Vaporizing Liquid Micro-resistojet experimentation

R. Hutten

Delft University of Technology

TU Delft

Vaporizing Liquid Micro-resistojet experimentation

by

R. Hutten

to obtain the degree of Master of Science
at the Delft University of Technology,
to be defended publicly on February 10, 2021.

Student number:	4151534	
Affiliation:	Chair of Space Systems Engineering, Faculty of Aerospace Engineering	
Supervisor:	Ir. B.T.C. Zandbergen	
Thesis committee:	Ir. B.T.C. Zandbergen,	TU Delft
	Prof.dr. E.K.A. Gill,	TU Delft
	Ir. R. Noomen,	TU Delft

TU Delft

Abstract

The Delfi program at the Delft University of Technology aims to develop nano satellites between 1 and 10 kg to provide high level education and to develop a platform for novel space technologies. Miniaturized satellites require miniaturized propulsion systems to provide orbital adjustments for functions like station keeping, extending mission duration and precise formation flying. Current research into micro-propulsion systems with aims to improve performance and efficiency is focused on Micro-electromechanical systems (MEMS), solar thermal and Commercial off-the-shelf (COTS) resistojet thrusters. The COTS design and prototype by Versteeg was the first leak resistant micro-thruster produced and successful experiments were performed using hot and cold nitrogen as propellant. The usage of liquid water as propellant for a Vaporizing Liquid Micro-resistojet (VLM) has been suggested as it is easy to store, has a high storage density, decent performance and is relatively safe to use. However as of writing this thesis, experimental tests using liquid water as propellant have been unsuccessful. In this thesis thrust tests with nitrogen have been repeated and show similar results to the data obtained by Versteeg verifying results of both experiments. In order for liquid water tests to be performed in the absence of a liquid mass flow sensor, a syringe pump was used to expel a constant volumetric flow. The liquid mass flow has been calculated by calibrating the syringe pump combined with the measured chamber pressure. Using liquid water, it was found that the chamber pressure increased over the course of the thrust experiment due to the feed system being volume based instead of driven by pressure. Since the test bench is dependent on the center of gravity of the thruster, thermal expansion significantly effects the measured thrust. Using nitrogen this effect can accurately be corrected for, while for water the effect is more difficult to correct due to the unpredictability of the liquid water remaining between the last propellant valve and the thruster chamber. This led to a decrease in accuracy of the measured thrust using liquid water compared to nitrogen, where the error grew from $\sim$1.5% to $\sim$13%. Thrust tests with water have been successfully performed at a chamber pressure of 1.02 bar and temperature of 300 °C for 15 minutes producing 8.0-8.3 mN of thrust with a specific impulse of 94-100 seconds with an accuracy of 14%. Several areas of improvement have been listed for both thruster design and experimental setup.

Contents

List of Tables

List of Figures

List of Symbols

A	Area
A_e	Area at the nozzle exit
A_t	Area at the nozzle throat
c^*	Characteristic velocity
C_d	Discharge coefficient
C_F	Thrust coefficient
$C_{F,loss}$	Viscous drag and heat transfer losses on thrust coefficient
C_θ	Divergence loss
D_h	Hydraulic diameter
F_m	Measured thrust
F_T	Produced thrust
h_c	Specific enthalpy of the propellant in the chamber
h_0	Specific enthalpy of the stored propellant
H_t	Nozzle throat height
I_{act}	Actuator coil current
I_{heat}	Heater current
I_{sp}	Specific impulse
I_{tot}	Total impulse
L	Characteristic length
$\dot{m}$	Mass flow
m_p	Mass of the propellant
M	Molar mass
p	Pressure
p_a	Ambient pressure
p_c	Chamber pressure
p_e	Pressure at the nozzle exit
p_t	Pressure at the nozzle throat
P_h	Change in energy per unit mass of propellant per second
P_{heat}	Heater power
r_c	Radius of the nozzle throat curvature
r_t	Radius of the nozzle throat cross-section
R_A	Universal gas constant
Re	Reynolds number
t_{open}	Time at which the propellant valve opens
t_{close}	Time at which the propellant valve closes
T	Temperature
T_c	Chamber temperature
T_{cu}	Casing temperature
T_e	Flow temperature at the nozzle exit
T_t	Flow temperature at the nozzle throat
T_{tube}	Temperature of the propellant tube
U	Flow velocity
U_e	Flow velocity at the nozzle exit
U_t	Flow velocity at the nozzle throat
U_{max}	Maximum flow velocity at nozzle exit
v_e	Effective exhaust velocity
V_{heat}	Heater voltage
W_t	Nozzle throat width
α	Actuator coil calibration factor

γ	Specific heat ratio
Γ	Vandenkerckhove function
δ	Boundary layer thickness in the nozzle throat
ΔP	Difference between ambient and chamber pressure
Δ_T	Difference in measured thrust due to thermal expansion
η_{heat}	Heating efficiency
θ	Nozzle divergent half angle
μ	Dynamic viscosity of the propellant
μ_c	Dynamic viscosity in the chamber
μ_t	Dynamic viscosity in the nozzle throat
ξ_{c^*}	Combustion quality
ξ_{C_F}	Nozzle quality
ξ_{F_T}	Thrust quality
$\xi_{I_{sp}}$	Propellant consumption quality
ρ	Density of the propellant
σ	Standard deviation

List of Acronyms

CFD	Computational Fluid Dynamics
CGG	Cool Gas Generator
CoG	Center of Gravity
COTS	Commercial off-the-shelf
IRT	Ideal Rocket Theory
MEMS	Micro-electromechanical systems
MFC	Mass Flow Controller
PWM	Pulse Width Modulation
RPT	Resistojet Performance Tool
VLM	Vaporizing Liquid Micro-resistojet
VTDC	Varying Turn-Density Coil

1

Introduction

The miniaturization of technology in the last few decades has enabled a reduction in size of satellites leading to the creation of so called smallsats, satellites with a mass of less than 500 kg. Reduced launch cost caused by this reduction in size and mass and the availability of Commercial off-the-shelf (COTS) technology saving in R&D cost allow small companies and educational institutions access to space. Miniaturized satellites require miniaturized propulsion systems to provide orbital adjustments for functions like station keeping, extending mission duration and precise formation flying. The Delfi program at the Delft University of Technology aims to develop nano satellites between 1 and 10 kg to provide high level education and to develop a platform for novel space technologies.[8] The first satellite launched was the Delfi-C^3, a tripple-unit CubeSat demonstrated solar cells, sun sensors, an electrical power subsystem and radio transmissions and was considered a full mission success.[15] Its successor the Delfi-n3Xt was also a tripple-unit CubeSat and was the first to demonstrate a micro-propulsion system based on solid propellant Cool Gas Generator (CGG).[9, 28]

Current research into micro-propulsion systems with aims to improve performance and efficiency have led to research into Micro-electromechanical systems (MEMS) [11], solar thermal [24, 39] and COTS resistojet [19, 37] thrusters. MEMS thrusters designed at TU Delft are etched on silicon wafers and are very efficient with respect to mass and volume. The main downside to this production method is the long lead times and high cost per batch. A COTS resistojet is made from as much COTS products as possible in order to significantly reduce cost. A resistojet is a class of thrusters that heat up propellant using electricity to increase performance. Prototypes made by Krusharev [19] and Stohr [37] provided valuable insights in theory and design but ultimately fell short in the experimental phase where the thruster failed to pass leak tests. This is one of the main problems encountered in development of micro thrusters at the TU Delft: the difficulty in creating a leak resistant prototype suitable for high operating temperatures since common practices for sealing requires materials like rubbers (o-rings, etc.), silicone or glues.[19, 26, 30, 37] The literature study performed preceding this thesis was focused on improving design and production methods to solve these issues. The improved design and prototype by Versteeg [47] was the first leak resistant COTS micro-thruster produced with which successful experiments were performed using hot and cold nitrogen as propellant. Although nitrogen can be a convenient propellant to work with, its low storage density provides a major downside on volume restricted small satellites. Storing liquid nitrogen requires cryogenic tanks which poses many challenges of its own, especially in a tight form factor such as the CubeSat. Cryogenic propellant tanks for CubeSats however have been developed and deployed for the CryoCube-1 mission.[5] Although some advanced resistojets require a specific type of propellant such as hydrazine to decompose into smaller molecules using a catalyst, the operating principle of a resistojet is to heat up propellant to increase the propellant efficiency of the thruster and generally can be operated with different propellants. Since the design by Versteeg does not require the use of a specific type of propellant, it is possible for other propellants with higher storage densities to be used. The usage of liquid water as propellant has been suggested as it is easy to store, has a high storage density, decent performance and is relatively safe to use.[14, 22] Using liquid propellants instead of gaseous classifies the resistojet as a Vaporizing Liquid Micro-resistojet (VLM). However as of writing this thesis, experimental tests using liquid water as propellant

have been unsuccessful. Liquid to gas phase changes and the different behaviour of liquids compared to gasses can provide obstacles that need to be overcome. Currently, many components of the test setup such as the feed system, propellant storage, as mass flow measurements are tailored towards the usage of gas and thus significant changes to the testing setup and procedures may be required. Since previous attempts for thrust tests using liquid propellant failed due to the lack of effective seals at high temperatures which has now been solved in the prototype of Versteeg, a new attempt to perform liquid propellant thrust experiments should provide valuable insight in future COTS VLM designs.

The research objective of this Master thesis stated as the following:

To perform experimental thrust tests using liquid water as propellant in order to validate the current VLM design and identify areas for improvement for future VLM development.

For the purpose of this thesis, validation of the VLM design refers to both how suitable the used design principles are for using a liquid propellant, and how accurately the performance of the VLM can be modelled. Testing with liquids is relatively new at TU Delft, and although the design is shown to be leak resistant at high temperatures, it should be researched what aspects of the design do or do not work well with liquids. In order to achieve the research objective, the following research questions have to be answered:

1. *How well can the characteristics of the thruster using liquid water be estimated from theory and how does this compare to nitrogen?*
2. *How can the current hot gas resistojet design be used for VLM testing using water as propellant?*
3. *How does the experimental setup need to be modified in order to allow for liquid water thrust tests?*
4. *What are the areas of improvement with respect to the current VLM design and experimentation?*

This report describes the work performed in order to give answers to the research questions and objective given above. First, an analytical model is made in chapter 2 in order to allow for the estimation and calculation of the thrusters performance. The experimental setup and VLM that will be used for all tests is described in chapter 3. In order to prepare for the thrust experiments multiple preliminary tests are performed and are described in chapter 4. Thrust tests with nitrogen as propellant are performed and described in chapter 5 in order to characterize the thrusters performance and verify the results with previous work. The thrust tests using water as propellant will be described in chapter 6 and compared to the results to the nitrogen experiments. Chapter 7 contains the conclusion of this thesis in which the answers to the research questions are given. Recommendations for future VLM design and to improve the experimental setup are found in chapter 8.

2

Analytical Model

This chapter describes the analytical model that is made in order to predict what values are to be expected during testing and how to describe the performance of the thruster in meaningful parameters. Section 2.1 describes Ideal Rocket Theory (IRT) which is the basis for the analytical model. In section 2.2 describes the corrections that can be made on top of this model to obtain a more accurate representation of the expected values. In section 2.3 is described how the error propagation of the analytical model works which is used to determine the confidence bounds of the obtained values from the analytical model. The model is validated with the obtained results in chapters 5 and 6. The model is verified using the results of previous work by Versteeg [47]. The model is named the Resistojet Performance Tool (RPT) and is hosted publicly on GitHub to be used for future use and is open to contributions for improvements and extensions.

2.1. Ideal Rocket Theory

The following section will describe the formulas needed to calculate the performance of the resistojet using Ideal Rocket Theory (IRT). This section will follow the work done by George P. Sutton and Oscar Biblarz.[38] All rocket engines rely on the law of conservation of momentum which is implied by Newton's laws of motion. The only way to propel a rocket engine forwards is by expelling a reaction mass in the opposite direction. The force acting on the rocket engine, i.e. the thrust, will depend on the mass flow rate $\dot{m}$ of the reaction mass (the propellant) and the effective exhaust velocity v_e:

$$F = \dot{m} \cdot v_e \tag{2.1}$$

The effective exhaust velocity v_e is not the actual flow velocity of the propellant. It rather is an artificial velocity that a reaction mass would have in order to attain a certain thrust. The actual exhaust velocity is not uniform over the entire cross section of the nozzle exit, one reason being the boundary layer which is especially prominent in small scale applications such as micro thrusters. The total impulse delivered by the system is given by the generated thrust integrated over the total thrust time,

$$I_{tot} = \int F \cdot dt \tag{2.2}$$

In order to maximize the efficiency of the rocket engine, i.e., maximizing the total impulse per unit mass of propellant, the exhaust velocity will have to be increased. A commonly used parameter to describe the performance of a rocket engine is the specific impulse I_{sp}, which is the total impulse per unit weight of the propellant

$$I_{sp} = \frac{I_{tot}}{m_p g_0} = \frac{v_e}{g_0}, \tag{2.3}$$

where g_0 is the gravitational acceleration of the Earth at sea level, 9.80665 m/s^2 and m_p is the mass of the propellant. The maximum flow velocity at the nozzle exit, U_{max}, occurs when the exhaust gasses

are infinitely expanded to a vacuum:

$$U_{max} = \sqrt{\frac{2\gamma}{\gamma - 1} \cdot \frac{R_A}{M} \cdot T_c} \tag{2.4}$$

where T_c is the chamber temperature, M is the molar mass of the propellant gas, γ the specific heat ratio of the propellant, and R_A is the universal gas constant. Combining formulas 2.3 and 2.4 and replacing v_e by U_{max} we find the first order approximation of the relation between the I_{sp} and the temperature:

$$I_{sp} \propto \sqrt{T} \tag{2.5}$$

This relation shows the benefit of a resistojet over cold gas propulsion in terms of propellant efficiency. The difference in real engines is that the pressure at the nozzle exit is not zero and U_{max} can't be attained. A pressure differential exists between the exhaust and ambient pressure that acts over the nozzle exit that has to be accounted for. The force acting on the rocket engine, depending on the actual flow velocity, U_e, that takes this pressure differential into account is written as

$$F = \dot{m} \cdot U_e + (p_e - p_a) \cdot A_e \tag{2.6}$$

Equation 2.6 is known as the rocket thrust equation, where p_e is the pressure at the nozzle exit, p_a is the ambient pressure, and A_e the area at the nozzle exit. To achieve maximum thrust, the pressure at the nozzle exit should be equal to the ambient pressure, although that is not what equation 2.6 might suggest.[1] The pressure at the nozzle exit depends on multiple factors and can be calculated using

$$\frac{A_e}{A_t} = \frac{\Gamma}{\sqrt{\frac{2\gamma}{\gamma - 1} \cdot \left(\frac{p_e}{p_c}\right)^{\frac{2}{\gamma}} \cdot \left(1 - \left(\frac{p_e}{p_c}\right)^{\frac{\gamma - 1}{\gamma}}\right)}} \tag{2.7}$$

where A_e is the area at the nozzle exit, A_t the area at the nozzle throat, p_c the pressure in the chamber and Γ is the Vandenkerckhove function given by

$$\Gamma = \sqrt{\gamma \left(\frac{2}{\gamma + 1}\right)^{\frac{\gamma + 1}{\gamma - 1}}} \tag{2.8}$$

which is a function of the specific heat ratio γ. The specific heat ratio is a property of a gas that is dependent on the temperature, pressure and type of propellant. The specific heat ratio is the ratio of the heat capacity at constant pressure (C_P) to the heat capacity at constant volume (C_V). The specific heat ratio is roughly equal to $\gamma = 1 + 2/f$ with f being the degrees of freedom of the gas. At the throat of the nozzle, where the mass flow per unit area is the largest, a unique situation exists where the maximum mass flow is reached for a given chamber pressure:

$$\frac{p_t}{p_c} = \left(\frac{2}{\gamma + 1}\right)^{\frac{\gamma}{\gamma - 1}} \tag{2.9}$$

At this critical pressure ratio the Mach number at the throat is equal to 1. Decreasing the exit pressure will not result in an increase in mass flow for a fixed chamber pressure. This limiting condition is often described as choked flow. Supersonic flow can only be attained when the exit pressure is smaller than the pressure at the throat or combined with equation 2.9:

$$\frac{p_c}{p_e} > \left(\frac{\gamma + 1}{2}\right)^{\frac{\gamma}{\gamma - 1}} \tag{2.10}$$

[1] It seems that a higher p_e would lead to higher thrust, but the energy required for a higher p_e is best spent by converting it to additional velocity. As can be seen in equation 2.13, increasing p_e will result to lower U_e.

At critical mass flow where the flow through the nozzle becomes supersonic, the relation between the chamber pressure and the throat area can be written as

$$A_t = \frac{1}{\Gamma} \cdot \frac{\dot{m}\sqrt{\frac{R_A}{M} \cdot T_c}}{p_c} \tag{2.11}$$

Assuming isentropic flow, the Poisson equations hold:

$$\frac{T}{T_c} = \left(\frac{p}{p_c}\right)^{\frac{\gamma-1}{\gamma}} \tag{2.12}$$

Where T and p are the temperature and pressure at some location in the nozzle. The flow velocity of the gas at any place in the nozzle can be written as:

$$U = U_{max} \cdot \sqrt{1 - \left(\frac{p}{p_c}\right)^{\frac{\gamma-1}{\gamma}}} \tag{2.13}$$

The thrust can be calculated with equation 2.6 by calculating exhaust velocity at nozzle exit U_e with the exit pressure p_e from equation 2.7.

2.2. Correction to Ideal Rocket Theory

The equations obtained from IRT come from a simplification of processes for which multiple assumptions are made that not necessarily have a negligible effect on the estimated values. Some important assumptions made when considering IRT that will affect the predicted thruster characteristics in comparison to a real thrust are listed below:[38]

- The propellant is gaseous, and any condensed phases are negligible to the total mass.
- The propellant gas obeys the ideal gas law.
- The propellant flow is adiabatic, no heat flows to or from the nozzle walls.
- The boundary layer effects are negligible, no friction occurs in the nozzle.
- There are no shocks occurring in the flow.
- The heat capacity of the gas is constant.
- The exhaust gasses leave the rocket in the axial direction.

This section lists some modifications that can be made to Ideal Rocket Theory in order to better estimate and describe specific characteristics of the thruster during experiments.

2.2.1. Quality factors

The performance of a real resistojet will be different from the performance calculated using IRT. There are multiple factors that will have an impact on the performance such as nozzle divergence loss, non-ideal gases, heat transfer losses and frictional effects which are not accounted for in section 2.1. It is difficult to account for all these physical processes individually since it is not clear what assumptions can be made and what the effects of these simplifications will be on the result. An easier method of determining the effects of these physical processes is to compare the theoretical values of the characteristic parameters to the ones obtained from experiments. The characteristic parameters C_F and c^* are used to determine the performance of the nozzle and the propellant. The characteristic velocity c^*, which reflects the energy level of the propellant and is independent of nozzle performance, is given by:

$$c^* = \frac{1}{\Gamma} \cdot \sqrt{\frac{R_A}{M} \cdot T_c} \tag{2.14}$$

The thrust coefficient C_F describes the ratio of the thrust due to the expansion of the propellant gasses in the nozzle to the force of the chamber pressure acting over the nozzle throat area:

$$C_F = \frac{F}{p_c \cdot A_t} = \frac{F}{\dot{m} \cdot c^*} \tag{2.15}$$

Combining 2.1, 2.3 and 2.15 shows that the thrust and I_{sp} correlate to the characteristic parameters as follows:

$$F = \dot{m} \cdot C_F \cdot c^* \tag{2.16}$$

$$I_{sp} = \frac{C_F \cdot c^*}{g_0} \tag{2.17}$$

With the characteristic parameters, multiple correction factors can be constructed. Correction factors describe the ratio between the experimental (subscript *exp*) and the ideal value (subscript *ideal*). The correction factors are a way to predict the performance ahead of testing. The correction factor for the thrust coefficient

$$\xi_{C_F} \equiv \frac{(C_F)_{exp}}{(C_F)_{ideal}} \tag{2.18}$$

is also known as the nozzle quality or nozzle efficiency and shows the efficiency of the nozzle design. Typical values of well-designed nozzles are above 0.90, although small nozzles usually are quite inefficient because of the relatively high friction forces due to the high surface to volume ratio.[38] The correction factor for the characteristic velocity

$$\xi_{c^*} \equiv \frac{(c^*)_{exp}}{(c^*)_{ideal}} \tag{2.19}$$

is also called combustion quality or combustion efficiency and combines the quality and irregular heating of the propellant. Sutton states typical values of ξ_{c^*} are between 92% and 99.5% for well-designed combustion chambers.[38] Since no chemical combustion occurs inside the resistojet and instead the chamber temperature is controlled directly by the power input, the value of ξ_{c^*} is set to 1 as the measured chamber temperatures are used as input to the model. The correction factor for the thrust and specific impulse are called the thrust quality and propellant consumption quality respectively and are given by:

$$\xi_{F_T} \equiv \frac{(F_T)_{exp}}{(F_T)_{ideal}} \tag{2.20}$$

$$\xi_{I_{sp}} \equiv \frac{(I_{sp})_{exp}}{(I_{sp})_{ideal}}. \tag{2.21}$$

At Reynolds numbers smaller than Re < $2.2 \cdot 10^5$, the boundary layer inside the throat can significantly reduce the effective throat area.[50] This reduction in throat area reduces the amount of mass flow needed to obtain a certain chamber pressure. The reduction of the effective throat area relative to the geometrical throat area is called the discharge coefficient and is given by:

$$C_d \equiv \frac{(A_t)_{eff}}{(A_t)_{geo}} = \xi_{c^*} \frac{(\dot{m})_{exp}}{(\dot{m})_{ideal}}. \tag{2.22}$$

The effective throat area can be calculated with experimental data using equation 2.11 when using a non-reacting gas. Since the value of ξ_{c^*} is set to 1, the discharge coefficient can also be defined as the ratio between the expected and ideal mass flow. Lastly, the correction factors can be correlated using the following equations:

$$\xi_{I_{sp}} = \xi_{C_F} = \xi_{F_T} / C_d. \tag{2.23}$$

For resistojets the efficiency of adding thermal energy to increase performance can be calculated using various ways. One method is by calculating the heating efficiency η_{heat} which is the ratio of the change in energy of the propellant P_h per second to the total heater power P_{heat}:

$$\eta_{heat} = \frac{P_h}{P_{heat}} = \frac{\dot{m}(h_c - h_0)}{P_{heat}} \tag{2.24}$$

where h_c is the specific enthalpy of the heated propellant in the chamber, and h_0 the specific enthalpy of the stored propellant. The of energy not directly used for heating the propellant during operation is lost due to thermal radiation to the environment and conduction to the thruster peripherals such as the thrust bench.

2.2.2. Boundary layer

Rocket theory in the ideal case does not include effects of the boundary layer in the thruster. The boundary layer is the layer of fluid (liquid or gas) that is in the vicinity of a surface in which viscous forces of the fluid are significant. Close to the surface, the velocity of the moving fluid approaches zero. The thickness of the boundary layer δ depends largely on the viscosity of the fluid, a fluid with a low viscosity will have a smaller boundary layer than a high viscosity fluid. The slow moving fluid along the nozzle wall reduces the overall momentum compared to the ideal case. The thickness of the boundary layer also reduces the effective throat area compared to the geometrical throat area. Especially for small thrusters with already a small throat area, the reduction of the nozzle throat area can be significant. The discharge coefficient C_d describes the ratio of the effective throat area to the actual geometric throat area, as can be seen in equation 2.22. An important factor in the estimation of the discharge coefficient is the Reynolds number Re which is a dimensionless number that describes the ratio of the inertial to viscous forces within a fluid and can be calculated with

$$Re = \frac{\rho U L}{\mu} \tag{2.25}$$

with ρ the density of the fluid, U the flow speed, L the characteristic length of the cross section, and μ the dynamic viscosity. The Reynolds number therefore changes depending at the location in the thruster. For the discharge coefficient specifically, the Reynolds number at the throat is the desired quantity and given by

$$Re_t = \frac{\rho_t U_t L_t}{\mu_c} = \frac{\dot{m} L_t}{\mu_c A_t} \tag{2.26}$$

where ρ_t is known for a fluid with a given pressure and temperature, which can be calculated using eq. 2.9 and 2.12. The flow velocity at the throat U_t can be calculated using eq. 2.13. According to the ISO 9300 standard, the throat Reynolds number is calculated using the chamber (stagnation) viscosity μ_c instead of the throat viscosity.[16] This differs from the model by Versteeg, where throat viscosity is assumed. This new method of calculation is used in other work such as the work by Kuluva and Hosack [21] and Johnson et al. [18] and effectively reduces the value of the Reynolds number by a factor of 0.84-0.90 for water with T_c between 150-1000°C and 0.86-0.91 for nitrogen with T_c between 20-1000°C.[4] The characteristic length of a circular throat would be the throat diameter, while for a rectangular nozzle this is not a defined quantity. Since the characteristic length is not an exact quantity, the Reynolds number is not always exact either and is mainly intended to indicate whether the flow is inertial or viscous. For calculating Re_t the characteristic length is taken as the hydraulic diameter D_h at the throat, which is widely used as replacement for equations that assume a circular tube. The hydraulic diameter is defined as

$$D_h = \frac{4A}{P} \tag{2.27}$$

$$D_{h,t} = \frac{2W_t H_t}{W_t + H_t} \tag{2.28}$$

where A is the cross-sectional area of the flow, P the wetted perimeter, and W_t and H_t the width and height of the throat. Another quantity that can be considered for the characteristic length is the throat width W_t itself, since for an infinitely long slit or where $H_t \gg W_t$, the height becomes irrelevant and L is dependent only on W_t. From the results of section 4.3.3 it can certainly be argued for this to be the case for this thruster. In the thesis by Versteeg the characteristic length was both taken to be W_t and $D_{h,t}$ resulting in two different Reynolds numbers. In this thesis it is believed that taking $L_t = W_t$ is incorrect. For a circular pipe of diameter a and a square pipe with sides a, the characteristic length is both a and satisfy equation 2.27. Taking $L_t = W_t$ is inconsistent with this definition and has only arisen from an educated guess and is thus disregarded. If $H_t \gg W_t$, the characteristic length should be equal to $L = 2W_t$ which is as expected only dependent on W_t.

Several expressions for estimating the discharge coefficient can be found in literature. Given below are theoretical relations for C_d by Kuluva and Hosack [21], Johnson et al. [18] and by Tang and Fenn [40]:

$$C_{d,KH} = \left(\frac{r_c + 0.05r_t}{r_c + 0.75r_t}\right)^{0.019} \times \left(1 - \left(\frac{r_c + 0.1r_t}{r_t}\right)^{0.21} \left(\frac{1}{Re_{t,ideal}}\right)^{\frac{1}{2}} (0.97 + 0.86\gamma)\right) \quad \text{(Kuluva and Hosack)} \tag{2.29}$$

$$C_{d,JS} = \alpha - \frac{\beta}{\sqrt{Re_{t,ideal}}} \quad \text{(Johnson et al.)} \tag{2.30}$$

$$C_{d,TF} = 1 - \left(\frac{\gamma+1}{2}\right)^{\frac{3}{4}} \left(\frac{4\sqrt{6}}{3} + \frac{8(9-4\sqrt{6})}{3(\gamma+1)}\right) \frac{1}{\sqrt{Re_D^*}} + \frac{2\sqrt{2}}{3} \frac{(\gamma-1)(\gamma+2)}{\sqrt{\gamma+1}} \frac{1}{Re_D^*} \quad \text{(Tang and Fenn)} \tag{2.31}$$

$$\text{with } Re_D^* = Re_{t,real} \sqrt{\frac{r_t \mu_c^2}{(Pr) r_c \mu_t^2}}$$

where r_c is the geometrical radius of the throat curvature, r_t the geometrical throat cross-sectional radius, γ the specific heat ratio, and Pr the Prandtl number at the throat. The relation by Kuluva and Hosack is derived from experiments using a axisymmetrical conical nozzle with 20° inlet and outlet angles and are valid for $0 \leq r_c/r_t \leq 20$ and $50 < Re_t < 10^4$. For the estimation of the discharge coefficient by Johnson et al., values of α and β depend on the propellant used and were initially only defined for CO_2, N_2, H_2 and Ar for axisymmetric nozzles with r_c/r_t = 4 and a nozzle divergent angle of 3° for $2000 < Re < 22000$. The relation by Tang and Fenn is analytically derived using the assumption of an infinitely long conical nozzle and was used by previous work by Versteeg [47] and Makhan [26] and is valid for Reynolds numbers greater than 200. Although the expression is analytical, the equation is experimentally validated and includes the Prandtl number as a small correction and "*has only empirical justification*".

For this thesis the work by Johnson et al. [18] is not used as the Reynolds number of some experiments will be lower than 2000, a divergent angle of 3° is far away from the designed 35° used here and the value of r_c/r_t is set at a fixed value of 4, whereas with the other two methods this is variable. As for choosing between the method by Kuluva and Hosack or Tang and Fenn, this is rather arbitrary as the values are very close together as will be shown in section 2.4. In the previous work by Versteeg and Makhan, the calculation of both models was incorrect as the model from Kuluva and Hosack was incorrectly calculated using the Reynolds number based on the throat viscosity instead of chamber viscosity, while the model used by Tang and Fenn incorrectly didn't include the Prandtl number. Therefore, it is not preferred to use one method over the other based on previous work alone. For this thesis it is chosen to use the method by Kuluva and Hosack [21] as this is an easier equation as it doesn't require calculation of $Re_{r,real}$ which is the Reynolds number in the throat using the effective values instead of the ideal ones.

The Reynolds number calculated using the right side of equation 2.26 is dependent on the mass flow, hydraulic diameter, and throat area. These parameters are all affected by the boundary layer in the throat. This means that the actual Reynolds number in the throat is different from the ideal situation. As the real values of the mass flow and throat area are both reduced by C_d (see equation 2.22), the effects cancel out and the only difference between the ideal and real Reynolds number is the reduction in hydraulic diameter. In order to calculate the hydraulic diameter for the reduced throat area it is assumed that the boundary layer thickness δ is equal along the height and width of the throat. The boundary layer thickness at the throat can be calculated as a function of the discharge coefficient as

follows:

$$C_d = \frac{(A_t)_{eff}}{(A_t)_{geo}} = \frac{(W_t)_{eff} \cdot (H_t)_{eff}}{W_t H_t} = \frac{(W_t - 2\delta)(H_t - 2\delta)}{W_t H_t} \tag{2.32}$$

$$\delta = \frac{1}{4}\left(-\sqrt{4H_t W_t C_d - 2H_t W_t + W_t^2 + H_t^2} + H_t + W_t\right) \tag{2.33}$$

where $(W_t)_{eff}$ and $(H_t)_{eff}$ are the effective width and height of the throat. Calculating the new hydraulic diameter with boundary layer thickness δ then becomes:

$$(D_{h,t})_{eff} = \frac{2(W_t)_{eff} \cdot (H_t)_{eff}}{(W_t)_{eff} + (H_t)_{eff}} = \frac{2(W_t - 2\delta)(H_t - 2\delta)}{W_t + H_t - 4\delta} \tag{2.34}$$

$$(D_{h,t})_{eff} = \frac{2W_t H_t C_d}{\sqrt{4W_t H_t C_d + (W_t - H_t)^2}}. \tag{2.35}$$

When $C_d = 1$, equation 2.35 reduces to equation 2.28 as expected. To clarify the definitions of the ideal and real Reynolds numbers, they are repeated here:

$$Re_{t,ideal} = \frac{\dot{m}_{ideal} \cdot (D_{h,t})_{geo}}{\mu_c \cdot (A_t)_{geo}} \tag{2.36}$$

$$Re_{t,real} = \frac{\dot{m}_{ideal} \cdot (D_{h,t})_{eff}}{\mu_c \cdot (A_t)_{geo}} \tag{2.37}$$

In equation 2.31, the value of C_d is dependent on the real Reynolds number which means the values of $Re_{t,real}$ and C_d have to be calculated over and over until they converge.

The boundary layer is not only present in the throat area, but also in the divergent part of the nozzle. This reduces the momentum of the exhaust gasses which therefore has an influence on the thrust that is produced. These losses are determined empirically by Spisz et al. [36] for Reynolds numbers between 500 and 18000 for area ratios A_e/A_t of 25 to 150 for conical nozzles of 20° half angle using hydrogen as propellant within an accuracy of 5%. These losses take into account the viscous drag on the divergent part of the nozzle and heat transfer losses to the nozzle wall and is as follows:

$$C_{F,loss} = 17.6 \exp\left(0.0032 \frac{A_e}{A_t}\right) \left(Re_{t,wall}\right)^{-0.5} \tag{2.38}$$

$$Re_{t,wall} = \frac{C_d \mu_c}{\mu_t} Re_{t,ideal} \left(\frac{T_t}{T_{t,wall}}\right)^{5/3} \tag{2.39}$$

where T_t is the gas temperature at the throat, and $T_{t,wall}$ is the temperature of the wall at the throat, and the ratio A_e/A_t is the geometrical area ratio. The factor $C_d \mu_c/\mu_t$ comes from the definition of the Reynolds number used in Spisz et al. which uses the real mass flow, but geometrical throat dimensions and throat viscosity instead of chamber viscosity. It is good to note that in the thesis by Versteeg, the power of 5/3 in equation 2.39 was changed to 1.727, which was due to the density scaling with T^{-1} and viscosity scaling close to $T^{0.727}$. However as the validity of the model was found to be lacking compared to the obtained results, the relation from Spisz et al. [36] is kept for now. Since $Re_{t,wall}$ depends on the value of C_d, the value of $C_{F,loss}$ has different values depending on the chosen method of estimating C_d. Since the resistojet is heated in its entirety, including the nozzle wall, the temperature of $T_{t,wall}$ can be approximated to be equal to the chamber temperature T_c. In this case, the ratio of T_t/T_c is actually already known in IRT by combining equations 2.12 and 2.9, which results in:

$$\frac{T_t}{T_{t,wall}} \approx \frac{T_t}{T_c} = \frac{2}{\gamma + 1} \tag{2.40}$$

$$C_{F,loss} = 17.6 \exp\left(0.0032 \frac{A_e}{A_t}\right) \left(\frac{C_d \mu_c}{\mu_t} Re_{t,ideal}\right)^{-0.5} \left(\frac{2}{\gamma + 1}\right)^{-5/6} \tag{2.41}$$

The ratio of T_t/T_c in the work by Spisz et al. [36] was set to a constant of 0.857, which coincide with a specific heat ratio of 1.33. To keep the model as free from assumptions as possible, the ratio of $2/(\gamma + 1)$ is seen as a more general expression. Although the wall at the throat is heated, it is actively cooled by the flowing propellant and is therefore presumably lower than T_c which means that $C_{F,loss}$ is likely an overestimation of the actual heat transfer losses.

2.2.3. Flow divergence losses

In Ideal Rocket Theory, the assumption is made that the propellant exits the nozzle in axial direction. However since exhaust gasses are diverging from the nozzle throat to the nozzle exit, part of the thrust vector of the individual gas molecules is directed radially outward decreasing the thrust in the axial direction. These losses are usually referred to as flow divergence losses. The amount of diverge loss depends on the shape and angle of the nozzle wall. For this reason launch vehicle rocket engine nozzles are usually bell shaped nozzles to reduce the amount of radial thrust at the nozzle exit, where the wall angle is small compared to the angle closer to the throat. For small thrusters this is more difficult to produce and conical nozzles are more common. The divergence loss C_θ for a two dimensional conical nozzle is calculated analytically by Berton [6] and is given by:

$$C_\theta = \frac{\sin\theta}{\theta} \tag{2.42}$$

with θ the divergent half angle of the nozzle in radians. The designed value for the divergent half angle of the nozzle is 20° which gives C_θ = 0.980, a loss of 2.0%. Together with the viscous and heat transfer losses in the nozzle $C_{F,loss}$, an estimate can be made for the thrust coefficient and nozzle quality:

$$C_{F,exp} = C_\theta C_{F,ideal} - C_{F,loss} \tag{2.43}$$

$$\xi_{C_F,exp} = \frac{C_{F,exp}}{C_{F,ideal}} \tag{2.44}$$

with subscript exp meaning expected from the correction based on the boundary layer and flow diverge effects, while $ideal$ is the value obtained from IRT.

2.3. Error propagation

The difference between experiments and theoretical models is that the latter is usually a simplification of the real world. The analytical model described above is no exception, and Ideal Rocket Theory makes several assumptions in order to keep equations simple and applicable in many different situations. Quality factors as described in section 2.2.1 again are simple (yet effective) methods to bridge the gap between ideal and real world situations. An important part of creating a theoretical model is to estimate how much the theoretical values can differ from a real life experiment. In order to say whether a measured variable is predicted correctly, the errors of both the theoretical and experimental variable have to be taken into account. The range in which a variable can fluctuate is set at three times its standard deviation, 3σ. The standard deviation σ can be calculated from a sample of N measurements using the following equation:

$$\sigma = \sqrt{\frac{\sum_i^N (x_i - \overline{x})^2}{N}} \tag{2.45}$$

where x_i is the value of the i-th measurement and $\overline{x}$ the average of all samples. If the samples are normally distributed, it is expected that 99.7% of the measurements are within $\overline{x} \pm 3\sigma$. The calculation of the standard deviation however does not require the data to be normally distributed, and can be calculated for every set of data. The 3σ rule is still kept for maximum error expectancy for non-normal data. Manufacturers of sensors generally declare the accuracy of the supplied values in terms of this 3σ value, which serves as an input for the accuracy of the measurements made. The question in a theoretical model becomes what to do with the errors if they take part in mathematical operations. Given A is a variable with error σ_A, and B a variable with error σ_B, a a constant with no error ($\sigma_a = 0$),

and σ_f the error of f, the propagation of uncertainty for various mathematical operations is given as follows [20]:

$$\begin{aligned}
&f = aA && \Rightarrow && \sigma_f = |a|\sigma_A \\
&\left.\begin{aligned} f = A + B \\ f = A - B \end{aligned}\right\} && \Rightarrow && \sigma_f = \sqrt{\sigma_A^2 + \sigma_B^2} \\
&\left.\begin{aligned} f = A \cdot B \\ f = A/B \end{aligned}\right\} && \Rightarrow && \sigma_f = |f|\sqrt{\left(\frac{\sigma_A}{A}\right)^2 + \left(\frac{\sigma_B}{B}\right)^2} \\
&f = A^a && \Rightarrow && \sigma_f = \left|\frac{fa\sigma_A}{A}\right| \\
&f = A^B && \Rightarrow && \sigma_f = |f|\sqrt{\left(\frac{B\sigma_A}{A}\right)^2 + \left(\ln(A)\sigma_B\right)^2}
\end{aligned} \tag{2.46}$$

The model produced in this thesis automatically keeps track of the propagation of uncertainty when any of the above mathematical operations are applied. This ensures that all errors that are calculated correctly. However this propagation of uncertainty is only valid for single mathematical operation where A and B are uncorrelated. An example for when this is not the case is when the chamber pressure and temperature are used to calculate a value for γ and then calculating a value such as c^* which depends on both the temperature and γ. In this case the temperature for both equations are seen as independent, and as a result the error of c^* will be overestimated. To combat this, the model is instead calculated with randomized input parameters taken from the a Gaussian distribution representing these input parameters. By repeating these calculations multiple times, the parameters of the model output form a distribution of which the standard deviation can be calculated from. Although the calculating the error of the output parameters this way is not exact, a high number of iterations of this process will eventually converge on the correct value. Unless otherwise specified, the number of iterations is set to 100.000 as this was found to be a good compromise between accuracy and computation time.

2.4. Model verification

In this section the model will be verified by comparing its output to the results of the model by Versteeg [47] on two different sets of input variables. The input and output of both models can be seen in table 2.1. Comparing the two outputs of the model, the results from IRT are identical barring some rounding differences, whereas results from the expected model are within 2% with the exception of the Reynolds number. This slight differences between the two models can be explained by the fact that the Reynolds number is now calculated correctly with respect to its definition in the associated papers as stated in section 2.2.2 and the different methods for calculating the discharge coefficient. The difference between the two methods (equation 2.29 and 2.31) is minimal. For the conditions of test TTH-1.1 performed in the work by Versteeg, the discharge coefficient changes between $C_{d,KH}$ = 0.9525 and $C_{d,TF}$ = 0.9522 and for test TTH-4.1 these are $C_{d,KH}$ = 0.9334 and $C_{d,TF}$ = 0.9300. The large difference in Reynolds number is caused by the different definitions used in the models: using the throat or chamber viscosity of the fluid. Other than this change in definition, the Reynolds numbers found are the same.

2.5. Conclusion

In this chapter a model is described for calculating ideal and expected Resistojet thruster performance. Compared to the predecessor of this thesis, the several errors in the model by Versteeg [47] are identified and fixed. The model applies a different technique or calculating the discharge coefficient as the calculation is easier while the difference between the two methods is insignificant. Also a slight modification to the calculation of the nozzle losses is made to stay closer to the definition in the paper as it did not provide good validity with the experimentally obtained results, while another modification of the nozzle losses replaced a constant with a variable that is dependent on the used propellant and stagnation conditions. In literature the Reynolds number was found to be defined in several different ways which means special care has to be taken implementing these results. For the sake of standardization, the definition of the Reynolds number is now taken as its definition in the ISO

Input		TTH-1.1		TTH-4.1	
Propellant		Nitrogen		Nitrogen	
T_c	[K]	305.5 ± 5.8		670.7 ± 5.8	
p_c	[kPa]	135.6 ± 5.0		166 ± 10	
p_a	[Pa]	184 ± 29		209 ± 32	
A_t	[10^3µm^2]	70.6 ± 4.8		70.6 ± 4.8	
A_e	[10^3µm^2]	531.7 ± 5.1		531.7 ± 5.1	
H_t	[µm]	496 ± 4		496 ± 4	
θ	[°]	20 ± 0		20 ± 0	
Output		This work	Versteeg	This work	Versteeg
Ideal:					
F_T	[mN]	15.45 ± 1.16	15.4 ± 1.2	19.02 ± 1.69	19.0 ± 1.7
$\dot{m}$	[mg/s]	21.78 ± 1.70	21.8 ± 1.7	17.87 ± 1.63	17.8 ± 1.6
I_{sp}	[s]	72.34 ± 0.73	72.34± 0.73	108.6 ± 0.62	108.58± 0.62
Expected:					
C_d	[%]	95.25 ± 0.17	94.91 ± 0.25	93.34 ± 0.28	92.55 ± 0.40
$\xi_{I_{sp}}$	[%]	77.74 ± 0.70	78.70 ± 0.66	68.13 ± 1.23	69.5 ± 1.1
F_T	[mN]	11.44 ± 0.97	11.54 ± 1.00	12.10 ± 1.32	12.2 ± 1.3
$\dot{m}$	[mg/s]	20.74 ± 1.66	20.7 ± 1.7	16.68 ± 1.57	16.5 ± 1.6
I_{sp}	[s]	56.25 ± 0.51	56.93 ± 0.50	73.97 ± 1.22	75.5 ± 1.1
Re_t	[-]	3641 ± 256	4120 ± 290	1677 ± 140	1820 ± 150

Table 2.1: Input parameters used for two different hot thrust tests performed by Versteeg [47] (TTH-1.1 and TTH-4.1) and corresponding output parameters of the model from this thesis compared to the results from the model by Versteeg.

9300 standard.[16] In the end, the model was verified with the results of Versteeg and show that they are identical for ideal case while having a maximum difference of 2% in the non-ideal case. As the model from Versteeg was found to be around 10% to 15% off from the experimental values, this implies that this model will have the similar validity as both models have within 2%.

In order to make the model available for future research, it is hosted on the GitHub repository RickHutten/ResistojetPerformanceTool. To allow other researchers and students to contribute and make improvements and extensions to the model, it is recommended to move the repository to a centralised account of the Space Flight track where multiple tools can be hosted. This prevents every student from recreating existing models and tools and instead build an ever improving set of tools for shared use.

3

Test Setup

The thrust tests in this thesis are performed with very similar test setups. This chapter will describe the test setup used for the thrust tests performed in this thesis. Section 3.1 describes the thruster and section 3.2 the thrust bench and equipment used for the thrust tests. Section 3.5 describes how the thruster is heated. Finally, section 3.6 describes the confidence bounds of the used equipment.

3.1. Micro resistojet

The micro resistojet used for this thesis is the one produced in the Master thesis of Versteeg [47]. The thruster is made up of two copper blocks that are clamped by six screws onto a stainless steel cutout hereafter called the nozzle profile, see figure 3.2. Specifications of the nozzle profile can be seen in table 3.1. The nozzle profile is open at the throat where it forms a two dimensional conical nozzle. The copper blocks clamped on the nozzle profile ensure the gas can only escape through the nozzle. Figure 3.1 shows a schematic of the assembled thruster of the fully assembled thruster and on the inside of the radiation shield, where the two copper blocks are visible. The propellant inlet is connected by a small tube to a valve which can be toggled using a LabView interface. This propellant valve, shown in figure 3.3, is the MINSTAC VHS type solenoid valve by The Lee Company [42]. This is the last valve to be switched for allowing mass flow to be entering the thruster. To measure the chamber pressure a p-T sensor is used from TE connectivity [41] at the end of a tube connected to the chamber to reduce the temperature at the sensor. The sensor has a maximum operating temperature of 85°C, which can be measured directly with its built-in temperature sensor. The thruster is mounted on a pendulum pole to the test bench, which is described in detail in section 3.2. The chamber temperature is measured using a thermocouple that is placed on the outside of the chamber touching the nozzle profile and copper sealing block. The chamber temperature sensor therefore technically measures the chamber body temperature instead of the gas temperature inside the chamber. Measuring the chamber temperature directly of the gas is very challenging for miniaturized thrusters due to the lack of space. Figure 4.12 shows more clearly the location of the thermocouple on the thruster. One heater is inserted in each of the two copper blocks to heat up the thruster body to operational temperatures. Not shown on the schematic drawing are three thermocouples that are placed on the propellant tube to measure the temperature at three different locations. These thermocouples are electrically insulated and attached using tape at distances of 18.5 ± 1.0, 31.5 ± 1.0, and 44.0 ± 1.0 mm from the copper sealing block.

The thruster by Versteeg [47] is an engineering model produced to verify the principles of design, fabrication, and operation of a COTS resistojet design. It is primarily designed to be used with gaseous propellant, although the use of liquid propellant is not explicitly excluded. Resistojets are a class of thrusters that could theoretically work with various gaseous and liquid propellants as long as enough heat is provided for vaporization. Since the thruster is an engineering model, there are still areas for improvement with respect to volume and mass. Table 3.1 shows some typical specifications of the thruster.

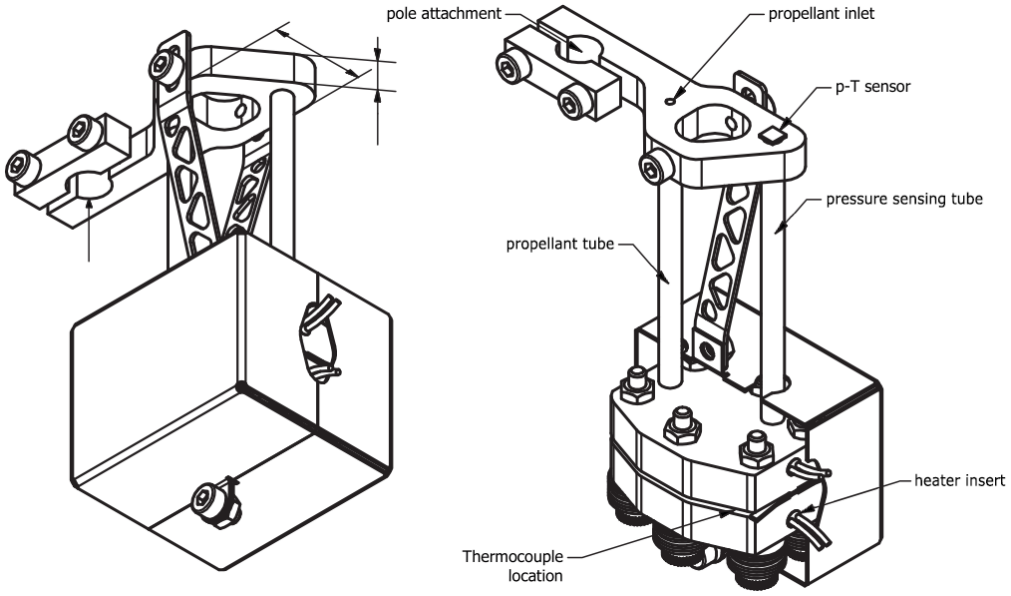

Figure 3.1: Schematic drawing of the assembled thruster with its radiation shield (left) and with half the radiation shield removed (right) showing the thruster body. Image by Versteeg [47].

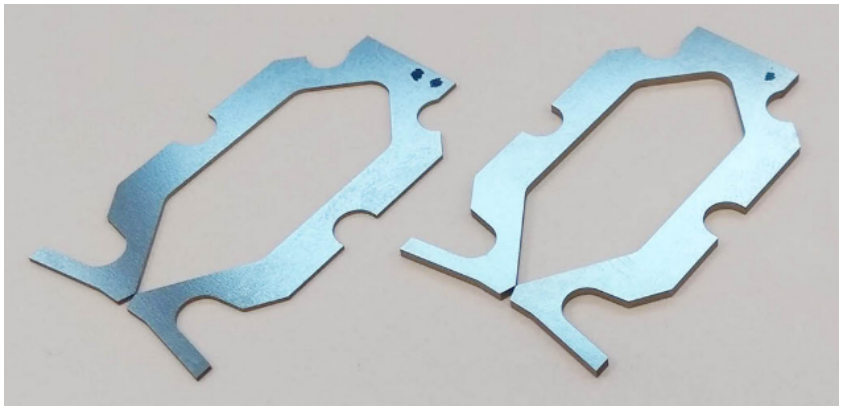

Figure 3.2: Stainless steel nozzle profiles cut by using wire-EDM with a thickness of 0.5 mm (left) and 1.0 mm (right). Image by Versteeg [47].

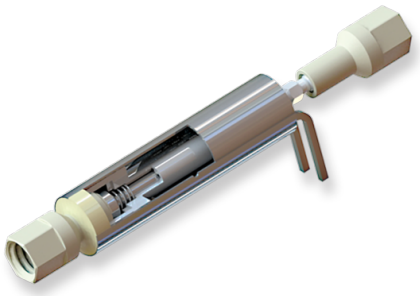

Figure 3.3: MINSTAC propellant valve by The Lee Company. Image from The Lee Difference [43].

3.2. Thrust bench

The TU Delft Faculty of Aerospace Engineering possesses a small number of thrust benches that can be used for micropropulsion. When starting this thesis only one of these thrust benches, the TB-5m, was fully assembled and working. This thrust bench made by Bijster [7] and later refined by Jansen [17], was also used to test the same thruster when it was fabricated by Versteeg [47]. Since this thrust bench

Parameter	Value	Unit
Nozzle throat height	500	µm
Nozzle throat width	130	µm
Nozzle exit height	500	µm
Nozzle exit width	1072.5	µm
Expansion ratio	8.25	-
Throat curvature radius	260	µm
Divergent half angle	20	°
Convergent half angle	35	°
Mass thruster body	0.149	kg
Max power	50	W

Table 3.1: Design values of the micro resistojet produced by Versteeg [47].

was already shown to be fully working with the same thruster that will be used in this thesis and was the only one that was fully operational, it was chosen to use this thrust bench for the experiments. The TB-5m, shown in figure 3.4 and 3.5, consists out of a pendulum that is suspended on a low friction pivot on which the thruster can be attached. Attached to the pivot is a spring to help dampen oscillations. When the pendulum is hanging freely, the mass of the pendulum and spring is causing the pendulum to oscillate around a certain equilibrium position. A capacitive distance sensor (Micro-Epsilon CS2, not visible in both figures) is used to measure the pendulum displacement up to an accuracy of 40 nm.[27] Attached perpendicular to the pendulum arm is a plastic arm that holds a magnet at the outer end. This magnet is located inside a coil which can exert a force on the magnet by running current run through it and creating a magnetic field. Since this magnet is attached to the pendulum arm, this will put a force on the pendulum and put the pendulum in a different position. With this setup it is possible to set the pendulum at a predefined position by actively controlling the current through the coil. If the thruster is operated, the thrust produced will put an additional force on the pendulum. The current required by the coil to keep the pendulum arm at a certain position will be different on whether the thruster is producing thrust or not. This difference is directly related to the thrust that is being produced by the thruster.

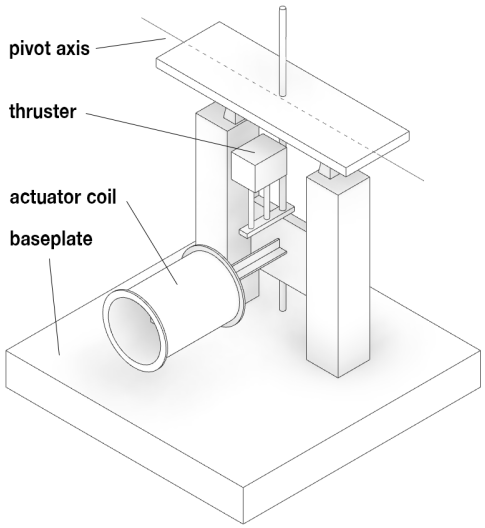

Figure 3.4: Sketch of the thrust bench, not to scale.

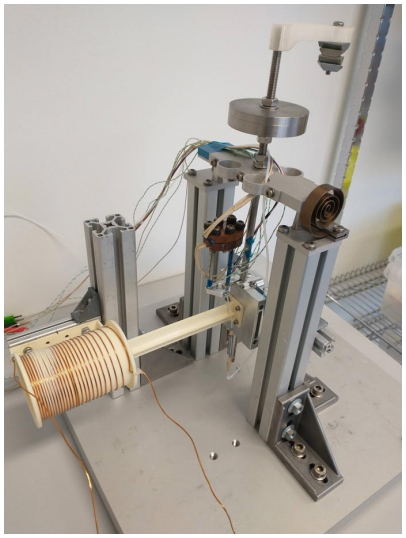

Figure 3.5: Photo of the thrust bench outside the vacuum chamber.

3.2.1. Thrust calculation

The thrust bench is fitted with a Varying Turn-Density Coil (VTDC) by Bijster so that the force on the pendulum arm is linear with the thrust.[7] In MSc thesis by Versteeg [47] and Pappadimitriou [30], the coil was calibrated producing a force of α = 0.826 ±0.006 mN/A. Both calibrations of the actuator coil

are in compliance with each other and are deemed stable enough so that a repeat of the calibration is not necessary. The TB-5m thrust bench was originally rated for thrust up to 5mN with the idea to mount the thruster on the bottom of the pendulum arm.[7] However, as also done by Versteeg, by mounting the thruster closer to the pivot axis it is possible to measure higher thrusts at the cost of some loss of accuracy. The thruster is expected to produce thrust of no more than 15mN, so the thruster need to be mounted around 1/3rd the distance or less from the length of the pendulum arm. The torque that the actuator delivers on the pendulum counters the torque the thruster delivers, and so to convert from actuator coil force to thruster force the following relation is used:

$$\begin{aligned} F_T \cdot L_F &= F_C \cdot L_C \\ F_T &= F_C \cdot \frac{L_C}{L_F} \end{aligned} \tag{3.1}$$

where F_T is the thrust delivered by the resistojet, L_F the distance along the pendulum from the point of thrust to the pivot, F_C the force that the actuator coil delivers, and L_C the distance along the pendulum from the actuator coil to the pivot. Figure 3.6 shows a side view of the thrust bench showing the lengths L_F and L_C. Distances L_F and L_C are difficult to measure directly, and have to be calculated. Instead the lengths L_{1-5} can be measured using a caliper. From this the values of L_F and L_C can be calculated as follows:

$$L_F = L_3 - \frac{L_1 + L_4}{2} \tag{3.2}$$

$$L_C = L_2 + \frac{L_1 + L_5}{2} \tag{3.3}$$

$$\frac{L_C}{L_F} = \frac{L_1 + 2L_2 + L_5}{-L_1 + 2L_3 - L_4} \tag{3.4}$$

Lengths L_2 and L_3 were difficult to measure and so the error is higher than L_1 and L_5. The height of the thruster, L_4, was not constant everywhere and so multiple measurements were taken from multiple sides. The error Δx is taken as the 3σ of the measured values. Measurements with a caliper for the dimensions of L_{1-5} are shown in table 3.2, with the values of L_C and L_F and their fraction included.

Length	x [mm]	Δx [mm]	$\Delta x/x$ [%]
L_1	10.00	0.01	0.10
L_2	123.5	0.50	0.40
L_3	71.54	0.38	0.52
L_4	16.53	0.50	3.05
L_5	70.04	0.03	0.04
L_F	58.28	0.45	0.776
L_C	163.52	0.50	0.306
L_C/L_F	2.806 [-]	0.0234 [-]	0.834

Table 3.2: Measured values of lengths L_{1-5} and the lever conversion factor of the test setup.

Together with the actuator coil calibration α from Versteeg and Pappadimitriou, the conversion from actuator coil current I_{act} to thruster force F_T is:

$$\begin{aligned} F_T &= \frac{L_C}{L_F} \cdot \alpha \cdot I_{act} \\ F_T &= (2.806 \pm 0.0234) \cdot (0.826 \pm 0.006) \cdot I_{act} \\ F_T &= (2.318 \pm 0.0256) \cdot I_{act} \end{aligned} \tag{3.5}$$

3.2.2. Pendulum control

To determine the current that is needed to set the pendulum arm at a certain position, a discrete time PID-controller was used. During exploratory testing it was found that the precision of the output signal

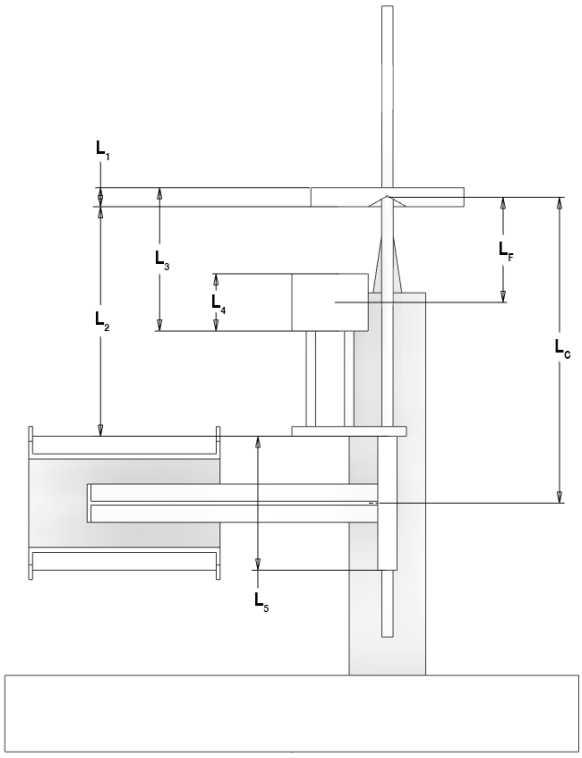

Figure 3.6: Sketch of the thrust bench as viewed from the side, not to scale.

was poor, in particular when using water as propellant, and could not be improved by further tuning the PID variables. An example of the unstable PID control resulting in measured thrust with high noise can be seen in figure B.2 in the appendix. It is unclear why the noise was found to be that high as the results of Versteeg do not show noise of similar proportion. In the thesis by Versteeg no experiments with water as propellant have been done, which could be more prone to noise as the the boiling of the water introduce extra vibrations that could have an effect on the movement of the pendulum. This could be one of the reasons why the instability was not encountered in the work by Versteeg. The experiments with nitrogen performed in this thesis show no significant difference in the magnitude of the noise. The PID control code written in the LabView program was cumbersome to debug and it was chosen to reimplement the PID algorithm with a more simplistic version. The control algorithm used is as follows:

$$
\begin{aligned}
e_i &= S - y_i \\
P_i &= e_i && \text{(proportional term)} \\
I_i &= I_{i-1} + e_i \cdot dt && \text{(integral term)} \\
D_i &= (e_i - e_{i-1})\,/dt && \text{(derivative term)} \\
U_i &= K_P \cdot P_i + K_I \cdot I_i + K_D \cdot D_i
\end{aligned}
$$

where subscript i denotes the i-th sample in time, S the setpoint of the controlled variable, y the measured variable, e the error between the setpoint and the measured variable, dt the size of the discrete time step (the inverse of the sampling rate), K_P, K_I and K_D are the three user variables that control the behaviour of the controller, and U the output signal for the actuator influencing the controlled variable. This algorithm is a more straightforward version of the one used in the setup by Versteeg [47], in which the algorithm by Astrom et al. [2] was used. It also reduces the amount of arbitrary input variables by one, which increases the simplicity of tuning the controller. It was found that the stability of the controller was increased and showed no noticeable downsides compared to the PID control from Versteeg [47]. The values of the control parameters K_P, K_I, and P_D that were chosen to be giving acceptable results were 1, 80, 3 respectively. The reason that the value of K_I is two orders of magnitude larger than the other parameters is that this is the only parameter that is

dependent on the sampling rate. The stability of the updated control algorithm can be seen in various figures in the results of chapter 6 for comparison.

3.3. Feed system

This section will describe the feed systems used in the experiments. Figure 3.7 shows the nitrogen feed system. Not shown in this figure is the pressurized nitrogen tank which is located at the back, from which a tube goes through a notch in the back board at the bottom. Following are a series of valves to control the flow and regulate the downstream gas pressure. The nitrogen first flows through a high pressure shut-off valve before arriving at the pressure regulator valve which is used to decrease the pressure from 200 bar to 1-10 bar. With the pressure regulator valve it is possible to control the downstream pressure by turning the handle. The downstream pressure can be read on the low pressure gauge, although this is relatively inaccurate as this is an analog gauge with lines at only every 0.5 bar. Further down the line is the low pressure shut-off valve. In this figure the valve is in the open position, rotating the handle by 90° clockwise will close the valve. The tubing after the low pressure shut-off valve splits into three different tubes to allow multiple simultaneous setups for different experiments. Every of the three tubes contain a selection valve which are used to block the flow for the individual paths. For this experiment, the rightmost path is connected to the Mass Flow Controller (MFC) that will be used to measure the flow of propellant. As can be seen in the figure, only the selection valve going to the MFC is opened, while the other two are in the closed position. On top of the mass flow sensor is a plastic hose which can be connected to the connection that leads into the vacuum chamber. The connection is a Swagelok Quick Connect which is designed for minimal air inclusion and minimal spillage when a connection is made.

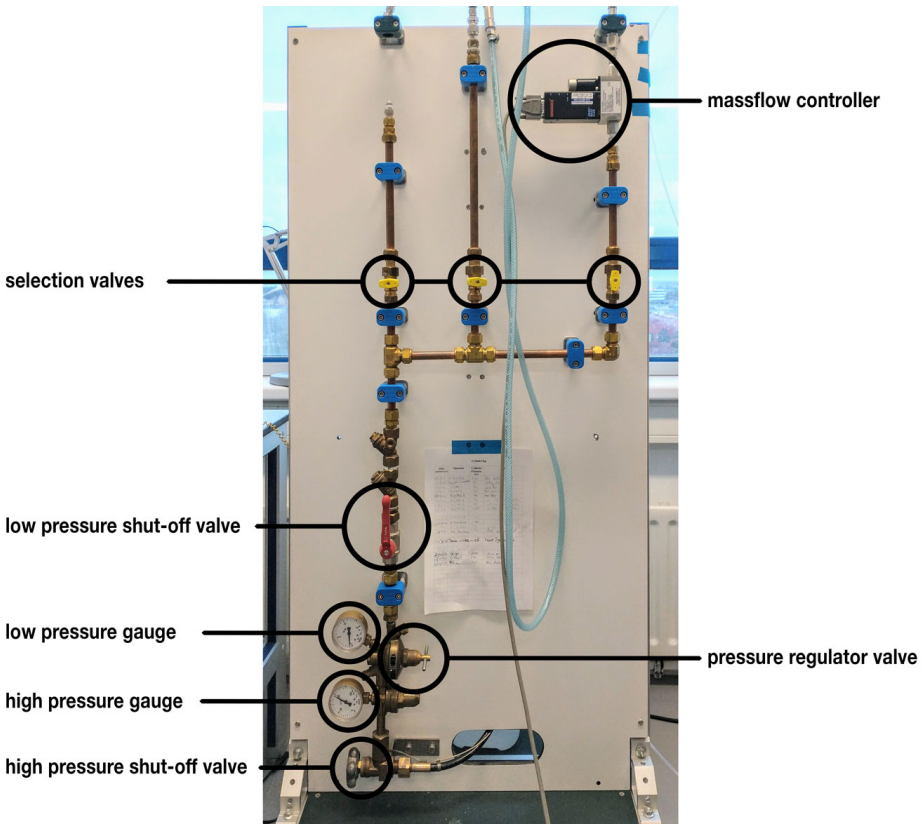

Figure 3.7: Nitrogen feed system.

The water feed system is different from the nitrogen feed system. There are different options for supplying water to the thruster. The main issue with determining the mass flow of water is that currently no sensor for liquids is available. One way to determine the mass flow is by suspending a water tank inside the vacuum chamber and using the nitrogen feed system to pressurize the tank, forcing liquid

water towards the thruster. Calculating the water mass flow can be done in multiple ways. One way is by measuring the tank pressure and mass flow of nitrogen to the tank which makes possible to calculate the change in volume of the nitrogen and therefore mass flow of the water expelled from the tank. Even without the mass flow sensor the tank can be pressurized and shut off from the nitrogen supply. Knowing the tank dimensions and water level, it is possible to calculate the mass flow by the decreasing rate in tank pressure. Because these methods are based on the displaced volume and since the density of nitrogen is much lower than liquid water, the pressure sensor and mass flow sensor needs to be able to measure very accurately. Another method is by using a syringe pump to supply a steady flow as was done previously at the university by Kurmanbay [22]. The syringe pump works by moving the plunger of the syringe at a constant rate into the barrel of the syringe. A syringe pump therefore dispenses propellant at a constant volume rate, instead of a mass flow rate. For fluids this is not a problem since they can be assumed to be incompressible. In practice however, small air bubbles will form when filling the syringe and propellant tube. The volume of these air bubbles greatly depend on the pressure inside the feed line compared to atmospheric pressure when the bubbles were created. Since the order of magnitude of the mass flow for the thruster is around 10 mg/s, which for water is equal to a volume flow of 10 µL/s, gaseous bubbles inside the feed system can have a large influence on the propellant that is dispensed down the line into the thruster. It is therefore important to keep air bubbles to a minimum when filling the syringe and propellant tube. An image of the syringe pump can be seen in figure 4.7. A syringe is placed in the syringe pump which can connect to a tube similar to the one coming from the nitrogen feed system, which in turn can be connected to the Swagelok Quick Connect to connect to the propellant connection of the vacuum chamber. Since the equipment for using the syringe pump was already available and used before, while creating the blow-down tank requires significantly more work it was chosen to use the syringe pump concept.

Both the nitrogen and water supply is attached on the same connector that leads into the vacuum chamber. Inside the vacuum chamber another Swagelock Quick Connect interface exists which connects to a MINSTAC VHS type solenoid valve from The Lee Company.[42] This valve can be controlled using the LabView script and is the main valve that determines the flow of propellant to the thruster. It can only be opened and closed fully, but can be controlled using Pulse Width Modulation (PWM) to restrict the flow of propellant. The tubing from the propellant valve to the thruster is made from PTFE/Teflon and is glued on the thruster inlet tube.

3.4. Equipment used and thruster installation

This section will summarize the equipment that is used in the setup and the procedure on how to mount the thruster on the test bench. Table 3.3 lists all the equipment used for the thrust experiments performed in this thesis. The thruster is mounted on the test bench by clamping it on the pendulum arm with the nozzle facing towards the actuator coil. As thruster is clamped onto the pendulum and can rotate around it, aligning the thruster perpendicular to the pendulum rotational axis has to be done by eye. After the thruster is secured tightly in place, the heat shield can be secured. Make sure the wiring from the heaters, propellant tube, thermocouples, propellant valve cables, and p-T sensor are fed through the openings on the top of pendulum platform. Guide the wired along the rotational axis away from the test bench and secure with the vacuum chamber appropriate blue tape. By securing the wires this way, the effect of rotation of the pendulum has minimal effect on the movement of the wires. The thin plastic propellant tube is then rotated 180°downwards and secured on the test bench with tape to minimize the effect of the flowing propellant on the movement of the pendulum. After all the wiring has been secured, the test bench can be placed inside the vacuum chamber after which all cables can be connected. Figure 3.9 shows the thruster mounted on the test bench fully connected inside the vacuum chamber.

3.5. Heating

The resistojet is heated by two Watlow FIREROD cartridge heaters. The cartridge heaters are 1/8-th inch in diameter, one inch long and can handle a maximum temperature of up to 760°C.[49] These heaters have also been used in the work by Versteeg to heat up the resistojet up to a temperature of 400°C, well within the heaters operating temperature range. However, the heaters were found to fail after a few heat cycles. The assumption was that the internal temperature of the heater had surpassed

Device	Description
Sensors	
Brooks 5850S	Gaseous mass flow controller to measure the nitrogen mass flow from the feed system.
TE Connectivity MS5837-30BA	Combined pressure and temperature (p-T) sensor to measure the chamber pressure.
Micro-Epsilon CS2	Capacitive displacement sensor that measures the pendulum position.
VACUUBRAND VSP 3000	Pressure sensor that measures the vacuum chamber pressure.
Power supplies	
Delta Elektronica D-030-10	Power supply for the spike and hold driver.
Delta Elektronica E-030-10	Power supply for the spike and hold driver.
Delta Elektronica ES 030-10	Power supply for one of the two heating elements.
Delta Elektronica SM-7020	Power supply for one of the two heating elements.
Delta Elektronica SM-7020-D	Power supply for the actuator coil.
Data Acquisition	
NI USB-8451	Reads out the MS5837-30BA p-T sensor.
NI USB-6008	Provides 2.5V power to the MS5837-30BA p-T sensor.
NI PCI-6229	Interfaces with SM-7020-D and 5850S.
NI-9211	Reads out the thermocouple sensors.
Micro-Epsolon DT6220/DL6230	Reads out the Micro-Epsilon CS2 sensor.
VACUUBRAND DCP 3000	Reads out the VSP 3000.
Actuators	
Vacuubrand RZ 6	Vacuum chamber pump.
ProSense NE-1000X2	Syringe pump used for liquid feed system.
1/8” Watlow FIREROD Cartridge Heater	Controls the chamber temperature.
Actuator coil	Creates a known force on the thrust bench.

Table 3.3: Equipment used and functionality used in the thrust test setup.

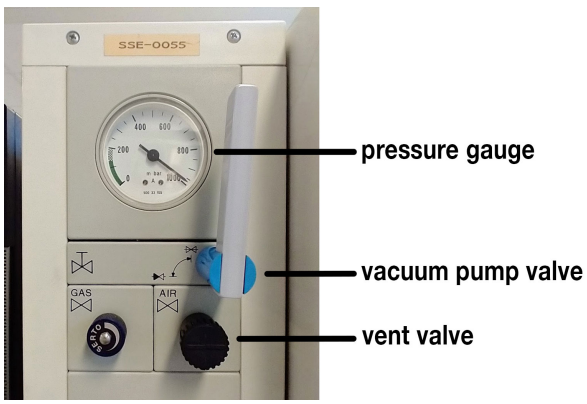

Figure 3.8: Vacuum chamber valves.

the maximum allowed temperature, since the point where the temperature was measured is on the thruster itself, around 1 cm away from the heater. A new heater was ordered by the university before the start of this thesis with an internal J-type thermocouple. This should measure the temperature of the heater more accurately and prevent overheating. However, with an exploratory test the heater with the internal thermocouple still failed while the internal temperature of the heater was 550 °C at maximum, well below 760 °C. Consultation with a representative of Kurval B.V., the company that supplied the

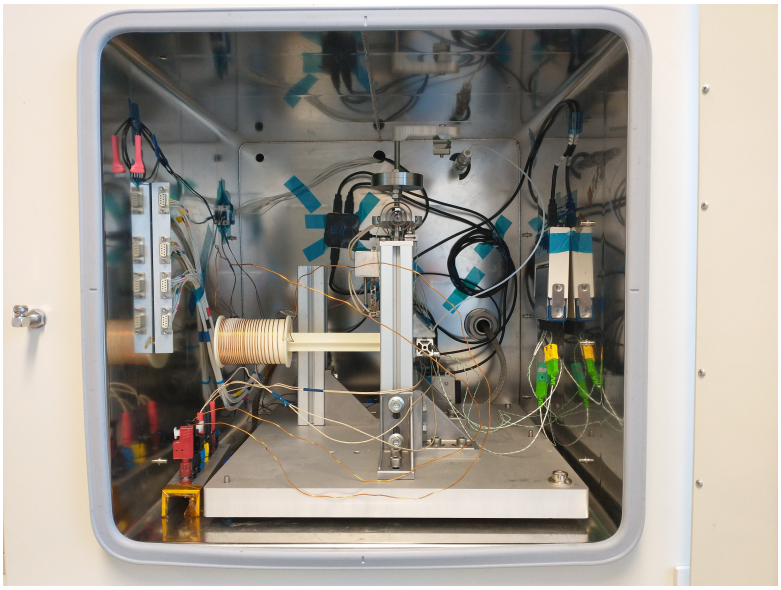

Figure 3.9: Thrust bench TB-5m inside the vacuum chamber with all sensors and equipment attached.

Watlow heaters, revealed that the internal thermocouple is not placed in the center where the largest amount of heat is generated. This means that the temperature of the heater at the point of highest heat generation could have been above its maximum allowed temperature. In addition to this, the fit of the heater inside the hole was most likely too large. The Watlow 1/8-th inch cartridge heater requires a fit so small that it generally is very difficult to fit the heater inside the hole. This is especially true for the 1/8-th inch heater since the shape is slightly oval because of the small diameter. In the case of the resistojet, the heater fits inside the hole very easily and even has enough space to move around. The maximum allowed wattage of the heater is actually a function of the engineering fit of the hole, as can be seen in figure B.4. The problem with a large fit is that the conductivity of the heater to its environment is heavily reduced. With a large fit, most of the surface of the heater resides in vacuum, which is a bad conductor of heat and therefore the heater can overheat very quickly.

Since the hole was already cut, either two new copper blocks had to be produced or a solution had to be found to increase the thermal conductivity between the heater and the copper block. Finding a way to increase thermal conductivity is the preferred solution as replacing the copper blocks is expensive as the material has to be machined again and the heater holes have to be very precise. Many commercial thermal pastes do not operate at temperatures of up to 400 °C, many having a maximum operating temperature between 120-200 °C. Since a higher temperature of the resistojet equals better performance, it is undesirable to use a thermal paste that limits the maximum temperature at which the resistojet can operate. The maximum temperature that was tested by Versteeg was 400 °C and so the thermal paste should have an operating temperature in that range. Ideally the maximum operating temperature of the thermal paste should be higher than the 400 °C, since the temperature at the heater surface is higher than the average temperature of the copper block. The thermal paste with the highest operating temperature found was Thermal Grizzly Kryonaut designed for use on electronic parts such as CPU heat sinks, with a maximum operating temperature of 350 °C.[44] Using this product would limit the maximum operating temperature slightly but could possibly be used as a last resort. On the other hand there are products geared towards the industrial market like the Thermon T-99 Heat Transfer Compound with a temperature rating of up to 1200 °C.[45] This would be an acceptable solution but since the product only comes in container sizes of 3.79 liter (1 gallon) and the product also hardens when cured which means the heaters are not able to be removed from the thruster, which is not ideal. The choice for the thermal compound eventually fell on copper grease. Copper grease is an anti-seize compound and is most commonly used in the automotive industry. Copper grease is a grease mixed with fine copper particles and is used as an anti-seize compound for e.g. nuts in high temperature conditions. Operating temperatures for copper grease is well over 1000 °C depending on the manufacturer. Copper grease is not usually applied as

a thermal conductor, but given the high amount of copper particles in the compound, the thermal conduction will be greatly increased. The copper grease that was used in this thesis is 'Protecton kopervet' bought at local hardware store Praxis for €9.45, but can be acquired at multiple vendors. It should be noted that although the grease is advertised as having a operating temperature of up to 1150 °C, the grease-like substance inside the compound will still start to liquefy and boil at much lower temperatures. This should be taken into account when applying the grease to the heaters, as in practice it was found that heating the thruster to only 200 °C will already make the grease start to boil.

3.5.1. Heater installation

This section will describe how the copper grease is applied to the heater to make sure that the copper grease fills up the space around the heater and increase the thermal conductivity. Firstly it is important to cover off the nozzle with a piece of tape to prevent the grease from getting in. The copper grease that was acquired came in a pressurized spray can which made it impossible to directly apply to the heater or hole. Simply spraying it inside the copper hole would make the grease fly out of the entry hole since the back of the hole is shut. Instead, the copper grease was first sprayed onto a paper towel, see figure 3.10a. The added benefit of this is that the grease is partially extracted from the compound into the paper towel which increases the relative copper content. Since the grease boils at high temperatures, the generated pressure in the hole behind the thruster can create enough force to move the heater out of its socket. This occurred once after the first time when the copper grease was applied, which is dangerous as the heater will be very hot, and will overheat very rapidly if it isn't noticed on time. Another possibility is that the heater might touch some wiring or other equipment inside the vacuum chamber when its blown out which might cause additional damage. Therefore it is very important to let the grease extract into the paper towel for a couple of minutes to reduce the chance of this happening. Figure 3.10b shows a closeup of what it looks like when the grease is extracted into the paper towel. The copper residue is then scraped off towel with a pair of tweezers and put inside the hole. Because of the extracted grease, the viscosity of the remaining substance is increased and is easier to work with. Make sure to fill the hole with enough copper grease, enough so that when the heater is inserted some of the grease will be forced out. Figure 3.10c shows the holes in the copper block filled with copper grease. The heaters are then slowly inserted into the holes. Slowly pressing the heaters in allows the air in the hole behind the grease to escape in a controlled manner. Some pressure will be felt of the air compressing behind the heater, and might push the heater back out when the heater is released. Keep pushing the heater until it is fully inside and copper grease comes out of the hole. If no copper grease is pushed out, remove the heater and apply more copper grease. Try to move the heaters in a sideways motion to feel if there is any wiggle room inside the hole, if the heater can wiggle around more grease needs to be applied. It is not a problem if the heater can rotate inside the hole. Finally, clean the copper grease that is pushed out and make sure there are no lumps on the side of the thruster. When the thruster heats up, any lumps of grease will start liquefying which might block the nozzle. Figure 3.10d shows the cleaned up heaters inside the thruster. Try to remove as much copper grease as possible before removing the tape over the nozzle.

3.5.2. Temperature control

The power of the heater can be manually set by inputting a desired wattage or voltage in the LabView user interface. In the thesis by Versteeg the thruster is brought to the desired temperature after which the heaters are turned off for the duration of the test. This is acceptable if the tests are short and the thruster does not cool too much by the propellant. However, the energy required to heat up and vaporize water is much larger than nitrogen, and as will be described in 6.3, the duration of the experiments will be 15 minutes. Because of this heaters can't be turned off during the experiments and the the temperature of the thruster will have to be regulated. This can be done by hand by adjusting the input wattage during the course of the test to keep the temperature even, but this requires constant attention and removes focus from the other aspects of the experiment. It was chosen to control the temperature of the chamber by a PID controller like the pendulum control from section 3.2.2. With this modification, it is possible to set a certain target temperature and let the algorithm control the amount of power required. The LabView interface to control the temperature of the thruster can be seen at the top of figure B.3. The temperature control is not designed to heat up the thruster from ambient temperature to the target temperature. The thruster will have to be heated manually by setting a certain power level, and should only be switched to automatic temperature control when the chamber temperature is

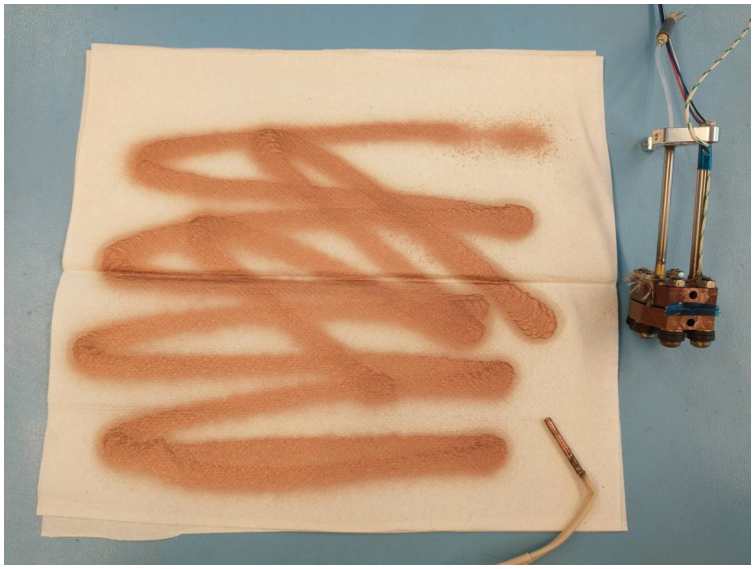

(a) Copper grease sprayed onto a paper towel.

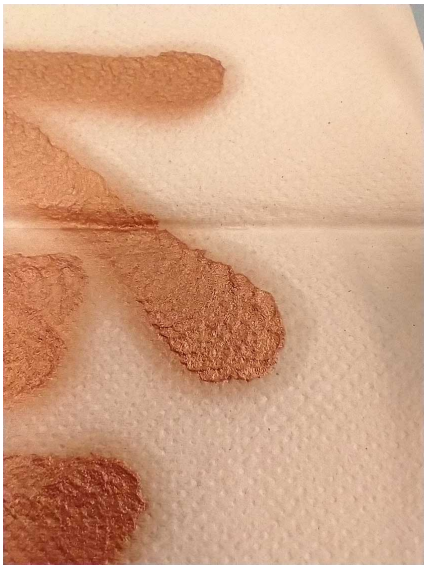

(b) Grease extracted into paper towel.

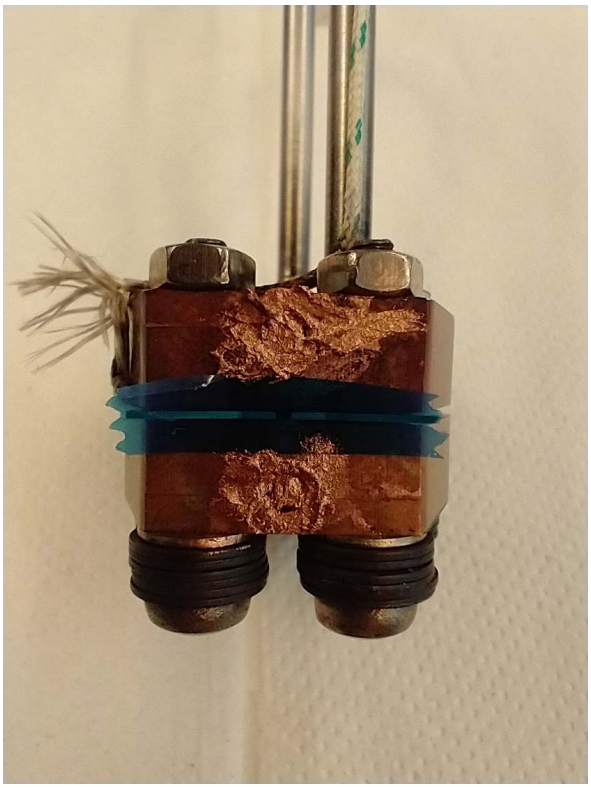

(c) Heater holes filled with copper grease.

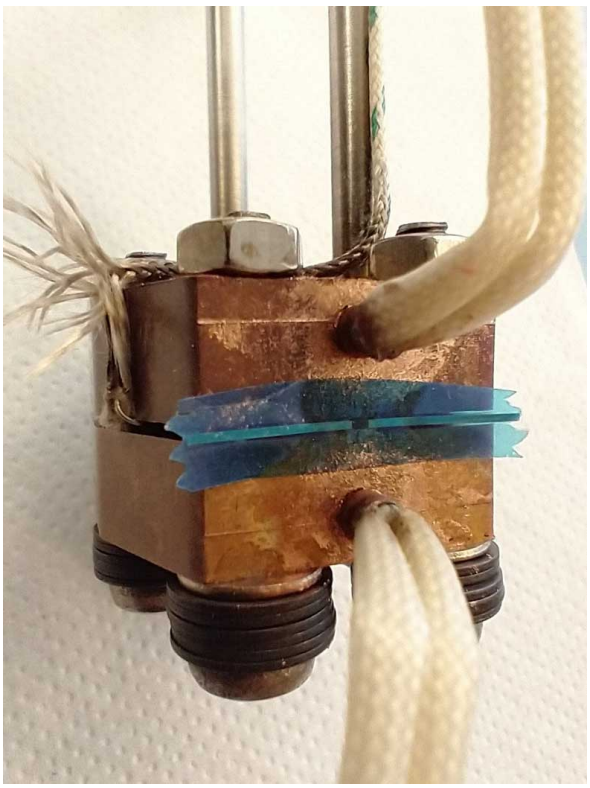

(d) Heaters inserted into copper block.

Figure 3.10: Applying copper grease to the heaters.

close to the target temperature. Since changing temperature is a slow physical process controlling the temperature with a PID controller is difficult. It is difficult to find the optimal parameters, and it might take several minutes before the temperature oscillations stabilizes within an acceptable range. The PID user variables are set to 2, 0.2, and 2 for K_P, K_I, and K_D respectively. These input values could most likely be improved upon, although the temperature responsiveness was found to be acceptable for the performed experiments and so not much time was invested into improving these.

3.6. Parameter confidence bounds

An important part of experimentation involves taking note of the accuracy of the equipment and setup used for measuring. This section will discuss the accuracy of the equipment and setup and summarize these effects on several important parameters used in the modelling and experimentation.

3.6.1. Equipment confidence bounds

This section will summarize the inherent errors of the measurement equipment. This error is the difference between the values recorded by the LabView software and their 'real' values. The errors introduced by the equipment and setup should be added on top of the statistical errors introduced in the data analysis after the experiments are performed. Since the statistical errors of the data analysis depend on the measurement itself, this will not be discussed here.

The power supply used for the actuator coil is the Delta Elektronika SM 7020-D [13]. Since it is used in the calibration of the actuator coil, which error is included in the calibration and formula 3.5, no additional error has to be included based on the actuator current. The mounting angle of the thruster on the pendulum is estimated to be within 2°, which results in an additional $1 - \cos(2°) = 0.06\%$ misalignment error. Since this misalignment error is so small compared to equation 3.5, it can be safely ignored. Since equation 3.5 also includes the lever conversion error, the error of the thrust measurement is fully included in this equation.

The sensor used for measuring the chamber pressure is the TE Connectivity MS5837 30BA01[41]. According to the specification sheet, the absolute accuracy is 50 mbar in the 0 to 45°C temperature range, and 100 mbar in the extended temperature range between -20 to 85°C. Since the signal is digitised inside the sensor, there is no additional analog to digital error that needs to be accounted for. It is important to check the internal temperature of the sensor at every experiment to determine which pressure error that needs to be used. Additionally, the pressure at the sensor is assumed to be equal to the chamber temperature, as the gas inside the pressure tube is stagnant at constant chamber pressure and therefore no pressure loss occurs.

The ambient pressure inside the vacuum chamber is measured with the Vacuubrand VSP 3000[46]. The specification sheet list an error of 15% in the 10 to 10^{-2} mbar pressure range. An measurement accuracy outside this pressure range is not given. Since the vacuum chamber pressures during the experiments are within this range, this is not a cause for concern. The VSP 3000 pressure sensor is a Pirani gauge, which measures the pressure by means of measuring the thermal conductivity of the surrounding gas. Although this allows for very accurate pressure reading at a wide range of pressures, the downside of this sensor is that it is dependent on the gas type to be measured, specifically its molar mass. The pressure sensor is calibrated for air (29 g/mol), and the manual refers to gasses with similar molar mass like O_2 (32 g/mol) and CO (28 g/mol) to be within the listed accuracy. This leads to the assumption that also for N_2, with a molar mass of 28 g/mol to be within this listed accuracy as well. However, the molar mass of water vapor with 18 g/mol can not be considered close to the calibrated molar mass of air, it needs to be checked whether the listed accuracy can be obtained. Switching to a different calibration is not easily done, and no setting on the device can correct for different gas types. Contact was made with Vacuubrand for this matter, in which a representative did not recommend the usage of the VSP 3000 for water vapor and instead recommended the VSK 3000 or a VACUU-SELECT sensor as they are gas type independent. Since the error of the ambient pressure does not have a large impact on the error of the performance indicators in the theoretical model such as I_{sp}, it was chosen to keep using the VSP 3000 and using correction factors and/or large accuracy errors. In conversation with Vacuubrand, correction factors for water vapor in the range of 1-10 mbar were asked for, but were not given. However a graph of gas type dependence of a Pirani gauge from a different manufacturer was found online, and is shown in figure B.5.[23] Since Pirani gauges are a very specific type of pressure gauge, the assumption was made that the gas dependence of the VSP 3000 is similar. The pressure range 4 to 6 mbar of water vapor (which is the range measured during the experiments with water) translate to true ambient pressures of around 3 to 5.5 mbar. Since reading out a graph is inaccurate, and since the pressure gauge is from a different manufacturer, a total error of 50% was assumed to be large enough to accommodate all the unknown uncertainties of measuring water vapor in the mentioned pressure range.

To measure the flow of nitrogen, the Brooks 5850S MFC is used. This mass flow controller can measure the flow of gas up to 2000 sccm (41.68 mg/s). Besides being a mass flow sensor, the device can control an internal orifice to limit the flow rate. The functionality to limit the maximum amount of flow was implemented in the LabView interface as can be seen in figure B.3. However, it was found that the time to reach the desired flow rate was quite significant, up to 15 seconds. Previously the mass flow was set by adjusting the valves in the feed system without limiting the flow by the MFC, and since this settle time is much faster, (≈3 seconds) it was chosen to not use the flow control. Brooks classifies the used 5850S model a legacy product, and therefore no data sheet can be found online as of writing this thesis. The accuracy of the MFC can be found in previous work by Bijster [7]. The accuracy is found to be 0.7% of the measured value, with a minimum of 0.2% of full scale (0.08 mg/s). For liquid (H_2O) testing, the mass flow is not directly measured but instead controlled using a syringe pump. The accuracy of the syringe pump has been determined by a performing a calibration described in section 4.2. From this calibration, the accuracy of 0.45% was found. On top of this in the case of any liquid, the propellant tube is not completely filled when the test starts, which introduces an additional error. In section 6.4.2 it is described how the mass flow is estimated from the chamber pressure. This means that the error of the mass flow is equal to the error of the chamber pressure (σ_{p_c}) plus the additional 0.45% found in the calibration of the syringe pump. The errors of these two sources are assumed to be independent.

For the measurement of the chamber temperature, a type K thermocouple is used that measures the temperature at chamber wall. Type K thermocouples typically have a measurement error of 2.2 K or 0.75%, whichever is greater. At 20 °C, these errors are the the same and so for all measurements the error of 0.75% can be simply taken as no temperatures significantly colder than 20 °C are going to be measured. The NI 9211 DAQ which is used to convert the analog thermocouple signal to a digital signal read by the LabView script introduces another 2.5 °C.[29] An additional 5 °C was taken as error due to temperature variations throughout the thruster, which was also taken into account in the thesis by Versteeg [47]. Assuming these errors are independent, the total error of the chamber temperature comes to

$$3\sigma_{T_c} = \sqrt{(0.75\% \cdot T_c)^2 + 2.5^2 + 5^2} \tag{3.6}$$

which is equals to ≈6-7°C for chamber temperatures of 20 to 300°C respectively. For simplicity, an absolute error of 7°C is taken independent of temperature. At room temperatures where the error is relatively largest this relates to a maximum error of 2.4%.

Lastly the accuracy of the input power is to be discussed. There are two Watlow Firerod heaters placed in the top and bottom copper block of the thruster. These two heaters are powered by two separate power supplies, the Delta Elektronica ES 030-10 and the Delta Elektronica SM-7020. Both the ES 030-10 and SM-7020 list a programming accuracy of 0.2% at constant voltage and 0.5% at constant current.[12, 13] Both power supplies are set to constant voltage, which is dynamically controlled through the LabView script. The previous LabView script included a separate power and voltage control for the heaters. As the voltage control is not as intuitive as power control, and an option to automatically control the chamber temperature was needed, the temperature control replaced the voltage control in the LabView interface, as can be seen in figure B.3. To convert a desired power level to a voltage for the power supply input, the resistance is estimated using a custom resistance estimator made by Versteeg and by using $P = U^2/R$. This resistance estimator filters the voltage and current of the power supply which causes the value of the resistance estimator to lag behind. Therefore the value of the resistance is not up to date and the power level required is only reached after ∼5 seconds. However, the logged data showing the heater power is still accurate up to the given 0.2% since the power is logged by multiplying the power supply voltage and current. In hindsight it is unclear why the current was not used directly to calculate the required voltage using $P = UI$, which would not have this downside. Versteeg mentioned to primarily use the voltage control and the power control to be mainly an experiment.[47] In future work this is an area that could be improved, although it is not believed to have a significant impact, as only large and quick changes in input power show a small temporary difference between the desired and measured heater power. If during an experiment the temperature control is used, the changes of the input power are relatively small enough for an input difference to be noticeable. On top

of this, by far the most important thing is to accurately know the value of the power into the heaters, not the accurately of the desired input power that is maintained.

3.6.2. Propellant properties confidence bounds

Part of calculating the thruster performance relies on the properties of the propellant used. These derived properties like specific heat ratio and speed of sound are derived from the temperature and pressure of the fluid. The library used for this purpose is Coolprop[4]. The library is based on the most accurate formulations in literature, and therefore depends on the type of propellant used. For water, the IAPWS-95 reference is used, which lists various accuracy's based on depending on the type of parameter requested and range from 0.001% to 0.2%.[48] For nitrogen a single source with confidence bounds could not be found, but is assumed to have a similar accuracy. It was decided to ignore the inaccuracy of the propellant properties as they are insignificant compared to the accuracy of the equipment. The values in the mathematical model obtained by CoolProp are therefore assumed as true values with perfect accuracy. Since the input values (the temperature and pressure of the fluid) are however not accurate, the errors of the fluid properties are obtained by also calculating the fluid properties at the extreme pressure and temperature (at $\pm 3\sigma$) and using the maximum differences of these values as the property confidence bounds.

3.6.3. Confidence bounds summary

As a quick reference of the material above, the confidence bounds of the setup equipment are summarized in table 3.4. These errors will be added on top of the statistical errors obtained from data analysis to obtain confidence bounds for the various parameters calculated in the results of the various tests that are performed.

Parameter	3σ error
T_c	7°C
p_c	50/100 mbar
p_a	N_2: 15 % H_2O: 50 %
$\dot{m}$	N_2: 0.7 % (min 0.08 mg/s) H_2O: σ_{p_c} + 0.45%
F_T	1.11 %
I_{act}	0 %
P_{heat}	0.2%
Fluid properties	0% + ($p_c \pm 3\sigma$, $T_c \pm 3\sigma$)

Table 3.4: Accuracy confidence bounds for equipment of test setup

4

Preliminary tests

This chapter describes the tests that have been performed in order to validate and characterize the test setup to be able to apply data correction and calculate the accuracy of future tests. Leak tests of the thrust have been performed and can be found in section 4.1. The syringe pump used for liquid water thrust testing has been calibrated in section 4.2. Section 4.3 describes the removal of a blockade in the nozzle throat which required reassembly of the thruster and redetermining the nozzle dimensions. In section 4.4 the effect of the heater current on the measured thrust is described. The angle of the thrust vector was determined in section 4.5 as it was found to be misaligned in certain circumstances. An overview of the performed tests can finally be found in section 4.6.

4.1. Leak test

One of the biggest challenges when designing a small thruster for high operating temperatures is to engineer a solution with a sufficiently low leak rate. Most solutions such as O-rings or glues fail in the range of 100-300 °C which is not desirable for resistojets since operating temperatures in that range significantly reduces the possible maximum performance. The thruster engineering model by Versteeg does not use a sealing compound but instead clamps polished metal surfaces onto each other to create a seal.[47] The difficulty in this design is that the touching surfaces have to be polished to a high degree and the clamping force has to be spread out evenly over the entire surface. Since copper is a relatively soft metal some leeway is obtained as it is possible for the copper to deform slightly to fill gaps in the sealing surface. When the thruster was first assembled by Versteeg the leak rate was determined to be 0.005%. When the thruster was reassembled at a later stage, the leak rate grew to the order of 1%.[47] For this thesis the leak rate will be determined again. Since halfway through the preliminary tests the nozzle was blocked and the thruster had to be reassembled to remove the blockage, and so the leak test was done before and after the reassembly. The results of which are shown in section 4.1.2.

As can be seen in sections 5.1.4 and 6.2.4, the maximum accuracy of the required mass flow in the analytical model is in the range of 9-10% due to mainly the inaccuracies of the nozzle throat size and the chamber pressure. Therefore it does not make sense to require small leakage rates in the order of 1% or smaller. The maximum allowed leakage is set at 5% as errors higher than this will start to significantly impact the error of the performance parameters, while still allowing some leeway that might be needed since reassembling the thruster is expected to negatively affect the smoothness of the sealing surface and therefore the sealing capability of the thruster.

4.1.1. Methodology and setup

To be able to measure the leak rate of the thruster, the nozzle has to be closed. In the thesis by Versteeg [47] the nozzle was closed off using two pieces of rubber and a clamp. One piece of rubber is placed over the nozzle while the other is placed on the back of the thruster to prevent damage the thruster if it comes in contact with the hard surface of the clamp. The clamp is tightened on the rubber to seal the nozzle shut, see figure 4.1. The leak tests will be performed with nitrogen gas at room temperature. There are two main methods of measuring the leak rate of the thruster. One way is by setting a certain

feed pressure on the feed system and measuring the leak rate directly with the mass flow sensor. The other method is by filling the thruster with a high pressure, closing the propellant valve, and measuring the rate at which the chamber pressure drops.

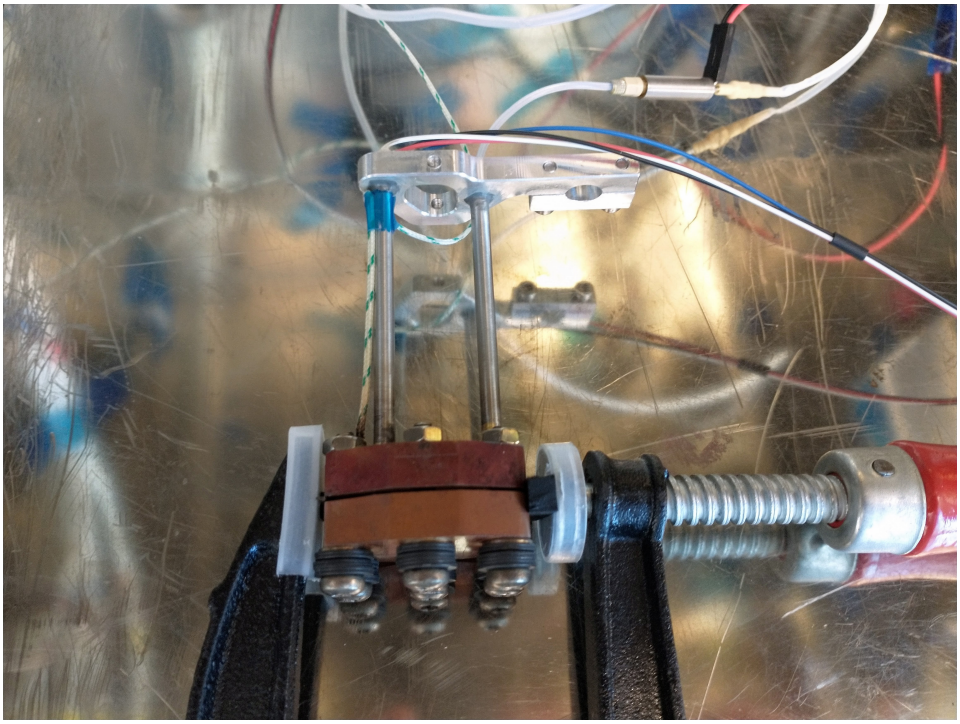

Figure 4.1: Thruster clamped between two rubber pieces to close off the nozzle.

4.1.1.1. Measuring leak rate with mass flow controller

The mass flow sensor used is the Brooks 5850S, which can measure flows of up to 2000 sccm (standard cubic centimeters per minute). This unit is a measurement of cubic centimeters per minute of a gas in standard conditions for temperature and pressure. The standard condition in this case is at 0 °C and 1013.25 hPa, at which a density of nitrogen of 1.2504 kg/m^3 is found.[4] The conversion of sccm to mg/s for nitrogen is therefore 1 sccm = 0.020840 mg/s. The mass flow sensor therefore has a range of up to 41.68 mg/s. From experimentation it was found that the Brooks 5850S mass flow sensor can not accurately measure a mass flow below ~0.5 mg/s, which is roughly equivalent of 1% of full scale (0.42 mg/s). From the manual it is not entirely clear what the minimum flow can be. There is a feature called Low flow cut-off which prevents the valve from opening whenever the set point is less than 1% of full scale. Although the sensor is set in Valve Override mode, which should open the valve fully independent of set point, a click is heard from the mass flow sensor whenever the sensor switches between measuring 0 mg/s and ~0.5 mg/s indicating that there is in fact a valve opening and closing preventing measurements to be made below 0.5 mg/s. Since the mass flow sensor is not accurate enough to measure flows in the range below 0.5 mg/s, the method of measuring the leak rate directly with the mass flow sensor was abandoned.

4.1.1.2. Measuring leak rate using differential pressure method

The second method of determining the leak rate is to measure the rate at which the pressure drops inside the chamber. With the nozzle closed and all valves open, the propellant feed pressure will set the pressure inside the chamber. Some propellant will leak out of the thruster, and thus some propellant will continue to flow from the feed system to the thruster. Closing the propellant valve attached to the thruster will shut off this flow of nitrogen and the pressure inside the chamber will start to drop. One advantage of this method compared to the previous one is that the leak rate can be determined over a continuous range of pressure differences instead of a single set pressure difference between the

chamber and ambient pressure. The leak rate can be determined using the following equation from ideal gas theory assuming constant temperature,

$$q_L = \dot{P}_c V \tag{4.1}$$

$$\dot{m}_L = \frac{\dot{P}_c V M}{RT} = \frac{q_L M}{RT}, \tag{4.2}$$

where q_L is the leak rate, $\dot{m}_L$ is the leaked mass flow, $\dot{P}_c$ is the change in chamber pressure over time, V the volume, M the molar mass of nitrogen gas (28.014 g/mol), R the ideal gas constant and T the temperature of the gas. The volume of gas inside the thruster was estimated by Versteeg to be 2.461 cm^3.[47] It is important to note that this volume is an upper limit of the actual volume inside the thruster and so the calculated leak rate will also be an upper limit of the actual. The temperature and pressure of the gas can be measured with the sensors already present on the thruster.

4.1.1.3. Leak rate conversion for changing gas types and temperatures

The method described above shows how the leak rate for nitrogen at room temperature can be measured. However, since some experiments will take place at elevated temperatures and with different gas types (N_2 & H_2O), it has to be shown how to determine the leak rate in these situations. The leak rate q_L as shown in equation 4.1 is commonly given in the unit mbar·l/sec or atm·cc/sec, which are equivalent. Conversion of leak rate based on gas type uses different formulas based on viscous or molecular flow. According to Amesz [1] and Rottländer et al. [32], leak rates larger than 10^{-4} atm·cc/sec can be considered viscous flow, while leak rates below 10^{-6} atm·cc/sec can be described by molecular flow. Since the leak rates in this instance are in the order of 10^{-1} atm·cc/sec, it is safe to assume that molecular flow can be ignored and only viscous flow conversion can be used. For viscous flow, it is shown in [1, 32] that from the Hagen–Poiseuille law:

$$q_{L,A}\nu_A = q_{L,B}\nu_B \tag{4.3}$$

where subscript A and B denote gas type A and B, and ν it's (dynamic) viscosity. From this equation it is possible to calculate the leak rate of any gas with a different viscosity. This is valid for nitrogen at elevated temperatures, as well as for water vapor. Introducing the product $\mathrm{X}_0 = q_L \cdot \nu$ for nitrogen gas at unheated conditions is a function of the pressure delta and can be used as a reference point to calculate the leak rates of other gas types and can be seen as the viscosity independent leak rate. The dynamic viscosity ν of the gas is a property that can be calculated using Bell et al. [4] given its pressure and temperature. The leaked mass flow rate of any gas can than be calculated using equation 4.2, as:

$$\mathrm{X}_0(\Delta P) = q_{L,N_2} \cdot \nu_{N_2} \qquad (N_2 \text{ at calibration temperature}) \tag{4.4}$$

$$\dot{m}_L(\Delta P, T_c, \nu) = \frac{\mathrm{X}_0(\Delta P) \cdot M}{\nu R T_c} \tag{4.5}$$

4.1.2. Results

This section will describe all the results from the leak test performed before and after reassembly. The reason for measuring the leak rate before reassembly is that it is good to see what the effects of taking the thruster apart are on the quality of the seal. In this section the leak rate is only calculated in terms of leaked mass flow at various pressure differences between the chamber and ambient pressure. The exact leak rate as a percentage of total mass flow during thrust testing is also a function of the throat size and chamber temperature amongst others, and therefore only a rough estimated is made in this section in order to compare the calculated values with the previous work from Versteeg [47]. Since the leak test is only done at room temperature and in ambient pressure, the effects of heating the thruster and vacuum conditions are not known. In this thesis the effects of thruster temperature on the leak rate is assumed to be negligible. It is also assumed that the leak rate is a function of the pressure delta $\Delta P = P_c - P_a$ and not of the absolute values of P_c or P_a themselves.

4.1.2.1. Before reassembly

This section shows the results of the leak test before the thruster was reassembled. Figure 4.2 shows the decrease in pressure over time. The leak rate of this data is calculated with equation 4.2 and

shown in figure 4.3 and tabulated at various pressure differences in table A.1. Since the data from the pressure sensor contains noise, in order to calculate the pressure drop at a certain time, the data in a time window of 1 second around the requested time is fit with a linear function to smooth out sensor noise and to be able to calculate a standard error. When looking at the data it becomes clear that the leak rate of test 1 is close to half of the leak rate of test 2 and 3. The most probable cause for this is that before starting test 2 the clamp holding the rubber in place was put on too tightly which forced the copper away from the sealing surface and thus reducing the sealing capability. The increase in leak rate was present in every subsequent measurement and the sealing capability from the first test could not be restored. It is therefore important for future leak tests to be careful of the force being exerted on the thruster by the clamp. Averaging the results from the second and third test, the average leak rate at a pressure delta of 1 bar is 0.122 mg/s. The first test is not taken into account since the sealing capability from the first test could not be repeated. From initial testing with nitrogen at 20 °C, the amount of mass flow needed to obtain a chamber pressure of 1 bar is around 17.5 mg/s. This means that the leak rate in this situation is roughly 0.70%. This value is around the same value found by Versteeg, and thus the result is deemed acceptable.

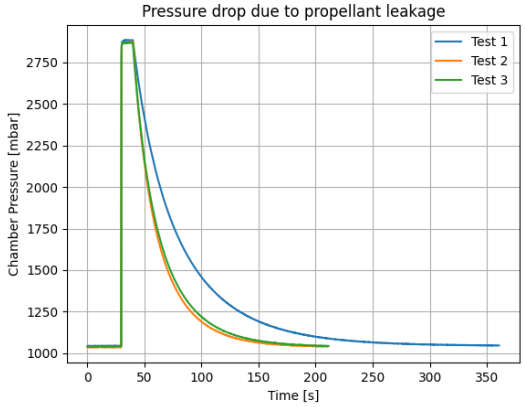

Figure 4.2: Pressure drop due to propellant leakage of the thruster before reassembly.

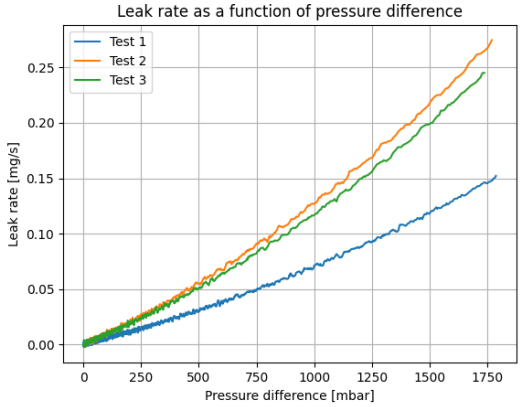

Figure 4.3: Leak rate as a function of the pressure difference between the chamber and ambient pressure before reassembly.

4.1.2.2. After reassembly

After the thruster has been reassembled, the leak test was performed again. Since the copper surface creating the seal is deformed slightly by being clamped on the nozzle cutout, the expectations are that additional gaps will arise when reassembling the thruster because of slight misalignments with respect to its original assembly. The results of this test will therefore determine if the copper needs to be polished again to restore the quality of the seal. The results of the leak test after disassembly are shown in figure 4.4. The leak rate is calculated using equation 4.2 and shown in figure 4.5 and tabulated at various pressure deltas in table A.2. What can be seen in the data is that the leak rate after reassembling the thruster is roughly doubled. At a pressure delta of 1 bar the leak rate averaged over the five tests is 0.240 mg/s, which equates to around 1.4% when assuming a total mass flow of 17.5 mg/s. Although the leak rate has doubled after reassembly, it is still considered acceptable for the purpose of this thesis. For convenience, the leak rate was fitted with a quadratic function that can be used in the data analysis to correct the mass flow for the expected leakage. The result of this fit is shown in figure 4.5 and is given by

$$\dot{m}_{L,N_2} = 5.64 \times 10^{-8} \Delta P^2 + 1.84 \cdot 10^{-4} \Delta P \tag{4.6}$$

with $\dot{m}_{L,N_2}$ the leak rate in mg/s of nitrogen at 20 °C and ΔP the pressure difference in mbar. Based on equation 4.5, leak rate of nitrogen and water vapor at various temperatures is shown in figure 4.6 and tabulated in table A.3. Note that this data is from a theoretical model is only based on the gas viscosity and molar mass, and ignores the effects of thermal expansion of the gaps in the sealing surface at those gas temperatures.

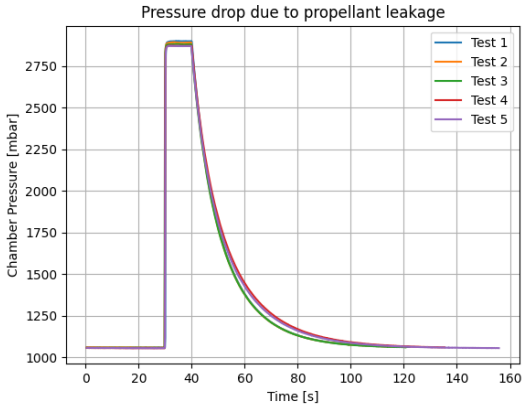

Figure 4.4: Pressure drop due to propellant leakage of the thruster after reassembly.

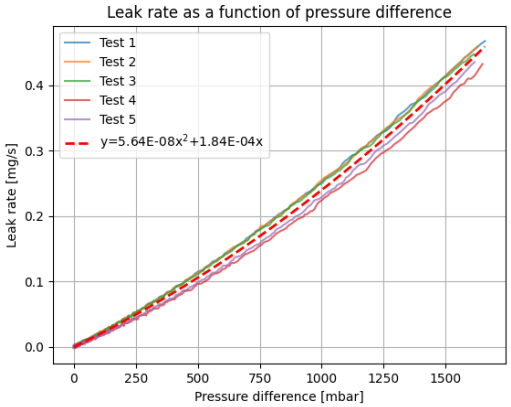

Figure 4.5: Leak rate as a function of the pressure difference between the chamber and ambient pressure after reassembly.

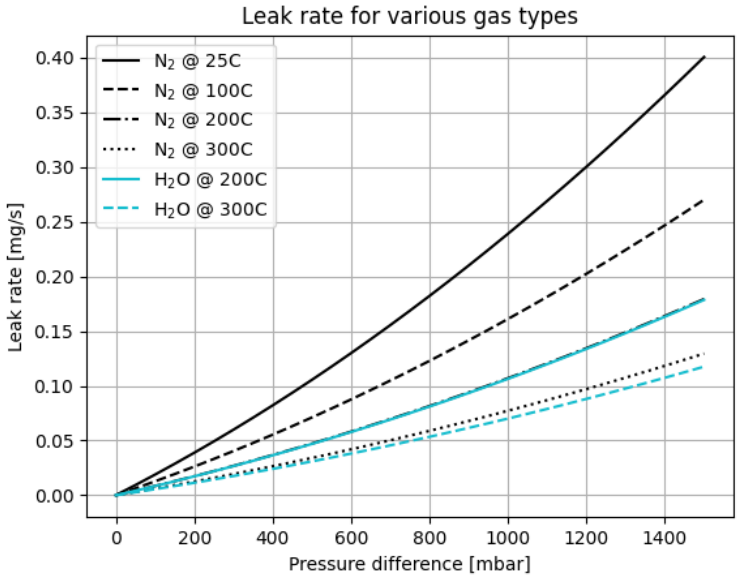

Figure 4.6: Leak rate for water and nitrogen as a function of the pressure difference between the chamber and ambient pressure at various temperatures.

4.1.3. Conclusion

The leak rate of the thruster was determined by sealing the nozzle shut with a piece of rubber and analysing the decrease in chamber pressure over time. The leak rate was determined at room temperature with chamber pressures up to 1500 mbar above ambient. A test was done before and after the thruster was reassembled and show that reassembly has a negative influence on the quality of the seal. The leak rate after reassembling the thruster has doubled compared to the leak rate before disassembly. To restore the quality of the seal the copper side of the sealing surface has to be polished, although in this case it was not necessary as the leak rate after reassembly was deemed to be acceptable for the purpose of this thesis. A theoretical model was made to adjust the leak rate based on the viscosity and molar mass of the gas. This allows the leak rate to be adjusted for the conditions in the experiments where measuring the leak rate is not directly possible due to the high temperatures.

4.2. Syringe pump calibration

As mentioned in section 3.3, a syringe pump will be used to supply a continuous flow of liquid propellant to the thruster. This syringe pump can be seen in figure 4.7. The volume rate dispensed by the syringe pump depends on the internal diameter of the syringe that is used. The syringe used for these experiments is a 10 mL syringe bought at a local retail store Kruidvat, which can be seen mounted on the syringe pump in figure 4.7 and packaged in figure 4.8. The internal diameter of the syringe was measured to be 15.56±0.20 mm, although because the plastic syringe is slightly flexible, a calibration is needed in order to more accurately determine and confirm the mass flow rate of the syringe pump feed system.

Figure 4.7: The ProSense NE-1000X2 syringe pump.[31]

Figure 4.8: Kruidvat 10mL syringe.

4.2.1. Methodology and setup

The syringe pump can be calibrated by measuring the mass dispensed by the pump after a predetermined time with a mass scale. The scale used for this experiment is the Mettler Toledo AG245 Analytical Balance, which displays masses with an accuracy of 0.1 mg and has a maximum capacity of 210 g. A cup is placed onto the scale and filled with a small layer of water. The syringe and propellant tube are filled with water and mounted onto the syringe pump. The end of the propellant tube is then submerged inside the water in the cup on the scale. This can be seen in figure 4.9. The propellant tube should avoid touching the side or bottom of the cup since that will introduce a lot of noise in the measurement of the scale. The end of the propellant tube has to be fully submerged inside the layer of water in the cup as to minimize the effects of surface tension on the measurements. Before starting the tests it is important to check that there are no significant air bubbles inside the tube. Since the time between starting and stopping the syringe pump will be measured with a stopwatch and is not controlled by a computer, the error of the duration of the test is estimated to be 1s. For every test the pumping time was set to be 5 minutes as to reduce the inaccuracies introduced of timing by hand. For the calibration of the syringe pump, the volume flow settings of 10, 20 and 40 mL/hr are tested. Assuming a density of water of 997 kg/m^3 for water at 1 bar and 25 °C[25], a volume flow of 1 mL/hr is equal to a mass flow of 997/3600 = 0.2769 mg/s. For the tested settings of 10, 20 and 40 mL/hr, the average mass flow measured is expected to be 2.769, 5.539 and 11.078 mg/s respectively. Since the accuracy of the expected mass flow is in part based on the syringe diameter set on the syringe pump, which was determined to be 15.56±0.20 mm, the measured mass flow is expected to deviate a maximum of $1 - (1 - \frac{0.20}{15.56})^2$ = 2.55% from the expected value based on the syringe diameter alone. This excludes errors from other origins such as the density of the water used and the accuracy of the syringe pump. The density of water at 1 bar and 18 °C is 0.156% larger than the density of water at 25 °C.[25] If the temperature of the water is assumed to be anywhere

between 18 and 25 °C during testing, an additional error of 0.156% has to be taken into account.

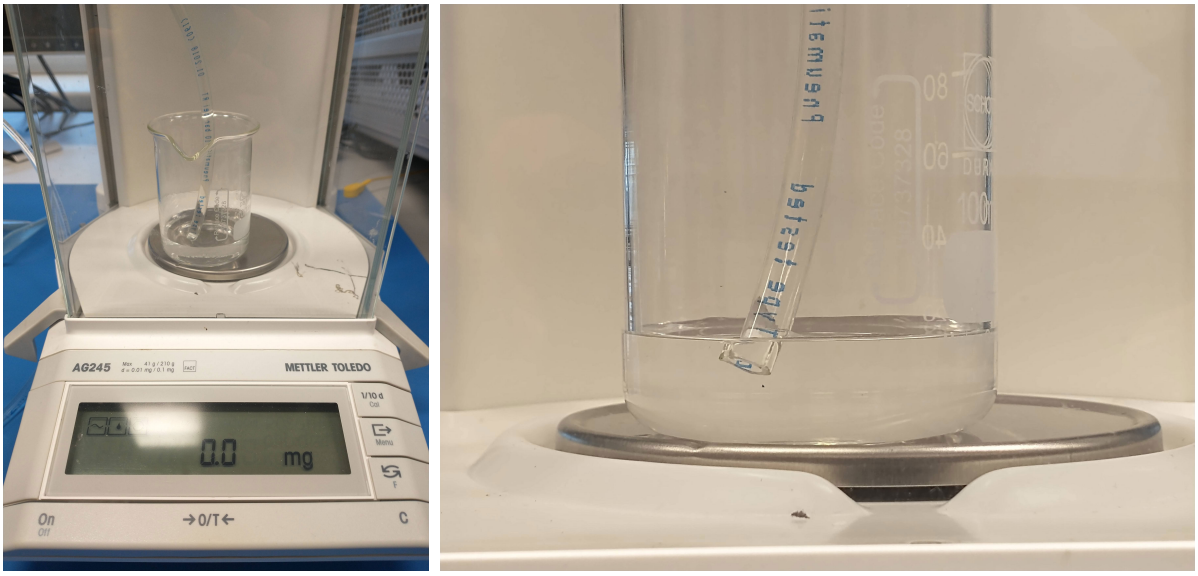

Figure 4.9: Syringe pump calibration setup with the Mettler Toledo AG245 Analytical Balance (left) and a closeup of the submerged tube on the scale (right).

4.2.2. Results

The results of the calibration test is shown in figure 4.10 and the measured data is tabulated in table A.4. A linear regression is done with the python package `scipy.optimize.curve_fit` which resulted in a slope of 0.2808 mg/s with a 3σ confidence interval of 0.00118 mg/s, which deviates 1.40% from the 0.2768 mg/s that was expected, and is within the aforementioned 2.55% maximum deviation. The error of the mass flow based on this calibration is 0.00118/0.2808 = 0.42%. Adding to this the error due to the unknown density of the water, the error of the mass flow dispensed by the syringe pump is found to be within 0.45%.

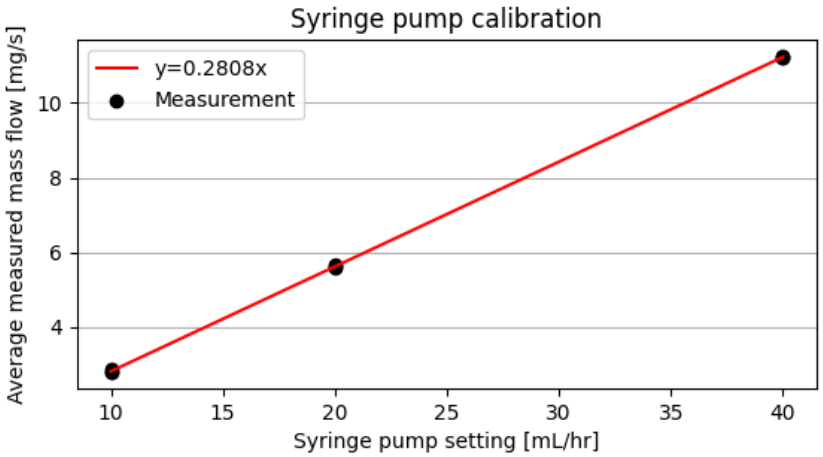

Figure 4.10: Measured mass flow as function of the volume flow setting of the syringe pump.

4.2.3. Conclusion

In this section the calibration of the syringe pump is described. The syringe pump is part of the feed system that provides a constant volume flow of liquid propellant. A 10 mL syringe is used which was bought at retail store Kruidvat. For this syringe, the internal diameter was measured to be 15.56 mm,

which is set as the input parameter of the syringe pump. Using this setup the conversion between dispensed volume $x[mL/hr]$, to the mass flow of water $y[mg/s]$, was found to be:

$$y[mg/s] = 0.2808 \cdot x[mL/hr] \tag{4.7}$$

with an error of 0.45% for the 3σ confidence interval.

4.3. Removing nozzle blockage

During initial testing it was observed that after a certain amount of testing with nitrogen the chamber pressure in relation to the mass flow and chamber temperature changed. It was seen that in tests with nitrogen the ratio of $p_c/\dot{m}$ increased by around 50% at constant chamber temperatures. According to IRT specifically equation 2.11 indicates that the throat area A_t is decreased by roughly a third. The pressure and temperature sensors were verified to still be giving sensible values and therefore not a probable cause of this effect. The only likely explanation that would cause this effect is that the nozzle could be blocked from the inside, therefore reducing the throat area. Attempts to remove the blockage by shaking the thruster and blowing through the thruster in either direction were not successful. Since the blockage in the throat could not be solved with simple methods, the only remaining method was to open the thruster, remove any blocking material, and reassembling the thruster. The downside of doing this is that the sealing capacity of the thruster will most likely be reduced, as later was shown to be the case in section 4.1. The throat and exit area also have to be determined again after reassembly as the nozzle alignment might change slightly.

4.3.1. Disassembling the thruster

The thruster can be opened by unscrewing the six M6 bolts around the copper blocks. The screws were found to be quite stuck and required some force to open up. After unscrewing all six screws and the bottom copper block was removed, it was not possible to locate any debris that was the culprit of blocking the throat. Since the nozzle is only around 0.15 mm wide, it is not remarkable that no piece could be found. There were however a number of small pieces of unknown material scattered in and around the thruster. Potentially all are possible culprits of the blockade, although they mostly came loose while opening the thruster. The source of these remnants could possibly be dust, flaked oxidation of the metals, or even burned oils from the screws or fingers that touched the thruster that gets caught in the small creases of the screws. Overall, the inside of the thruster looked very clean, as can be seen in figure 4.11, although the nozzle profile is discolored.

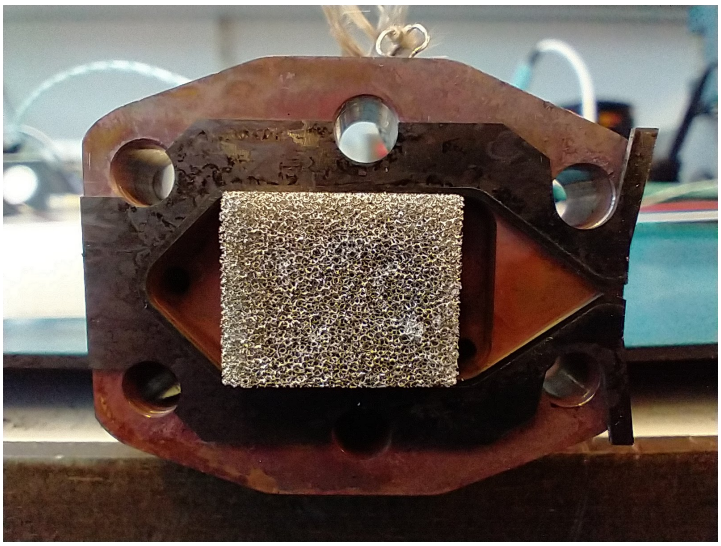

Figure 4.11: Thruster with the bottom copper block removed showing the used nozzle profile.

4.3.2. Reassembling the thruster

After the debris removed that came loose from opening up the thruster, the thruster had to be reassembled again. During the fabrication of the nozzle profiles two different types of profiles were made with one being 0.5 mm thick and one 1 mm thick.[47] The thickness of the nozzle profile determines the height of the nozzle throat and therefore the characteristics of the thruster. Of each type two profiles were cut using the wire EDM process. Therefore instead of reusing the slightly dirty nozzle profile, a new clean nozzle profile could be used. Since there was no direct need to use a larger throat area and to simplify the comparison to the previous results it was chosen to keep the same nozzle profile thickness of 0.5 mm. The thruster is designed to be assembled using two

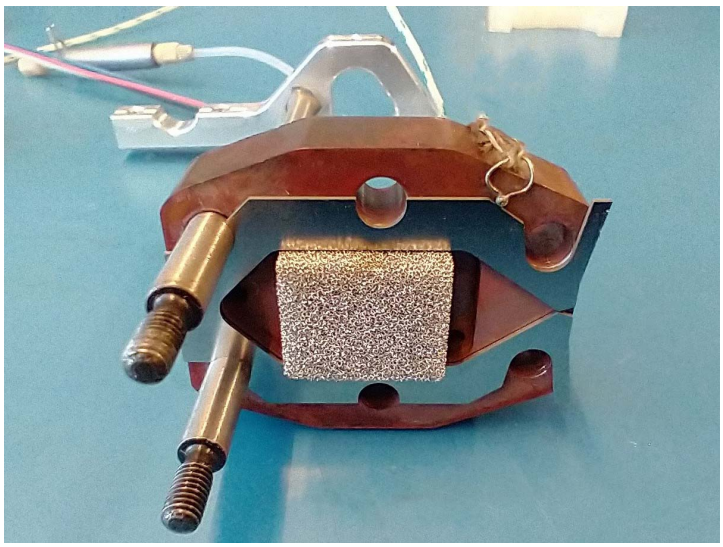

Figure 4.12: Thruster with the bottom copper block removed and the nozzle profile replaced.

shoulder bolts to precisely align the bottom and top copper block to the nozzle profile. Two shoulder bolts were fitted in the back two holes on the opposite side of the nozzle for alignment. Figure 4.12 shows the thruster with the two shoulder bolts fitted and the replaced clean nozzle profile. After that, the bottom copper block and the remaining four regular bolts are fitted to the thruster and tightened until the nozzle profile is firm in place so that the shoulder bolts can be replaced by the regular bolts. This method of assembly is how the thruster was assembled in the first place. However it was found that after tightening the four regular bolts, the shoulder bolts were stuck and could not be removed. Even only tightening the two bolts near the nozzle throat did not provide enough wiggle room for the shoulder bolts to be removed. All bolts including the shoulder bolts were removed and the thruster was reassembled without using the shoulder bolts. Even without using the shoulder bolts, there was not much room for the nozzle profile to move. In the assembly performed by Versteeg, the bolts were fastened with a torque of 1.4 Nm. The bolts were tightened with the FACOM A.402 0.5-2.5 Nm torque wrench up to 1.0 Nm and eventually tightened to 1.6 Nm together with performing the leak test in section 4.1.

4.3.3. Determining the nozzle dimensions

Since fitting a new nozzle profile could alter the nozzle throat and exit dimensions, these will have to be determined again. This section will discuss the various measurements taken to make an estimate on these nozzle dimensions. Before and after disassembly the thruster was inspected with the Keyence VR-5000 microscope, and once more when the thruster was reassembled. The VR-5000 microscope is a 3D optical profiles which allows measurements in 3D of small objects. This makes it possible to measure distances such as nozzle profile dimensions and the nozzle exit of the thruster. It is not possible to determine the throat area directly with the microscope, since the throat is too dark to capture when the thruster is assembled. However the throat area can be determined indirectly by measuring the nozzle profile and nozzle exit area. Figure 4.13 shows the nozzle exit width and height as measured with the VR-5000 of the thruster before and after the reassembly. The accuracy of the dimensions shown in the figure is estimated to be ± 8 µm, depending on where exactly the line or cursor is placed

to measure the dimensions. The nozzle profiles are measured using the same microscope in order

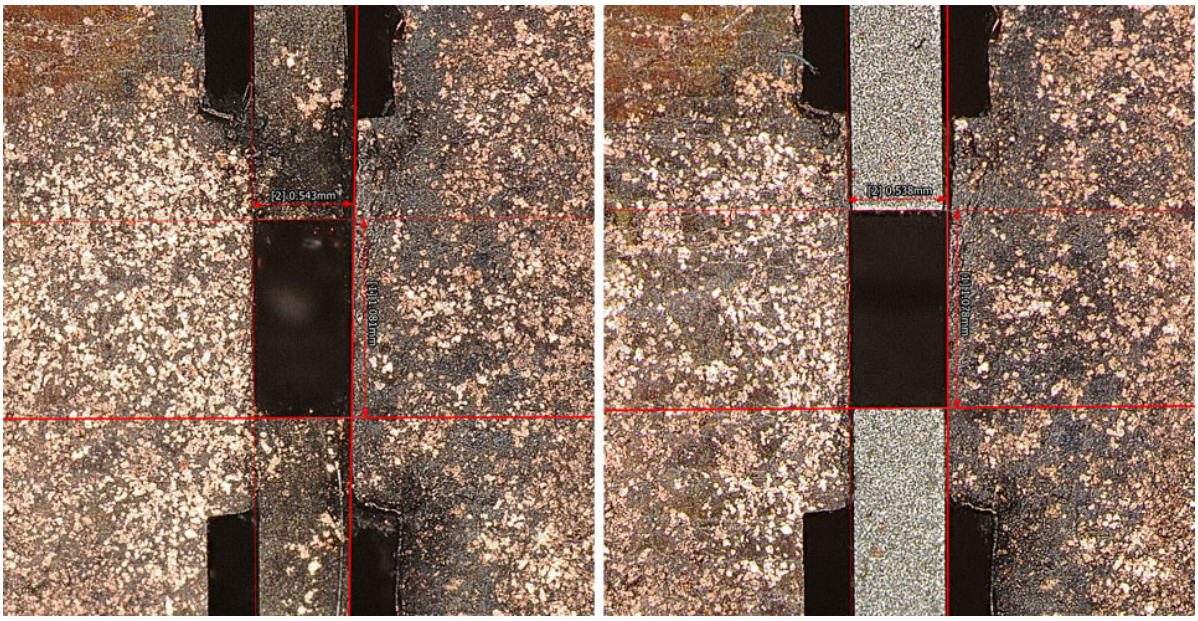

Figure 4.13: Nozzle exit dimensions before (left) and after (right) reassembly.

to relate the size of the nozzle exit to the size of the nozzle throat. Even though the old and new nozzle profiles are supposed to have the exact same dimensions, they are placed under the microscope individually for validation. Figure 4.14 shows the old and new nozzle profiles dimensions of the nozzle exit and throat width. The old nozzle profile shows discoloration and residue on the inner walls of the nozzle which is not present on the new nozzle profile. Also the edges of the new profile are more defined. The accuracy of the dimensions shown in this figure is set to ± 5 µm. From images 4.13 and

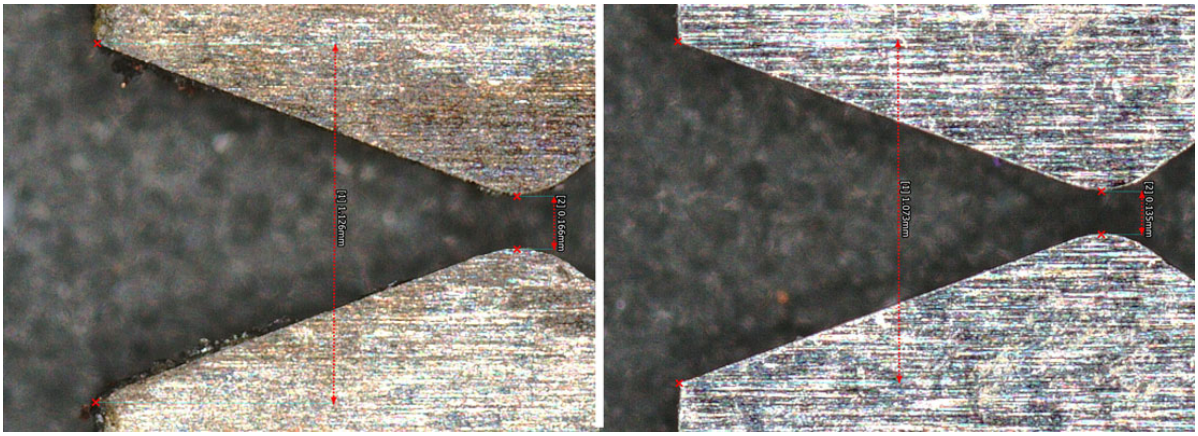

Figure 4.14: Dimensions of the old (left) and new (right) nozzle profiles.

4.14 it is possible to calculate the throat area using the measured width W and height H of the nozzle exit and throat values. The height of the nozzle exit and throat is determined by the thickness of the nozzle profile, and is assumed to be the same for the throat as for the nozzle exit. Since the profile is squeezed into the thruster, the width of the throat and nozzle exit are not necessarily equal to the dimensions measured of the profile when it lies unconstrained under the microscope in figure 4.14. However the difference between the nozzle exit width W_e and the throat width W_t should still be the same when the nozzle walls are squeezed slightly inwards or outwards since the rotation angle of the profile is negligible. This difference, together with the nozzle exit width measured in the assembled thruster from figure 4.13 can be used to calculate the throat width. The results of these measurements

are listed in table 4.1. Nozzle exit and throat area and their area ratio are derived from these nozzle dimensions and are listed in table 4.2.

	Nozzle height	Unconstrained nozzle profile		Assembled nozzle profile	
	H [µm]	W_e [µm]	W_t [µm]	W_e [µm]	W_t [µm]
Old profile	543(8)	1126(5)	166(5)	1081(8)	121(11)
New profile	538(8)	1073(5)	135(5)	1078(8)	140(11)

Table 4.1: Nozzle dimensions of the unconstrained and assembled nozzle profiles.

	Throat area	Exit area	Area ratio
	A_t [mm^2]	A_e [mm^2]	A_e/A_t [–]
Old profile	0.0657(59)	0.587(10)	8.93(81)
New profile	0.0753(59)	0.580(10)	7.70(61)

Table 4.2: Nozzle exit and throat areas and ratio based on microscope measurements.

4.4. Heater current effect on thrust measurement

On the TB-5m test bench, the thrust is measured by controlling the position of a magnet inside a coil that is attached to the pendulum arm. The coil creates a magnetic field which puts a force on the magnet according to

$$F = \nabla(m \cdot B) \tag{4.8}$$

when using the current loop model for the magnetic dipole.[10] Here, F is the force on the magnet, m is the magnetic moment of the dipole pointing from the south to the north pole of the magnet, and B is the magnetic field in which the magnet resides. This equation shows that the force on the magnet is zero inside a uniform magnetic field. In this test setup a VTDC is used to create a constant magnetic field gradient, which therefore creates a force that is linear with the current through the coil.[7] The measured thrust is calculated directly using this coil current, which is explained in more detail in section 3.2.1. However, the magnetic field from the VTDC is not the only magnetic field acting on the magnet. The resistojet is brought up to temperature by two electric heaters. The current through the heaters and wiring create a magnetic field that will in turn put an additional force on the magnet. The magnetic field caused by a current is calculated through the Biot-Savart law:

$$B(r) = \frac{\mu_0}{4\pi} \int_C \frac{I d\ell \times r'}{|r'|^3} \tag{4.9}$$

with μ_0 the permeability of free space, I the current through the wire, ℓ is a point on path C, $r' = r - \ell$ the vector from ℓ to r, and r a position in 3D space at which the field is being computed. Since there is no parallel circuit inside the heater or wiring, the current I is constant over the whole path C and can be taken outside of the integral. This also counts for the gradient of the magnetic field, which relates to the force on the magnet as seen in equation 4.8. The current through the wire relates therefore linearly with the force exerted on the magnet. Since there are two wires connected to the individual heaters with opposite current, most of the the magnetic field generated by the wires are cancelled out. This is because the wires are in close proximity to each other when building the setup. The best way to ensure the magnetic field is cancelled out is by revolving the wires tightly around each other, however this was not done during the experiments since this was not realised when the experiments took place.

In the experiments performed by Versteeg, the heaters were turned off while measuring the thrust to avoid any influence of the heaters.[47] This is possible if the duration of the test is short and the propellant does not reduce the heat of the copper block, and therefore the chamber temperature by a significant amount. For nitrogen, the amount of power needed to increase the temperature from 20 to

300 °C at 1 bar at a mass flow rate of 10 mg/s is 2.94 W, while for water this is 29.9 W.[4] Given that the mass of the copper block is 0.149 kg[47] and copper has a specific heat capacity of 415 J/(kg·K) at 300 °C[25], the heat capacity of the copper block is 61.9 J/K. Assuming the temperature of the copper is uniform throughout the volume, the decrease in temperature of the block from heating up the propellant to 300 °C is therefore 0.0475 K/s for nitrogen and 0.483 K/s for water. As can be read in chapter 6, it is especially the water thrust tests that require long duration testing of at least 5 minutes for accurate measurements. Because of the long thrust duration, the heaters have to be turned on to keep the chamber temperature at the target temperature. The effects of the heater current on the thrust measurements therefore have to be analysed so that its effects can be corrected for.

4.4.1. Methodology and setup

To measure the effects of the heater current on the thrust measurements, the difference in setpoint current of the pendulum is measured at various heater currents without allowing flow of propellant through the thruster. As the thruster does not actually produce thrust since there is no flow of propellant, there are still multiple sources that can cause a change in setpoint current besides the effects of the heater current on the setup. Due to the heater being turned on, the increase in temperature will expand the metals of the thruster and setup meaning the equilibrium position of the pendulum will change. This means that the force required to keep the pendulum at a given setpoint will change which results in a change in the thrust that is measured. The temperature effects on the measured thrust was noticed in the experiments by Versteeg and also play a significant part in the experiments done in chapter 5 and 6. To minimize the effects of the changing temperature in this experiment, the time at which the heaters are turned on should be kept to a minimum. The test procedure for this experiment is divided into three parts,

1. Prepare test setup
2. Environment setup
3. Perform measurement
4. Experiment shutdown

which are described in more detail in the following sections.

4.4.1.1. Prepare test setup

This phase of the procedure entails all the steps needed to ensure the thruster is mounted on the test bench and all sensors and equipment are working as expected. This procedure is described step by step in section 5.2.1. Note that since the experiments will be performed without propellant, all steps involving the mass flow sensor or feed system should be skipped.

4.4.1.2. Environment setup

This section describes only the steps to turn on the vacuum chamber, as this is the only requirement for the conditions in which to perform the experiment. These procedures require the completion of the procedures listed in section 4.4.1.1.

1. Turn on the vacuum chamber:
   (a) Specify a folder and test name and click run to start the LabView program.
   (b) Make sure the heating power is set to 0 Watt and the temperature control setpoint to 0 °C.
   (c) Make sure the vacuum chamber door is properly closed.
   (d) Turn the handle on the vacuum chamber such that the connection to the vacuum pump is open.
   (e) Rotate the black knob on the vacuum chamber such that the vacuum chamber is closed off from the outside air.
   (f) Turn on the vacuum pump and make sure the pressure sensors in the LabView program show that the pressure is decreasing.
   (g) Wait for the vacuum chamber to have reached a pressure of 5 mbar or lower.
   (h) Stop recording using the **STOP TEST** button.
   (i) Press the **Abort Execution** button to stop the LabView program

4.4.1.3. Perform measurement

This section describes the procedures to follow to perform the measurements. The procedures described in this section require the completion of the procedures in section 4.4.1.2. This experiment requires the user to quickly turn both heaters on/off simultaneously. Manually setting the individual heater power is too slow. It is advised that the user sets the temperature control to 0°C and switch to temperature control when the heaters are supposed to be turned off. While the heaters are turned off, the power of the individual heaters can be set at the correct level. This will not change the heater power as the heaters are determined by the temperature control. When the heaters need to be turned on, switch from temperature control to power control by clocking on the corresponding button in the LabView program. Afterwards, the heater power can be turned off instantly again by switching back to temperature control.

By powering the heaters the thruster will warm up which will also have a slight influence on the measurement of the thrust due to thermal expansion of the thruster, thruster mounting, and test bench. The heaters can't be removed from the thruster to avoid thermal expansion, as this setup would not be equal to a setup where thrust is produced. To minimize the effects of thermal expansion, the duration of heating is kept short, and was set to 20 seconds. In order to allow the thruster to cool down as the heater power increased, the duration between periods of heating was also increased. The steps to perform the measurement are as follows:

1. Perform ambient thrust measurements
   (a) Read the actions to undertake in the test from table 4.3.
   (b) Specify a folder and test name and click run to start recording data.
   (c) Follow the actions from table 4.3.
   (d) Stop recording using the **STOP TEST** button.
   (e) Press the **Abort Execution** button to stop the LabView program

Time	Actions
0:00	Start recording
1:00	Turn on the actuator coil PID control
2:00	Turn on heaters at 5 Watt each (10 Watt total)
2:20	Turn off both heaters
4:00	Turn on heaters at 10 Watt each (20 Watt total)
4:20	Turn off both heaters
7:00	Turn on heaters at 15 Watt each (30 Watt total)
7:20	Turn off both heaters
10:00	Turn on heaters at 20 Watt each (40 Watt total)
10:20	Turn off both heaters
14:00	Turn on heaters at 25 Watt each (50 Watt total)
14:20	Turn off both heaters
19:00	Turn off the actuator coil PID control
20:00	Stop recording

Table 4.3: Actions to undertake to measure the effect of heater current on the thrust measurement.

4.4.1.4. Experiment shutdown

After the experiment is finished, there are several steps that need to be taken to make sure the experiment is safely shutdown. The thruster can be hot and the vacuum chamber is under low pressure. The following steps should be taken in order to safely shutdown the experiment without damaging the equipment.

1. Turning off power:

(a) Specify a folder and test name and click run to start the LabView program.

(b) Make sure the heating power is set to 0 Watt and the temperature control setpoint to 0 °C. Note that the temperature of the thruster is dropping.

(c) Make sure the actuator coil PID control is off.

(d) Stop the LabView program.

2. Stop the vacuum pump:

(a) Turn the handle on the vacuum chamber such that the connection to the vacuum pump is closed.

(b) Turn off the vacuum pump. Some air will go through the vacuum pump in the opposite direction to fill the tube leading to the vacuum chamber (where the tube is shut off). If air is moving through the pump in the opposite direction for more than 3 seconds, which can be noted by the sound of the pump being forcibly rotated by the outside pressure, quickly turn the pump back on and verify the vacuum chamber is properly shut off from the pump and try again. Air moving in the opposite direction than what the pump is designed for can damage the pump.

(c) DON'T TURN THE VACUUM CHAMBER VENT VALVE! Keep the vacuum chamber under low pressure as long as the thruster is still hot to prevent oxidation of the thruster.

3. Turn off the equipment:

(a) Turn off the SM-7020, SM-7020-D, ES-030-10, E-030-1 and D-030-1 power supplies.

(b) Unplug the Micro-Epsilon DT6220/DL6230 distance sensor DAQ.

4. Release the vacuum of the vacuum chamber:

(a) Wait for the temperature of the thruster to be below 40 °C so it can be safely touched. Check the temperature by starting the LabView program.

(b) Release the vacuum of the vacuum chamber by rotating the vent valve.

5. Dismantle the thrust bench:

(a) Open the vacuum chamber door.

(b) Disconnect the heaters and actuator coil from the power supply inside the vacuum chamber.

(c) Disconnect the temperature sensors from the DAQ.

(d) Disconnect the propellant Swagelok Quick Connect inside the vacuum chamber.

(e) Disconnect the distance sensor inside the vacuum chamber.

(f) Disconnect the p-T sensor.

(g) Carefully take out the test bench from the vacuum chamber making sure no wires are still connected. Note that the test bench is heavy.

(h) Place the vacuum chamber outside the vacuum chamber and close the vacuum chamber door.

(i) Dismantle the thruster from the test bench.

4.4.2. Results

The experiment was repeated three times. As an example, the results of the second test are shown in figure 4.15. The black and blue line show the measured thrust during the experiment. It is important to note that no actual thrust is produced during this experiment. The thrust that is shown is merely the actuator current to keep the pendulum at a certain setpoint, converted in terms of a thrust by the calibration factor and the lever conversion factor as seen in equation 3.5. The magnitude of the measured thrust therefore has no meaning and depends on the chosen setpoint in relation to the equilibrium point of the pendulum. Instead the change in thrust is the property of interest. Although it is not easily apparent from the raw data shown in black, the filtered thrust shown in blue does clearly

show a small decrease in measured thrust during periods when the heaters are turned on. Furthermore, figure 4.15 suggests that an increase in heater power also increases the magnitude of this effect. Signal drift in measured thrust is visible when comparing the measured thrust just before and after periods where the heater is turned on. And lastly a signal drift is visible over the entire duration of the experiment. Figure 4.16 shows a closeup of the effect of heater current on the

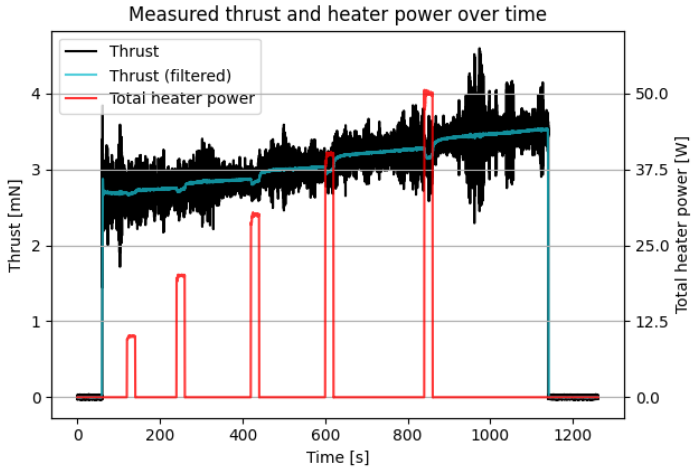

Figure 4.15: Measured thrust and power during the experiment.

measured thrust, in this instance 40W of heater power is applied. Figure 4.16a shows a clear dip in measured thrust and figure 4.16b shows the lines used to calculate the value of the change in measured thrust. The green, red and yellow lines in graph 4.16b show the baseline that represents the expected thrust measured without the effect of the heater current. Note that the baseline is relatively constant before, increases during, and slowly increases after the heater is turned on. This change in the measured thrust baseline is due to the heater heating up the thruster and therefore changing the equilibrium position of the pendulum. The baseline is an attempt to correct for this effect in order to calculate the different thrust measured due to the heater current. The baseline is constructed by linear regression on the 15 seconds before the heater is turned on and linear regression on the 5 to 20 seconds after the heater is turned on. These two linear fits are shown in green. The reason to skip the first 5 seconds after the heater is turned off is to give the pendulum control time to to stabilize. The yellow line is a extension of the latter linear regression to connect to the point where the heater is turned off. The red line connects the baseline in the range where the heater is turned on between the first green and yellow line. To calculate the value of the change in measured thrust, the baseline is subtracted from the measured thrust values. The average value of this difference is taken to be the average offset from the baseline shown in pink. The period where the offset is calculated is between 5 seconds after the heater is turned on, and 1 second before the heater is turned off. To filter the noise out of the signal and calculate the uncertainty of the value, the signal is filtered with a Savitzky–Golay filter with a filter window of 2 seconds as also performed in section 4.5.2. From this filtered signal and the subtraction from the baseline, the standard deviation is calculated which is used to calculate the 3σ uncertainty shown in orange in figure 4.16b. The results of all three experiments are shown in figure 4.17 in terms of both the total heater current and total heater power. The total heater current and total heater power are defined as the sum of the current and power of the two individual heaters respectively. As the fitted line has to go through the origin, the change in thrust in terms of heater current does not seem to be linear as expected. Instead the results show a quadratic relation between the heater current and change in measured thrust. The relation between the change in measured thrust and heater power however does seem to be linear. Since the resistance of both heaters deviates less than 1% during the course of the experiment, it is expected that the power is linear with the change in thrust (given that the current is quadratic) due to $P = I^2R$. Indeed this is appears to be the case looking at the results from figure 4.17. The cause of the unexpected relation between the heater current and the change in thrust is currently not known,

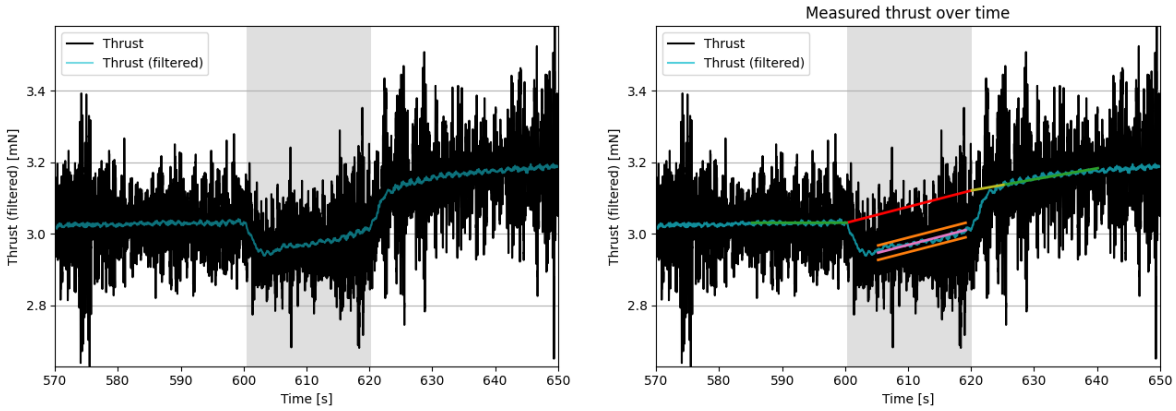

(a) Temporary dip in measured thrust when heater power is on.

(b) Analysis of the measured thrust showing the assumed baseline (green, red, yellow), average change from baseline (pink) and the uncertainty (orange, 3σ).

Figure 4.16: Change in measured thrust due to 40W of total heater power in the gray zone.

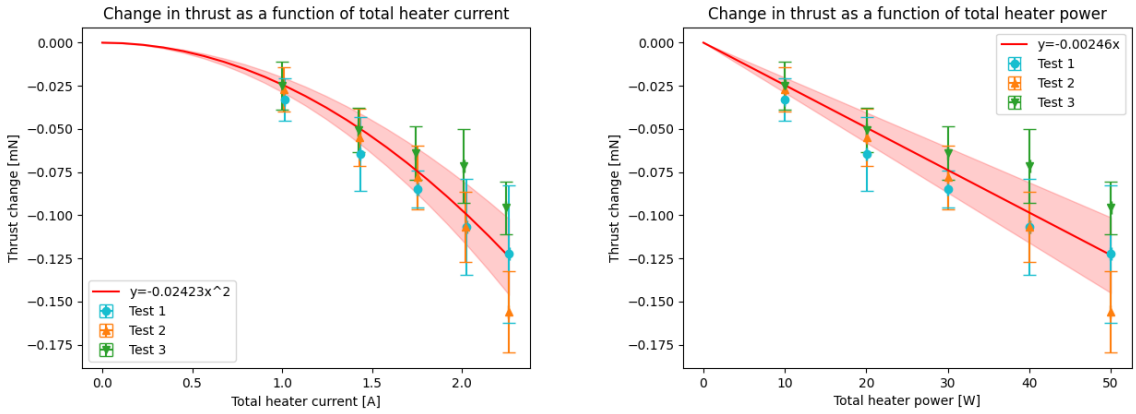

Figure 4.17: Change in measured thrust as a function of total heater current (left) and power (right). Marked surface shows the 3σ uncertainty of the fit.

even after consultation with multiple peers. Although the lack of proper explanation of the effect is unsatisfying, the most important part of the obtained result is that the effect of heater current can and should be corrected for.

4.4.3. Conclusion

Since the measurement of the thrust relies on controlling a magnet inside a magnetic field, any external magnetic fields, such as the one produced by the electric current of the heaters, can have an influence on the signal. An experiment was conducted to measure the influence of this heater current on the measured thrust. Using equation 4.9 and 4.8, it was expected that the heater current behalves linearly with a change in measured thrust. However, figure 4.17 shows the relation between the current and the change in measured thrust behaves quadratically. Therefore effect of the aforementioned hypothesis is found to be either incomplete or incorrect. However, from the results it is clear that the heater current has a measurable effect on the measured thrust which can still be corrected for.

4.5. Thrust vector determination

It was noted that when operating the thruster at room temperatures in atmospheric pressure that the exhaust plume of the thruster was not pointing out of the thruster at the expected angle. By holding a hand behind the thruster it was found that the horizontal angle at which the exhaust plume left the

thruster favored one specific side and was significant. This behaviour was unexpected and raised questions on whether this effect would also occur in vacuum. One possible reason for the misaligned thrust is that the thrust is subsonic the flow separates with a certain preference on one of the sides of the nozzle wall. This preference to one side could be caused by a small difference in geometry or surface roughness between the two sides. The misalignment of the thrust vector can negatively affect the measured thrust, as only the thrust in one dimension can be measured. If this situation would occur on a satellite in space it could potentially make the thruster become unusable as it would induce a torque on the satellite. This section describes the tests that were performed to find out the horizontal angle of the thrust in atmospheric (subsonic) and near vacuum conditions to find out the cause and if this thrust vector misalignment is of concern for operations in (near) vacuum conditions.

4.5.1. Methodology and setup

The thruster is mounted on the pendulum by clamping a piece of metal around the circular rod of the pendulum. This way, it is possible to mount the thruster at different horizontal angles. By measuring the thrust at different mounting angles, it is possible to measure the horizontal angle of the thrust vector. In the thesis by Versteeg, the alignment of the thruster is done by eye where the maximum misalignment is estimated to be 2°. This however is only possible to do by eye when the mounting angle is 0°, and this angle needs to be measured when the thruster is mounted at different angles. Measuring the mounting angle of the thruster is made difficult because of the small components, and the test bench and cables that get in the way. The thruster mounting clamp that mounts the thruster onto the pendulum arm was found to also be able to hold a small plastic stick that would point in the opposite direction to the thruster with respect to the pendulum arm. Using this plastic stick, it is possible to measure the mounting angle with a geo triangle. Figure 4.18 shows the method used to measure the mounting angle. The maximum error of the horizontal mounting angle using this method was estimated to be 2°. Since the plastic stick moves with the pendulum arm, it is important to check whether it is not in contact with any cables when the pendulum moves as that would interfere with the thrust measurements made. The maximum angle that the thruster can be mounted on the pendulum arm was found to be around ±30°, and so the decision was made to measure the thrust at angles of -30°, -15°, 0°, +15° and +30°. In this case, a positive angle is defined as a counterclockwise rotation as viewed from above. The test procedure for this experiment is separated into the following three different phases which are described in more detail in the following sections:

1. Prepare test setup
2. Perform measurement
3. Experiment shutdown

4.5.1.1. Prepare test setup

This phase of the procedure entails all the steps needed to ensure the thruster is mounted on the test bench and all sensors and equipment are working as expected. This procedure is described step by step in section 5.2.1. Note that since the experiments will be performed unheated, the steps involving the heaters should be skipped.

4.5.1.2. Perform measurement

This section describes the procedures to follow to perform the measurements. The procedures described in this section require the completion of the procedures in section 4.5.1.1. The following steps are the procedures for measuring the thrust at a single mounting angle. Therefore, all following steps need to be repeated for all the desired mounting angles.

1. Prepare for thrust measurement
   (a) Mount the thruster to the desired angle.
   (b) Specify a folder and test name and click run to start receiving signals from the sensors.
   (c) Set the pendulum equilibrium position with the counterweights such that it sits anywhere between 500 and 1000 µm.
   (d) Close the door of the vacuum chamber.

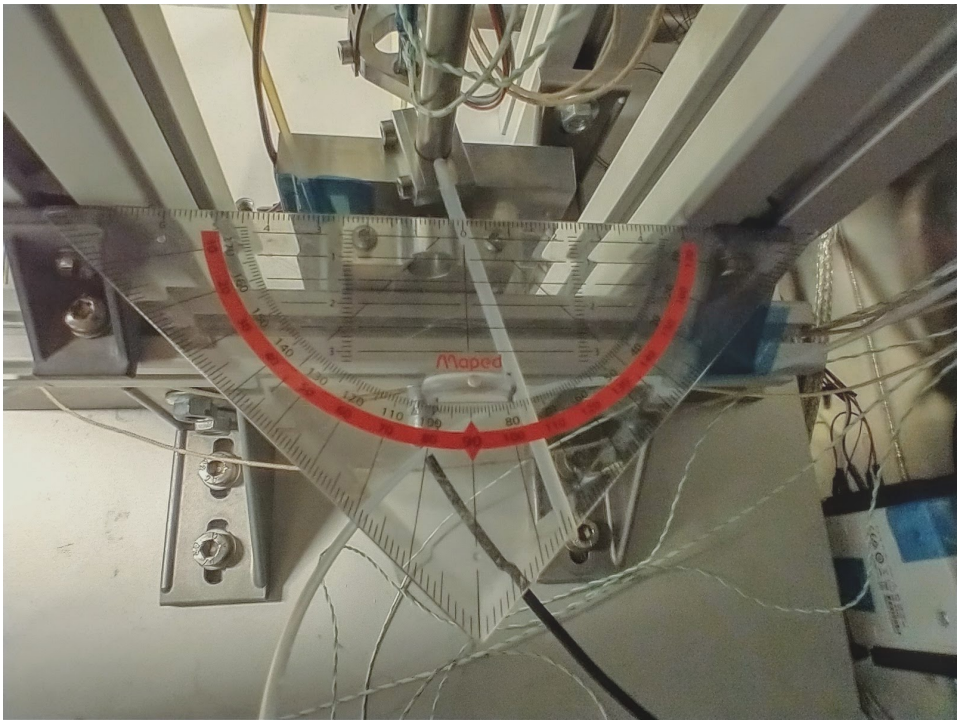

Figure 4.18: Method to measure the mounting angle of the thruster on the pendulum.

(e) Set the setpoint of the pendulum distance to around 75 µm above the pendulum equilibrium and turn on the PID of the actuator coil. Verify that the pendulum is brought to the given setpoint. The current through the actuator coil should be 2±0.5A. Adjust the setpoint distance if the current is not in this range. Turn the PID of the actuator coil off.

(f) Open the propellant valve for a few seconds until the chamber pressure stabilizes and read the chamber pressure. Close the valve immediately after.

(g) Adjust the pressure regulator valve on the nitrogen feed system to target a chamber pressure of 1500 mbar.

(h) Repeat steps 1f and 1g until a chamber pressure of 1500±10 mbar is reached.

(i) Stop the LabView program.

2. Perform ambient thrust measurements

(a) Read the actions to undertake in the test from table 4.4.

(b) Specify a folder and test name and click run to start recording data.

(c) Follow the actions from table 4.4 and make sure the recording is stopped at the end of the test.

(d) Repeat steps 2b and 2c once more so that the measurement is performed twice.

3. Prepare for vacuum measurement

(a) Open the vacuum pump valve on the vacuum chamber (see figure 3.8) by rotating the handle to the vertical position.

(b) Close the vacuum chamber vent valve.

(c) Specify a folder and test name and click run to start receiving signals from the sensors.

(d) Turn on the vacuum pump and wait until the pressure in the vacuum chamber is below 5 mbar.

(e) Since the vacuum chamber pressure affects the thruster chamber pressure, repeat steps 1f and 1g again until a chamber pressure of 1500±10 mbar is reached.

(f) Opening the propellant valve will have increased the vacuum chamber pressure. Wait until the vacuum chamber pressure is below 5 mbar.

(g) Stop the LabView program.

4. Perform vacuum thrust measurements

   (a) Read the actions to undertake in the test from table 4.4.

   (b) Specify a folder and test name and click run to start recording data.

   (c) Follow the actions from table 4.4 and make sure the recording is stopped at the end of the test.

   (d) Repeat steps 4b and 4c once more so that the measurement is performed twice.

5. Venting the vacuum chamber

   (a) Close the vacuum pump valve on the vacuum chamber (see figure 3.8) by rotating the handle to the horizontal position.

   (b) Turn off the vacuum pump.

   (c) Open the vacuum chamber vent valve.

   (d) Wait for the pressure in the vacuum chamber to reach atmospheric pressure.

Time	Actions
0:00	Start recording
0:10	Turn on the actuator coil PID control
0:40	Open the propellant valve
1:10	Close the propellant valve
1:40	Turn off the actuator coil PID control
1:50	Stop recording

Table 4.4: Actions to undertake during the nitrogen thrust measurement for thrust vector determination.

4.5.1.3. Experiment shutdown

After the experiment is finished, there are several steps that need to be taken to make sure the experiment is safely shutdown. However since the thruster is unheated and the vacuum chamber is already vented, the steps to shutdown the experiment are minimal. The steps taken to stop and dismantle the experiment are listed below.

1. Depressurize the nitrogen feed system:

   (a) Close the high pressure shut-off valve.

   (b) Close the pressure regulator valve.

   (c) Open one of the unconnected selection valves to release the pressure inside the feed system. Note that the low pressure gauge drops to zero.

   (d) Close the low pressure shut-off valve.

   (e) Close all selection valves.

2. Turn off the equipment:

   (a) Turn off the SM-7020, SM-7020-D, ES-030-10, E-030-1 and D-030-1 power supplies.

   (b) Unplug the Brooks 5850S 2000sccm mass flow sensor.

   (c) Unplug the Micro-Epsilon DT6220/DL6230 distance sensor DAQ.

3. Dismantle the thrust bench:

(a) Open the vacuum chamber door.

(b) Disconnect the heaters and actuator coil from the power supply inside the vacuum chamber.

(c) Disconnect the temperature sensors from the DAQ.

(d) Disconnect the propellant Swagelok Quick Connect inside the vacuum chamber.

(e) Disconnect the distance sensor inside the vacuum chamber.

(f) Disconnect the p-T sensor.

(g) Carefully take out the test bench from the vacuum chamber making sure no wires are still connected. Note that the test bench is heavy.

(h) Place the vacuum chamber outside the vacuum chamber and close the vacuum chamber door.

(i) Dismantle the thruster from the test bench.

4.5.2. Results

This section consists of two parts. The first part will describe the results and how the analysis is performed on a single test and the second part will describe how the results of the individual tests are combined to calculate the horizontal angle of the thrust vector.

4.5.2.1. Single test analysis

This section describes the analysis that is performed on a single test. As mentioned before, the thrust is measured at angles -30°, -15°, 0°, +15° and +30° in both ambient pressure and vacuum. On top of that, all these tests are performed twice so that the total number of tests is equal to 20. The test that will be analysed in this section is the situation of a mounting angle of 15° in (near) vacuum conditions. The reason for singling out this test in particular is that all the features that will be described in the analysis can be clearly visualised in graphs for this particular test. However, all methods that are being used in this section will be applied in the exact same way for every test.

Figure 4.19 shows the raw data of the operating conditions, namely the chamber pressure, the ambient pressure (vacuum chamber pressure), mass flow and chamber temperature. From the chamber pressure and especially the mass flow, it can be seen that the thruster needs some time for the conditions to stabilize. In this example, the chamber pressure needs around 3-5 seconds before a stable pressure is reached, and the mass flow converges to a constant constant number in a time span of 10±5 seconds. Because of this, all values from the measurement in the first half of the thrust period (40 to 55 seconds) are not taken into account for the analysis. The ambient pressure from figure 4.19c shows a decreasing pressure in the first 40 seconds, increasing pressure between 40 to 70 seconds, and decreasing pressure again from 70 seconds onward. This is a direct result of the propellant valve being opened and releasing nitrogen into the vacuum chamber, causing the pressure inside the vacuum chamber to rise. During the periods when the propellant valve is closed, the pressure drops inside the vacuum chamber due to the vacuum pump being turned on. Lastly figure 4.19d shows that the nitrogen gas has a negligible effect on the chamber temperature, which remains constant with a deviation of less than 0.06% during the entire duration of the test. The thrust that is produced by the thruster is shown in figure 4.20. The thrust is a linear transform from the current through the actuator coil as described in section 3.2.1. The periods in the data from 0 to 10 seconds, and from 100 to 110 seconds are periods where the actuator coil is off, and the current is zero. The period between 10 and 40 seconds is a period where no thrust is produced and thus can be used to zero out the thrust. Since the current through coil is determined by a PID controller and takes some time to stabilize, the value that is used to determine the point of zero thrust, is taken to be the average value between 15 and 39 seconds. Although the period where no thrust is produced ends at 40 seconds, since everything is timed by hand an additional second at the end of the period is discarded to be sure to not include any data of the transition.

Zeroing out the thrust by looking at the average thrust between the 15 and 39th second mark still leaves a problem that need to be accounted for. Figure 4.21a shows that the produced thrust before and after the thrusting period is not the same. The figure also shows a line where the thrust is filtered with a `scipy.signal.savgol_filter` Python filter, an implementation of the Savitzky–Golay smoothing

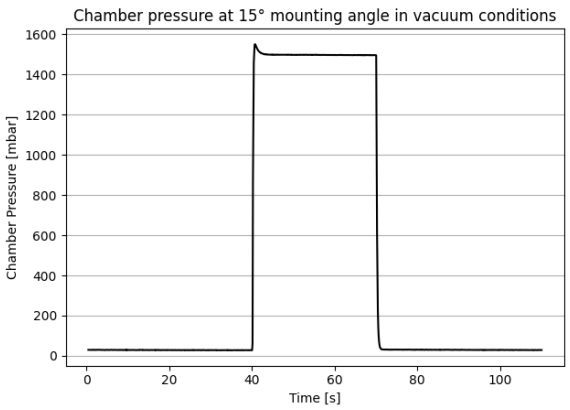

(a) Chamber pressure

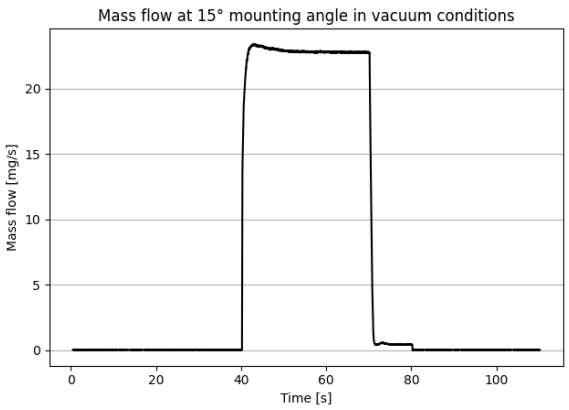

(b) Mass flow

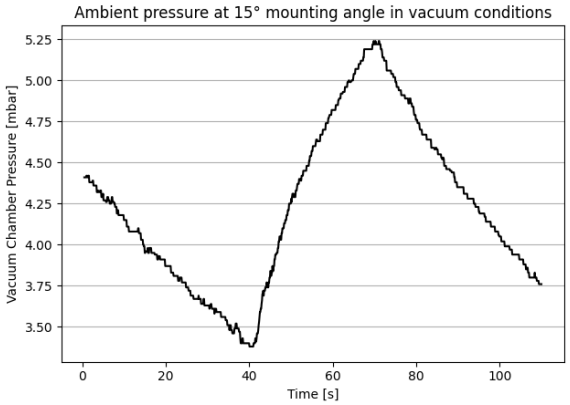

(c) Ambient (vacuum chamber) pressure

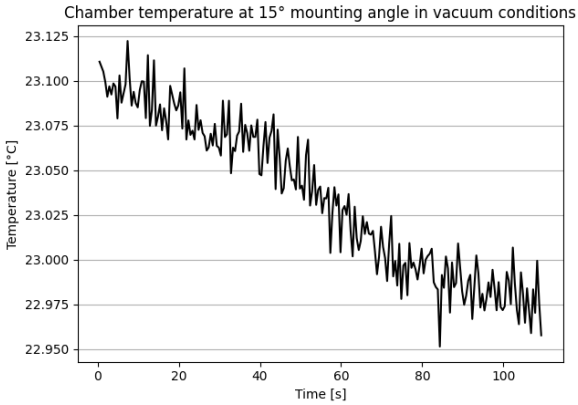

(d) Chamber temperature

Figure 4.19: Operating conditions of a thrust test at mounting angle of 15° in vacuum conditions.

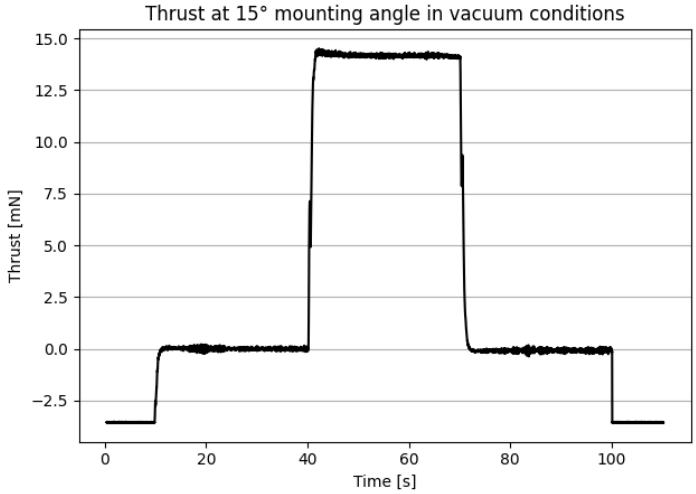

Figure 4.20: Measured thrust with a mounting angle of 15° in vacuum conditions.

filtering.[33] This filter is used as an attempt to reduce the sensor and PID control noise and and to show the trend of the signal. Next to the thrust measured before and after the thrusting period not being the same, it also seems that the thrust in these periods is not entirely constant, but there seems to be a slight

increasing or decreasing trend. An attempt was made to compensate for these types of signal drift. First, a separate linear regression is done using the the Python `scipy.stats.linregress` method on the time periods before and after the thrust period. Secondly, for the thrusting period between 40 and 70 seconds, a linear connection is made between these two linear trends to estimate the drift when thrust is produced. The resulting baseline that corrects for the signal drift is shown in red in figure 4.21a. Subtracting this baseline from the measured thrust signal results in a drift corrected thrust as can be seen in figure 4.21b. The effects of this drift correction on the value of the thrust is shown in figure 4.22.

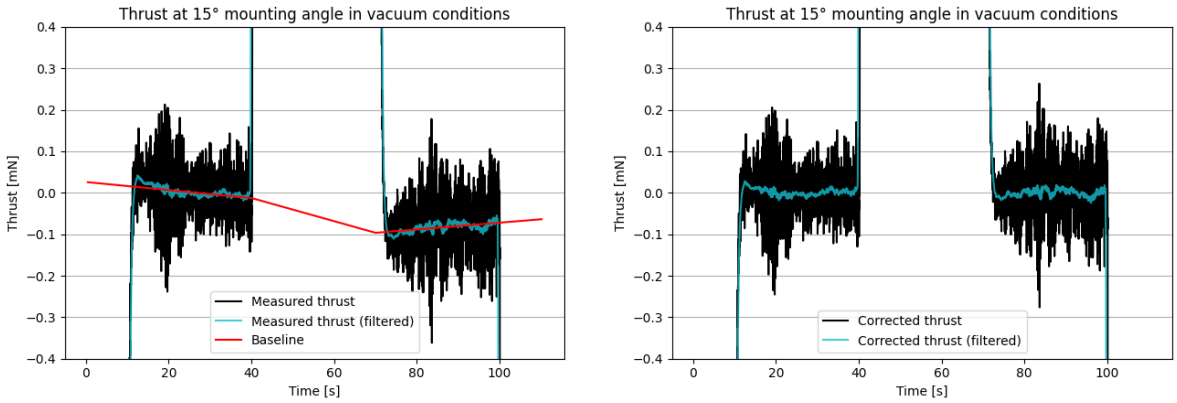

(a) Difference in measured thrust before and after thrust period. Red line shows the assumed drift.

(b) Baseline corrected thrust

Figure 4.21: Linear signal drift correction of the thrust.

The value of the thrust can now be obtained by averaging the individual data points of the corrected thrust over a certain time period. The remaining analysis needed for a single test is determining the error of the calculated average produced thrust. The problem with determining the error of the thrust is that simply calculating the standard deviation of the raw data over a certain time period is not accurate. The resulting standard deviation is influenced too much by the signal noise. In a formula this can be expressed as:

$$\sigma_{F,m} = \sqrt{\sigma_{F,T}^2 + \sigma_N^2}, \tag{4.10}$$

where $\sigma_{F,T}$ is the standard deviation of the theoretical thrust that is produced by the thruster, σ_N the standard deviation of all the combined noise contributions and $\sigma_{F,m}$ the standard deviation of the measured thrust. In order to calculate the standard deviation of the produced thrust, which can be used to describe the accuracy of the produced thrust, the standard deviation of the noise needs to be either determined or removed from the signal. One way to remove the noise from the signal is to apply a smoothing function on the data to reduce the noise. In the case where $\sigma_N \ll \sigma_{F,T}$, equation 4.10 reduces to:

$$\sigma_{F,m} \approx \sigma_{F,T} \qquad \text{for } \sigma_N \ll \sigma_{F,T} \tag{4.11}$$

As mentioned before, a Savitzky–Golay filter is used to reduce the noise of the signal. In this situation a polynomial of order 1 is used together with a window size of 1 second, the result of which can be seen in figure 4.22. This filter fits a linear function on all data points that are within half a second on both sides of the data point that needs to be smoothed. It was found that increasing the polynomial order would fit the data on a small timescale better, but therefore would be worse in smoothing out the small timescale noise. Increasing the window size would increase the smoothness of the filter, although with diminishing returns. Having a larger filter window will also negatively affect the smoothed values near the start and end of the thrust period. As can be seen in figure 4.22, the filtered values drop slightly earlier when the propellant valve is closed at 70 seconds than the unfiltered measurement data. Because a filter window of 1 second is used, the filtered graph start dropping half a second earlier than the unfiltered data. Increasing the window size therefore also negatively affects the amount of data that

can be used for steady state calculations. Because of this reason and the reasons mentioned before in this section, the time period over which to calculate the steady state thrust is defined to be from 55 to 68 seconds.

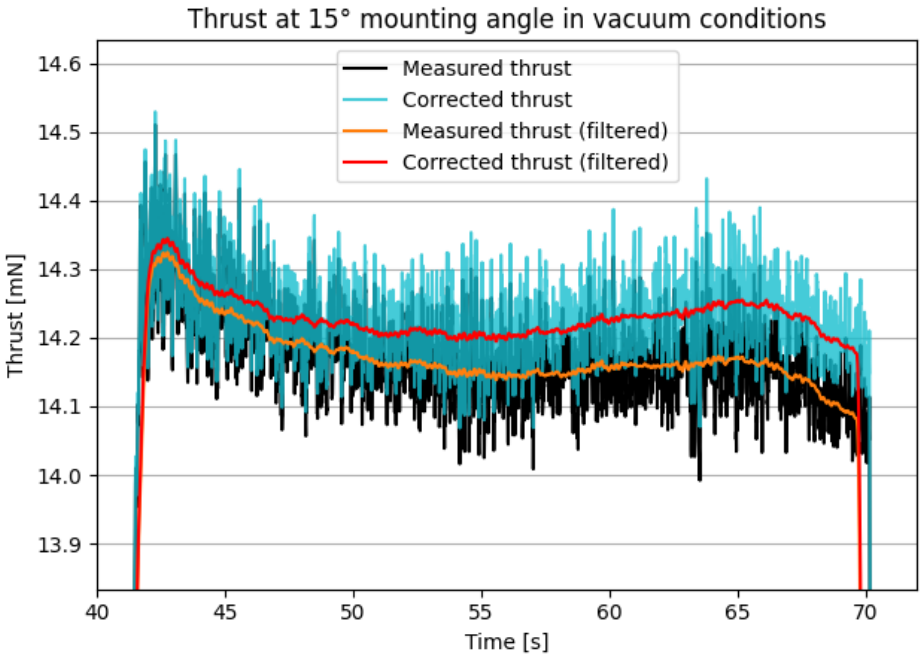

Figure 4.22: Difference between the measured and corrected thrust.

Before equation 4.11 can be used, it must first be proven that the condition $\sigma_N \ll \sigma_F$ is true. By using the Savitzky–Golay filter, it is assumed that the high frequency noise with a period smaller than one second is caused by the sensor noise and PID control instability. The low frequency changes in thrust, such as the trend of the thrust, is of various origins and will be captured in the thrust inaccuracy that will be calculated here. Calculating the standard deviation over a time window of 1 second gives a measure of the amount of noise in the signal. The average standard deviation of the individual 1 second intervals of the unfiltered thrust between 55 and 68 seconds is $\sigma_{N,unfilt}$ = 0.0499 mN, while the same for the filtered thrust gives an average of $\sigma_{N,filt}$ = 0.00339 mN. This means the noise is reduced 14.7 times by the filtering. The standard deviation of the entire time period of the filtered thrust by comparison is $\sigma_{F,filt}$ = 0.0162 mN. Using equation 4.10, the contribution of the noise on the error of the data is

$$\begin{aligned} \sigma_{F,filt} &= \sqrt{\sigma_{F,T}^2 + \sigma_{N,filt}^2} \\ 0.0162 &= \sqrt{\sigma_{F_T}^2 + 0.00339^2} \\ \sigma_{F,T} &= 0.0158 \text{ mN} \\ 1 - \frac{0.0158}{0.0162} &= \boxed{2.2\%} \end{aligned}$$

when the data is filtered. Because the contribution of the low frequency noise over a 1 second time period is small but not entirely zero, the measurement of the noise is not exact and therefore the measurement of $\sigma_{F,T}$ is not exact but merely shows that the contribution of the noise is small and can be ignored so that equation 4.11 holds. In this case, the 3σ error of the thrust is therefore $3\sigma_{F,filt} = 3 \cdot 0.0162 = 0.0486$ mN.

In addition to the error calculated above, the error of determining the baseline has to be added to complete the total error calculation. Since the baseline is already a straight line, the following formula

for the confidence interval can be used:

$$CI = \overline{x} \pm z\frac{\sigma}{\sqrt{N}} \tag{4.12}$$

with CI being the confidence interval, and z the confidence level value. To calculate the 3σ error z is equal to 3, and in the case of the baseline corrected thrust, $\overline{x}$ is always zero. The confidence interval is calculated over the data before and after the thrust period, from 15 to 39 seconds and from 75 to 99 seconds. This is the exact same time period over which the baseline was corrected. In this instance, the confidence interval of the zero thrust is $3\sigma_{zero} = 0.00294$ mN.

At last a final correction is made based on the chamber pressure of the test. The average chamber pressure of all the tests are within the predefined range of 1500±10 mbar. This size of the range was chosen because of the limitations of the nitrogen feed system. Since the thrust is linear with the chamber pressure, the thrust is calculated at exactly 1500 mbar to correct for the small variations between the experiments.

4.5.2.2. Thrust vector angle

Now that the thrust of a single test can be determined, the horizontal angle of the thrust vector can be determined. The data is fit with a cosine function of the shape:

$$F(x, \alpha, \beta) = \alpha \cdot \cos(x - \beta) \tag{4.13}$$

where F is the measured thrust, α stands for the thrust if the thrust angle is aligned with the thrust bench and thus measures maximum thrust, x is the mounting angle, and β the offset angle at which the maximum amount of thrust is measured. The data is fit using the `scipy.optimize.curve_fit` python function. Since the data is heteroscedastic, meaning the errors are different across the data points, a weighted least squares is used to fit the data. This is similar to linear least squares but the residuals are weighted into the cost calculation. In particular, they are weighted by the reciprocal of the thrust inaccuracies of the individual measurements. Therefore a value with a high error has a smaller effect on the fit than a value with a small error. However, a weighted least squares assumes the error in the x-axis, the mounting angle, is zero. In this instance, the inaccuracy of the mounting angle is determined to be 2°. In areas on the x-axis where the slope of function 4.13 is large, a slight change in the mounting angle results in a relatively large change in the y-value, the thrust. To compensate for the fact that the least squares method does not compensate for x-axis inaccuracy, another error in the y-direction has to be introduced for fitting purposes. The error in the y-direction as a result of the error in the x-direction is equal the slope of function 4.13 times the error in the x-direction. The size of the mounting angle in the x direction is named σ_x, the error that compensates for this x-error in the y-direction is called $\sigma_{x\to y}$, and the errors that are calculated according to section 4.5.2.1 are called σ_y. First, an initial fit is made with just the errors calculated in section 4.5.2.1. Then the errors $\sigma_{x\to y}$ are calculated and added to σ_y. The resulting errors are then used for another iteration of fitting an error calculation until convergence is reached. Algorithm 1 shows the psuedo code for the iterative weighted fitting method used, vectors and matrices are shown in bold.

The results of this algorithm is a vector $\boldsymbol{P}$ that contains the values of α and β of equation 4.13. The curve fitting function also calculates the covariance matrix $\boldsymbol{\Sigma}$ which contains the variances of the parameters along the diagonal, the square root of which gives the standard deviation. The results of the fit can be seen in figure 4.23. In this figure, the σ_y errors are shown, not the fitting errors σ_{fit}. From figure 4.23a it can be seen that a theoretical maximum thrust is reached at an angle of 23.4±2.6°. This result corresponds to the initial observation that the thrust vector was not properly aligned with the expected thrust direction. Figure 4.23b shows the thrust in vacuum conditions. This figure shows that the thrust in vacuum does not suffer from thrust vector misalignment as the maximum is found to be at 1.1±2.3° and can be neglected.

Algorithm 1: Iterative weighted fitting

Result: $\boldsymbol{P} \Rightarrow [\alpha, \beta]$ and $\boldsymbol{\Sigma}$

```
// make initial fit
[P_i, Σ] ← Fit(F, x, y, σ_y)
P_{i-1} ← [∞, ∞]

// loop until P converges
while ( P_i ≁ P_{i-1} ) do
    σ_{x→y} ← σ_x · F'(x, P_i)          // F' is the derivative of F
    σ_fit ← Sqrt(σ_y^2 + σ_{x→y}^2)
    P_{i-1} ← P_i
    [P_i, Σ] ← Fit(F, x, y, σ_fit)      // fit again with the new errors
end
```

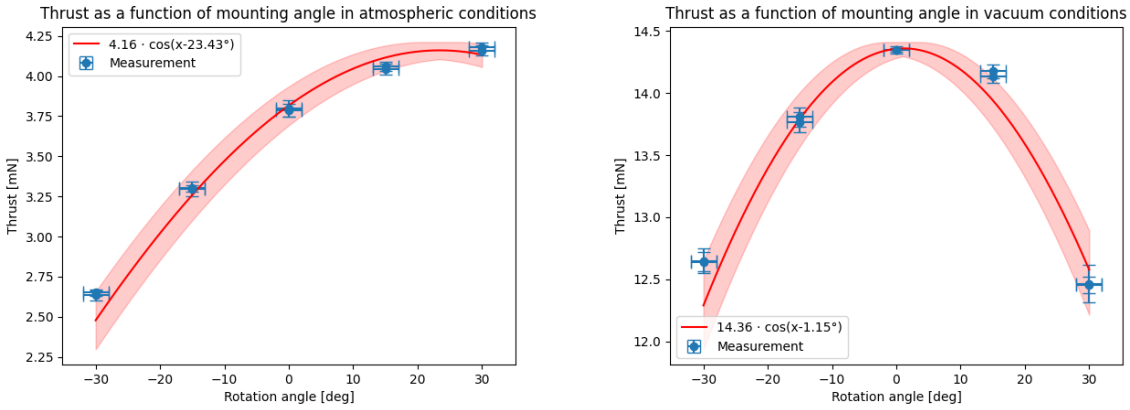

(a) Atmospheric conditions.

(b) Vacuum conditions

Figure 4.23: Horizontal thrust vector angle in atmospheric and vacuum conditions. Marked surface shows the 3σ uncertainty.

4.5.3. Conclusion

It was found that when operating the thruster at atmospheric pressure that the nitrogen gas does not get expelled by the thruster under a right angle. An experiment was performed in order to measure the thrust vector in atmospheric and vacuum conditions. Only the horizontal angle of the thrust vector can be measured with the method used, limited by the dynamics of the test bench and thruster mounting. In atmospheric conditions, the horizontal thrust vector angle is measured to be 23.4±2.6°, which corresponds to the initial observation that the thrust vector was misaligned. Using the same method to measure the thrust vector angle in vacuum conditions did not result in a significant vector misalignment of the thrust vector, as an angle of 1.1±2.6° was found. A correction on the thrust based on thrust vector misalignment is not necessary when the thruster operates in a near vacuum conditions with supersonic outflow.

4.5.4. Discussion

The results show that the thrust misalignment occurs in atmospheric conditions where the flow is over-expanded and subsonic but does not occur in supersonic flow in vacuum conditions. This result is in accordance with the hypothesis that the possible flow separation at atmospheric conditions occurs which affects the thrust angle. Sutton and Biblarz [38] mentions that flow separation is usually symmetric except during transients such as start and stop, although this mention is specifically guided towards large launch vehicle nozzles. Other possible reasons for misalignment mentioned are unsymmetrical surface roughness of the nozzle surface. Unequal surface roughness could cause a preference for flow separation on one specific side, which would explain the consistent preference for one side over the other. One way of verifying this hypothesis is with Computational Fluid Dynamics

(CFD), although this is beyond the scope of this thesis.

4.6. Conclusion

In this chapter several tests were performed in order to prepare for the thrust experiments. A leak test was performed in order to check if the leak rate was still acceptable after the thruster was reassembled. The leak rate was found to be 1.4% of the mass flow at a chamber temperature of 20 °C and a chamber pressure of 1 bar, which is well within the 5% that was set as the maximum allowed leak rate. For experiments at elevated temperatures, the leak rate is smaller than this number because of the higher viscosity of the fluid. The syringe pump that is used for the liquid water feed system was calibrated and was found linear with an accuracy of 0.45%. The effect of live heater current on the thrust measurement was measured. The relation between the heater current and the change in measured thrust was estimated to be linear but experimentally determined to be quadratic. The reason for this has not been found. The effect could be corrected for which allows the heaters to be turned on during experimentation to enable long duration tests. Lastly, the thrust vector was found to be misaligned during subsonic outflow in atmospheric conditions. An experiment was performed to determine the thrust angle in atmospheric (subsonic) and vacuum (supersonic) conditions. A thrust angle of 23.4(26)° was found in atmospheric conditions while this misalignment was not present in vacuum conditions where an angle of 1.1(23)° was measured. A possible reason for this misalignment is unsymmetrical surface roughness of the nozzle surface creating a preference on one side for flow separation to occur.

5

Nitrogen testing

This chapter describes the experiments that have been performed using cold and hot nitrogen gas as propellant. These experiments are done in order to verify the functionality, characteristics and performance of the thruster and thrust bench. The results are compared to the model predictions, previous experiments, and similar thrusters. The test plan will be discussed in section 5.1, and the test procedure in section 5.2. The result of the tests are shown in section 5.3 and further discussed in section 5.4. Finally, a summary, conclusion and recommendation for future tests for the nitrogen test campaign can be found in section 5.5.

5.1. Test plan

This section will describe the test plan for the experiments that are being performed with nitrogen as propellant. The experiments will be performed at a maximum of 300 °C since to reduce the risk of overheating the heaters. Since the water test has to be performed at a chamber pressure of 1 bar (see section 6.1.2), the experiments with nitrogen are also performed at a chamber pressure of 1 bar. Since the experiments by Versteeg are performed at room temperature, 200 °C and 400 °C, the experiments are also repeated at 200 °C to allow for direct comparison of the results.[47] Since the test at 200 °C was performed at a chamber pressure of 1.5 bar, they will be repeated in this chapter at 1 and 1.5 bar. Table 5.1 shows all the planned nitrogen tests that are going to be performed in this chapter. Note that the test at 20 °C is unheated, which is therefore a cold gas thrust test.

ID	p_c [bar]	T_c [°C]
NIT-1	1.0	20
NIT-2	1.0	200
NIT-3	1.5	200
NIT-4	1.0	300

Table 5.1: Planned nitrogen thrust tests.

5.1.1. Test objective

The purpose of the test is to be able to determine the performance parameters listed in table 5.4 with an accuracy of 15%. As can be seen in section 5.1.4, the accuracy of the mass flow is around 9% which means the discharge coefficient will have a minimum error of 9% as well. The value of 15% was chosen as this is roughly double the error of the analytical model ($\sqrt{9\%^2 + 9\%^2} \approx 13\%$) which thus allows a similar for experimental error. Results of this test can be compared to previous tests performed by Versteeg [47] for validation. These tests are needed to characterize the behaviour of the test bench so that for future tests with water the features of the test bench can be separated from the features specific to testing with water. Furthermore, they will provide verification for the used mathematical model and by comparing the results to previous work on the same thruster, the test procedure and data analysis can be verified as well.

5.1.2. Relevant parameters

There are several parameters that are required for characterizing the setup and performance related traits of the thruster. Table 5.2 shows the relevant parameters that need to be measured directly, while table 5.3 shows the most important parameters that can be calculated directly from the measured values. The temperature of the propellant tube is of interest because it is suspected in the work by Versteeg [47] that thermal expansion in this tube causes a change in measured thrust. The workings of this is described in more detail in section 5.3.1. Most of these parameters serve as input for the analytical model for comparison and are needed to eventually calculate the performance parameters to describe the thruster. The performance parameters are listed in table 5.4.

Symbol	Description	Location of measurement
$\dot{m}$	Propellant mass flow	Measured in the feed system before entering the vacuum chamber. See section 3.3.
p_c	Chamber pressure	Measured at the end of the pressure sensing tube connected to the thruster. See section 3.1.
p_a	Ambient pressure	Measured inside the vacuum chamber.
T_c	Chamber temperature	Measured on the thruster on the metal profile. See section 3.1.
I_{act}	Current through the actuator coil	Measured internally by the power supply.
I_{heat}	Heater current	Measured internally by the power supply.
V_{heat}	Heater voltage	Measured internally by the power supply.
T_{tube}	Temperature of the propellant tube	Measured at three different locations along the propellant tube. See section 3.1.

Table 5.2: Relevant parameters to be measured for the tests using nitrogen as propellant.

Symbol	Description	Dependent on
F_T	Thrust force	I_{act}
P_{heat}	Heater power	V_{heat}, I_{heat}

Table 5.3: Relevant parameters to be calculated for the tests using nitrogen as propellant.

Symbol	Description
I_{sp}	Specific impulse
η_{heat}	Heating efficiency
$\xi_{I_{sp}}$	Propellant consumption quality
C_d	Discharge coefficient

Table 5.4: Relevant parameters that are used for describing the performance of the thruster.

5.1.3. Acceptance criteria

Table 5.5 shows the acceptance criteria that have been set to define a successful nitrogen thrust test. Criteria AC-NIT-01 ensures that all parameters that need to be measured are being recorded. Criteria AC-NIT-02 ensures that the thrust that is being produced is supersonic. Although the exhaust velocity is not directly measured, it can be calculated if equation 2.10 is satisfied. AC-NIT-03 ensures that the

performance parameters resulting from the analysis is within the allowed 15% 3σ error as stated in the test objective. Acceptance criteria AC-NIT-04a, AC-NIT-05a and AC-NIT-06 ensure that the operating conditions of the thruster remain constant (max ±1% deviation, excluding sensor noise) over the course of the experiment. A value of 1% for the maximum deviation from the average was chosen to be so small compared to the overall 15% allowed inaccuracy to limit noise from controllable sources as much as possible. It is estimated that these input parameters are controllable within 1%, but a smaller deviation would be difficult to obtain with relatively little gain in overall accuracy and thus not worth the effort. Lastly, criteria AC-NIT-04b and AC-NIT-05b ensure that the chamber temperature and pressure are within 5% of the targeted value. The allowed deviation is chosen to be higher as the exact value of the controllable parameters are not as important as their stability during a single experiment. Note that there is no acceptance criteria for the average value of the mass flow. This is because in these experiments the mass flow is driven by the chamber temperature and chamber pressure.

ID	Description
AC-NIT-01	All parameters from table 5.2 are measured over time through their respective sensors.
AC-NIT-02	The exhaust is supersonic.
AC-NIT-03	The performance parameters from table 5.4 can be calculated with an accuracy of 15% or smaller.
AC-NIT-04a	The measured chamber temperature remains constant during operation.*
AC-NIT-04b	The average chamber temperature is within 5% of the target.
AC-NIT-05a	The measured chamber pressure remains constant during operation.*
AC-NIT-05b	The average chamber pressure is within 5% of the target.
AC-NIT-06	The measured mass flow remains constant during operation.*

* Maximum deviation of ±1% of average value excluding sensor noise, first 10 seconds of startup excluded.

Table 5.5: Acceptance criteria for nitrogen thrust test

5.1.4. Test predictions

The parameters of the experiments to be performed are used as input into the analytical model in order to estimate the performance of the thruster. This will make sure the resulting output parameters are within the capabilities of the testing equipment and allows for comparison with the experimental results. The input and output parameters of the analytical model for the performed experiments are shown in table 5.6. The values in this table are the ideal values and thus are uncorrected for the estimated correction factors.

5.2. Test procedure

In order to be able to measure the change in equilibrium of the pendulum, multiple thrusts intervals will be done in one single test. There will be 3 periods where thrust will be generated, alternated with periods where no thrust will be produced. This will be done by opening and closing the propellant valve at predefined times. The length of both thrust, and non-thrust producing intervals will be set at 5 minutes in order to give the setup enough time to converge to an equilibrium, and make additional measurements after the equilibrium has been reached. The test procedure is separated into four different phases and are in order:

1. Prepare test setup
2. Environment setup
3. Thrust measurement
4. Experiment shutdown

The following sections describe the steps for each the phase individually. Remember that if the test to be performed is a cold thrust test, all steps regarding the heaters should be skipped.

		NIT-1	±[%]	NIT-2	±[%]	NIT-3	±[%]	NIT-4	±[%]
Input									
T_c	[K]	293	2.4	473	1.5	473	1.5	573	1.2
p_c	[mbar]	1000	5.0	1000	5.0	1500	3.3	1000	5.0
p_a	[mbar]	5.00	15.0	5.00	15.0	5.00	15.0	5.00	15.0
A_t	[10^3µm^2]	75.32	7.8	75.32	7.8	75.32	7.8	75.32	7.8
A_e	[10^3µm^2]	580.0	1.7	580.0	1.7	580.0	1.7	580.0	1.7
H_t	[µm]	538	1.5	538	1.5	538	1.5	538	1.5
θ	[°]	20	0.0	20	0.0	20	0.0	20	0.0
Output									
Ideal									
γ	[-]	1.40	0.0	1.39	0.0	1.39	0.2	1.38	0.1
F_T	[mN]	11.96	9.2	11.98	9.1	18.11	8.2	12.00	9.1
$\dot{m}$	[mg/s]	17.49	9.4	13.74	9.3	20.6	8.5	12.46	9.3
I_{sp}	[s]	69.72	1.3	88.88	0.9	89.59	0.8	98.23	0.8
c^*	[m/s]	431	1.2	548	0.8	548	0.8	605	0.6
C_F	[-]	1.59	0.4	1.59	0.4	1.60	0.4	1.59	0.4
P_h	[W]	0.0	0.0	2.58	9.8	3.88	9.0	3.66	8.0
Re_t	[-]	2936	8.4	1617	8.0	2425	7.1	1282	8.0
p_t	[mbar]	528	5.0	529	5.0	794	3.3	531	5.0
T_t	[K]	244	2.4	395	1.5	395	1.5	481	1.3
U_t	[m/s]	319	1.2	405	0.7	405	0.7	445	0.6
p_e	[mbar]	10.8	11.9	11.0	11.8	16.5	11.2	11.2	11.8
T_e	[K]	80	3.9	132	3.4	132	3.4	165	3.3
U_e	[m/s]	664	1.3	846	1.0	846	1.0	934	0.9
Expected									
C_d	[-]	0.947	0.2	0.930	0.3	0.942	0.2	0.923	0.4
$\xi_{I_{sp}}$	[-]	0.746	1.4	0.662	2.0	0.724	1.3	0.621	2.5
ξ_{F_T}	[-]	0.707	1.6	0.615	2.4	0.682	1.5	0.573	2.8
F_T	[mN]	8.45	10.7	7.37	11.4	12.35	9.7	6.88	11.9
$\dot{m}$	[mg/s]	16.56	9.6	12.79	9.6	19.42	8.7	11.49	9.6
I_{sp}	[s]	52.04	1.5	58.79	2.0	64.82	1.2	61.03	2.4
Re_t	[-]	2830	8.7	1540	8.3	2330	7.4	1214	8.3

Table 5.6: Input and output parameters of the analytical model showing the predicted parameters for the tests to be performed using nitrogen as propellant.

5.2.1. Prepare test setup

This section contains the step by step procedure to make sure all equipment is connected and working. The steps to prepare the test setup are:

1. Turn on equipment that require warm up:
   (a) Turn on the SM-7020, SM-7020-D, ES-030-10, E-030-1 and D-030-1 power supplies (warm-up time: 60 min).
   (b) Plug in the power to the Brooks 5850S 2000sccm mass flow sensor. (warm-up time: 45 min).
   (c) Plug in the power to the Micro-Epsilon DT6220/DL6230 distance sensor DAQ. (warm-up time: 15 min).
2. Connect the test bench to the computer and equipment:
   (a) Install the thruster on the test bench as described in section 3.4.
   (b) Move the test bench inside the vacuum chamber.

(c) Turn the adjustable feet on the test bench such that the bench is level.

(d) Connect the connector of the p-T sensor to the NI USB-6008 and NI USB-8451 DAQs.

(e) Connect the distance sensor cable to the CS2 sensor.

(f) Connect the propellant feed to the quick connect inside the vacuum chamber.

(g) Plug in the cables of the actuator coil in the power feedthrough in the vacuum chamber. Make sure the cables are as perpendicular to the coil as possible.

(h) Plug in the cables of both heaters in the power feedthrough in the vacuum chamber.

(i) Make sure all connections on the power feedthrough match up to the correct power supplies outside the vacuum chamber.

(j) Plug in the thermocouples into the NI 9211 DAQ.

(k) Connect the red and black jumper cables inside the vacuum chamber to the connector pins on the MINSTAC valve. Route the wires over the pivot and parallel to the rotational axis with the other wires. Secure the cable with tape.

(l) Verify that the pendulum can rotate freely.

(m) Turn on the computer and open the LabView program.

3. Open the nitrogen feed system (shown in figure 3.7):

(a) Connect the output of the feed system to the propellant inlet of the vacuum chamber.

(b) Make sure all valves shown in figure 3.7 are closed.

(c) Open the valve on top of the nitrogen cylinder.

(d) Open the high pressure shut-off valve. Note: the high pressure gauge will now show how much nitrogen is left in the cylinder. A full cylinder will show approximately 200 bar.

(e) Open the pressure regulator valve slowly until the desired feed pressure is reached. This is the pressure displayed on the low pressure gauge.

(f) Open the low pressure shut-off valve.

(g) Slowly open the selection valve that is connected to the vacuum chamber.

4. Test if all sensors are working:

(a) Specify a folder and test name and click **Run** to start the LabView program.

(b) Verify that all temperature sensors are reading around 20°C.

(c) Verify that all pressure sensors are reading around 1 atm.

(d) Temporarily open the MINSTAC valve and verify that the mass flow sensor is measuring a flow of propellant. Set the PWM control slider to 255 (fully open).

(e) Turn on one of the heaters at 20 Watt and verify that the temperature of the thruster is going up. Turn the heater off. Repeat this step for the other heater.

(f) Set the pendulum equilibrium position of the pendulum using the counterweights such that it sits anywhere between 500 and 1000 µm.

(g) Set the setpoint of the pendulum distance to around 75 µm above the pendulum equilibrium and turn on the PID of the actuator coil. Verify that the pendulum is brought to the given setpoint. The current through the actuator coil should be 2±0.5A. Adjust the setpoint distance if the current is not in this range. Turn the PID of the actuator coil off.

5. Stop the LabView program:

(a) Click on the **STOP TEST** button to stop recording data.

(b) Wait at least 5 seconds to ensure all data is being written to the file.

(c) Click on the **Abort Execution** button to stop the LabView program.

5.2.2. Environment setup

This section describes the steps to turn on the vacuum chamber and heat up the thruster. These procedures require the completion of the procedures listed in section 5.2.1.

1. Turn on the vacuum chamber:
   (a) Specify a folder and test name and click run to start the LabView program.
   (b) Make sure the heating power is set to 0 Watt and the temperature control setpoint to 0 °C.
   (c) Make sure the vacuum chamber door is properly closed.
   (d) Turn the handle on the vacuum chamber such that the connection to the vacuum pump is open.
   (e) Rotate the black knob on the vacuum chamber such that the vacuum chamber is closed off from the outside air.
   (f) Turn on the vacuum pump and make sure the pressure sensors in the LabView program show that the pressure is decreasing.
2. Preheat thruster to desired temperature:
   (a) Wait for the vacuum chamber to have reached a pressure of 100 mbar or lower.
   (b) Turn on the heaters by setting the power level of the individual heaters to max 20 Watt and selecting **Power Control** by clicking the heating control selector button.
   (c) Continue heating until the chamber temperature has reached a temperature of 10 °C below the desired temperature. Set the heating power to 0 Watt.
   (d) Set the input of the temperature controller to the desired temperature and click the heating control selector button to select **Temperature Control**. The temperature will now automatically rise to the desired temperature.
3. Set correct mass flow:
   (a) Fully open the MINSTAC propellant valve for no more than 5 seconds and read the produced chamber pressure from the chamber pressure sensor.
   (b) Adjust the pressure regulator valve on the feed system to increase of decrease mass flow so that the chamber pressure is as close to the desired chamber pressure as possible and in accordance with AC-NIT-05b.
   (c) Repeat the above two steps if necessary.
4. Wait up to 5 minutes for the temperature oscillation to stabilize to an acceptable range (±1 °C) and for the pressure inside the vacuum chamber to reach 5 mbar or lower.

Note: Do not stop the LabView program yet! Stopping the LabView program will stop the control of the chamber temperature. The time between stopping this test and starting the thrust measurements should not be much longer than 10 seconds to keep the chamber temperature stable. The procedures for stopping the current program and starting the measurements for the test are listed in section 5.2.3.

5.2.3. Thrust measurement

This section describes the procedures for performing a thrust measurement. These procedures require the completion of the procedures for the environment setup listed in section 5.2.2. Some of the following procedures are time sensitive so in order not to miss the time window for a certain step, please read the procedure in full and locate all buttons on the LabView interface before starting the first step. At every step try to keep in mind the upcoming procedures.

1. Start the measurements:
   (a) Specify a folder and test name to save the upcoming thrust measurement.

(b) Repeat step 4g of section 5.2.1 since the change in temperature and chamber pressure might change the equilibrium position of the pendulum.

(c) Turning off pendulum distance control releases the pendulum. Wait until the pendulum distance amplitude has reached a minimum (±30 to 60 seconds).

(d) Click the **STOP TEST** button to stop the LabView program started for the environment setup.

(e) Click on the **Abort Execution** button to stop the LabView program.

(f) Click on **Run** to start the LabView program to start recording for the thrust measurement.

2. Perform the test:

(a) Perform the actions from table 5.7 at the given time.

(b) During the experiment, make sure the variables shown in the LabView interface are within the expected values.

3. Stop the test:

(a) At the end of the experiment, stop recording using the **STOP TEST** button.

(b) Press the **Abort Execution** button to stop the LabView program.

Time	Actions
0:00	Start recording
1:00	Turn on the actuator coil PID control
6:00	Open the propellant valve
11:00	Close the propellant valve
16:00	Open the propellant valve
21:00	Close the propellant valve
26:00	Open the propellant valve
31:00	Close the propellant valve
36:00	Turn off the actuator coil PID control
37:00	Stop recording

Table 5.7: Actions to undertake during the nitrogen thrust measurement.

5.2.4. Experiment shutdown

After the experiment is finished, there are several steps that need to be taken to make sure the experiment is safely shutdown. The thruster can be hot and the vacuum chamber is under low pressure. The following steps should be taken in order to safely shutdown the experiment without damaging the equipment.

1. Turning off power:

(a) Specify a folder and test name and click run to start the LabView program.

(b) Make sure the heating power is set to 0 Watt and the temperature control setpoint to 0 °C. Note that the temperature of the thruster is dropping.

(c) Make sure the actuator coil PID control is off.

(d) Make sure the MINSTAC propellant valve is closed.

(e) Stop the LabView program.

2. Stop the vacuum pump:

(a) Turn the handle on the vacuum chamber such that the connection to the vacuum pump is closed.

(b) Turn off the vacuum pump. Some air will go through the vacuum pump in the opposite direction to fill the tube leading to the vacuum chamber (where the tube is shut off). If air is moving through the pump in the opposite direction for more than 3 seconds, which can be noted by the sound of the pump being forcibly rotated by the outside pressure, quickly turn the pump back on and verify the vacuum chamber is properly shut off from the pump and try again. Air moving in the opposite direction than what the pump is designed for can damage the pump.

(c) DON'T TURN THE VACUUM CHAMBER VENT VALVE! Keep the vacuum chamber under low pressure as long as the thruster is still hot to prevent oxidation of the thruster.

3. Depressurize the nitrogen feed system:

(a) Close the high pressure shut-off valve.

(b) Close the pressure regulator valve.

(c) Open one of the unconnected selection valves to release the pressure inside the feed system. Note that the low pressure gauge drops to zero.

(d) Close the low pressure shut-off valve.

(e) Close all selection valves.

4. Turn off the equipment:

(a) Turn off the SM-7020, SM-7020-D, ES-030-10, E-030-1 and D-030-1 power supplies.

(b) Unplug the Brooks 5850S 2000sccm mass flow sensor.

(c) Unplug the Micro-Epsilon DT6220/DL6230 distance sensor DAQ.

5. Release the vacuum of the vacuum chamber:

(a) Wait for the temperature of the thruster to be below 40 °C so it can be safely touched. This can take up to several hours. Check the temperature by starting the LabView program.

(b) Release the vacuum of the vacuum chamber by rotating the vent valve.

6. Dismantle the thrust bench:

(a) Open the vacuum chamber door.

(b) Disconnect the heaters and actuator coil from the power supply inside the vacuum chamber.

(c) Disconnect the temperature sensors from the DAQ.

(d) Disconnect the propellant Swagelok Quick Connect inside the vacuum chamber.

(e) Disconnect the distance sensor inside the vacuum chamber.

(f) Disconnect the p-T sensor.

(g) Carefully take out the test bench from the vacuum chamber making sure no wires are still connected. Note that the test bench is heavy.

(h) Place the vacuum chamber outside the vacuum chamber and close the vacuum chamber door.

(i) Dismantle the thruster from the test bench.

5.3. Test results

Results of test TST-NIT-04 are shown in figure 5.1. These graphs show the relevant parameters from table 5.2, where the actuator coil current is converted into a thrust using formula 3.5 and the heater current and voltage are combined into total heater power. Initial impressions of the different graphs show some interesting characteristics of the experiment. First the chamber pressure and the mass flow decrease slightly over time. For this particular experiment the high pressure shut-off valve was closed before starting the experiment, as this was also the method used by Makhan [26] and Versteeg [47] before it was later improved. Closing the high pressure shut-off valve traps high pressure gas between

this valve and the pressure regulator valve which drives the feed system. Because the volume between these two valve is relatively small, the pressure of the small reservoir drops and with it the pressure behind the pressure regulator over the course of the experiment. For the updated procedures, the high pressure shut-off valve is kept open. Since the volume of the tank is much higher, the escaping mass flow does not measurably decrease the tank pressure and therefore the pressure behind the regulator valve. The results of the experiments are still kept however, since it doesn't significantly affect the measurements. The peaks in the chamber temperature are caused by the behaviour of the PID controller with changes in the chamber temperature due to the change in propellant supply. This PID control characteristic is also seen in the total heater power, which controls the chamber temperature. Initially the power is relatively constant around 8.2 Watt and rises when the propellant starts flowing. It overshoots its target slightly and starts to level out at the end of the thrust period. Interesting is that between thrust periods, the power level does not go back to the initial 8.2 Watt. It is important to note that the chamber temperature is only measured at a single location, on the opposite side of the propellant inlet close to the throat. After the mass flow of (initially) cold nitrogen stops, the throat side of the thruster is still (close to) 300 °C, but near the propellant inlet the temperature is lower than during the start of the experiment. This means more heat flows towards this cold part of the thruster meaning more power is needed to keep the temperature near the throat at a constant 300 °C. The measured thrust shown in figure 5.1f is the actuator coil converted directly into thrust using formula 3.5. Note that the measured thrust is not directly equal to produced thrust due to the nature of how the thrust is measured. How this measured thrust is converted into thrust produced by the resistojet is described in detail in section 5.3.1 and 5.3.2. The performance of the thruster is given in section 5.3.3 and compared to other work in section 5.3.4.

The temperature of the propellant tube is shown separately in figure 5.4, and thus AC-NIT-01 is satisfied. As can be seen in figure 5.1a and 5.1c, the mass flow and chamber pressure lightly decrease over time, but stay within 1% from their respective means. The chamber temperature from figure 5.1b shows the chamber temperature to stay within -1.5 °C and +1.0 °C, well within the 1% limit. This satisfies acceptance criteria AC-NIT-04a, AC-NIT-04b, AC-NIT-05a, AC-NIT-05b, and AC-NIT-06.

5.3.1. Thrust analysis

The measured thrust shown in figure 5.1f is not absolute, but relative to the arbitrary pendulum setpoint. Therefore, when the actuator coil is turned on at the 1:00 minute mark in accordance with table 5.7, the measured thrust rises to just over 4 mN. Since the thruster is not producing thrust at that time, this amount of measured thrust corresponds to zero produced thrust.

The first step in calculating the thrust is to corrected for the heater power as shown in section 4.4. After this, an attempt to correct for the drift is made. Two types of signal drift are observed when the thruster is turned off. The first type of signal drift is signified by the steady increase of measured thrust over the entire duration of the test. The second type of signal drift is observed immediately after the thruster is turned off and shows a significant decrease in measured thrust which effect seems to dissipate over a 2 or 3 minute time period. This effect is also seen when at the beginning of the thrust period, but in the opposite magnitude. This type of drift was also noticed in the work by Versteeg [47], where the measured thrust after the thrust period dropped below zero. The difference in this experiment is that more data is available to correct for these drifts in greater detail. In order to study both effects, an attempt is made to remove the first type of signal drift. This long term drift is from this point on called the baseline, which represents the line where zero thrust is produced by the thruster. The measured thrust after closing the valve can't directly be used to calculate the baseline since it is affected by the second type of drift. Therefore only the last half of the data in periods of no thrust is kept for fitting the baseline. In addition, the last 5 seconds are omitted to ensure no transitional effects influence the baseline. Since the periods where no thrust is produced last 300 seconds (see table 5.7), there are four periods of roughly 145 seconds of data, which is more than enough for fitting. The shape of the baseline is close to linear, but it was chosen to increase the polynomial order to a quadratic function to improve the quality of the fit. Figure 5.2a shows the measured thrust and baseline, while figure 5.2b shows the measured thrust with the baseline subtracted. When the baseline is removed from the measured thrust, the second type of signal drift which shows up directly after opening and closing the propellant valve is still visible. Comparing the results of figure 5.2b to figures 5.3a and 5.3b hints that the operating chamber temperature has a big effect on this type of drift. The effect is largest at 300°C,

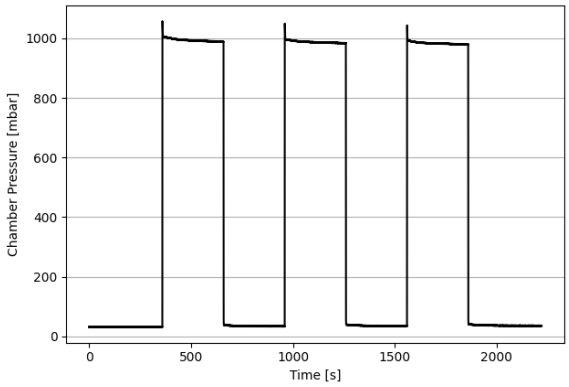

(a) Chamber pressure

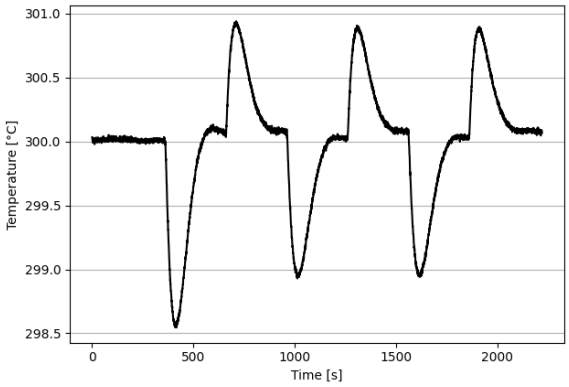

(b) Chamber temperature

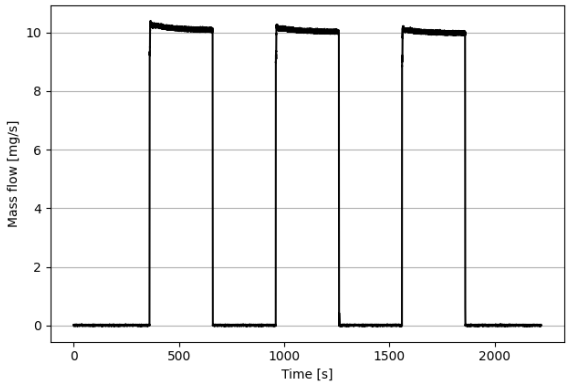

(c) Mass flow

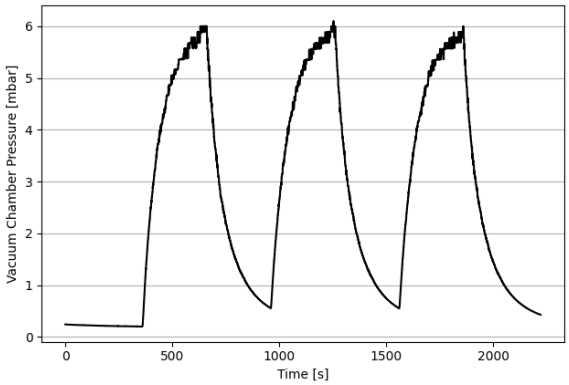

(d) Ambient pressure

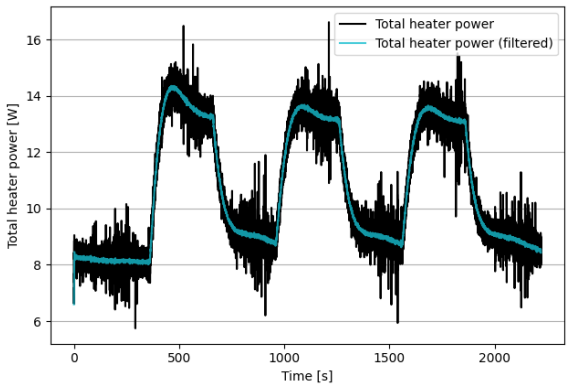

(e) Total heater power

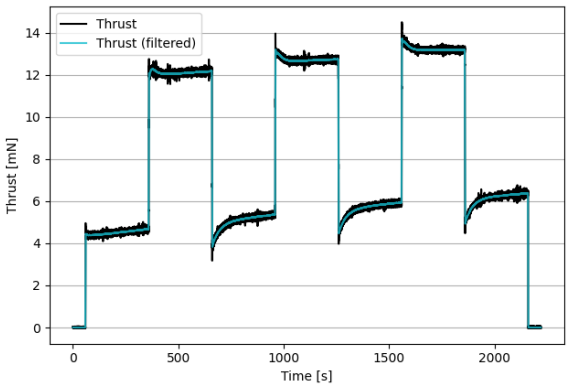

(f) Measured thrust

Figure 5.1: Three consecutive nitrogen tests with 5 minute valve open and close intervals.

smaller at 200°C, and is no longer visible at room temperature. The thrust is measured in reference to the equilibrium position of the pendulum, in which the center of mass of the pendulum is directly beneath its pivot axis. However, thermal expansion of certain components on the pivot may lead to a shift in center of gravity which alters the equilibrium position of the pendulum, and therefore the thrust that is measured. This problem has also been mentioned in the work by Versteeg [47], which raised concern for the temperature changes in the metal propellant tube leading up to the thruster body. In the experiments by Versteeg, it was noted that for experiments other than room temperature the actuator current after firing would be consistently lower than the current before firing. This effect also found to be

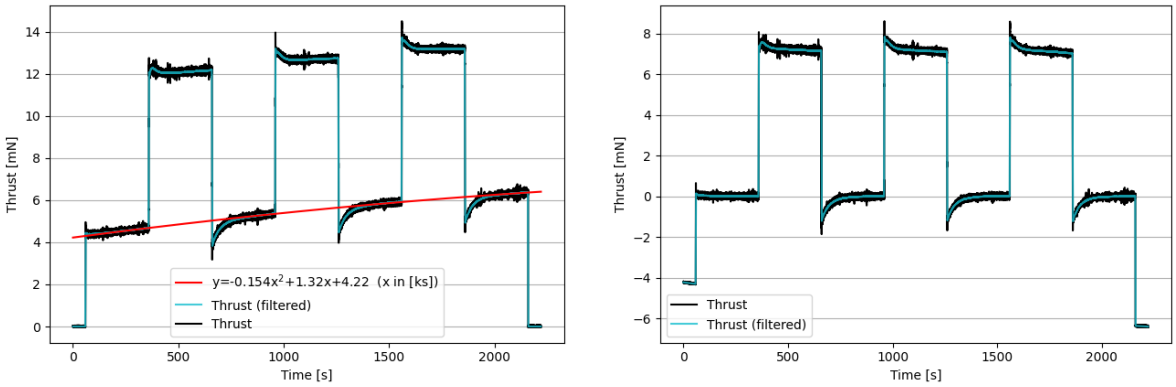

(a) Measured thrust together with the baseline showing in red in terms of kiloseconds.

(b) Baseline corrected thrust

Figure 5.2: Measured thrust and drift correction for hot nitrogen thrust test at 300°C chamber temperature.

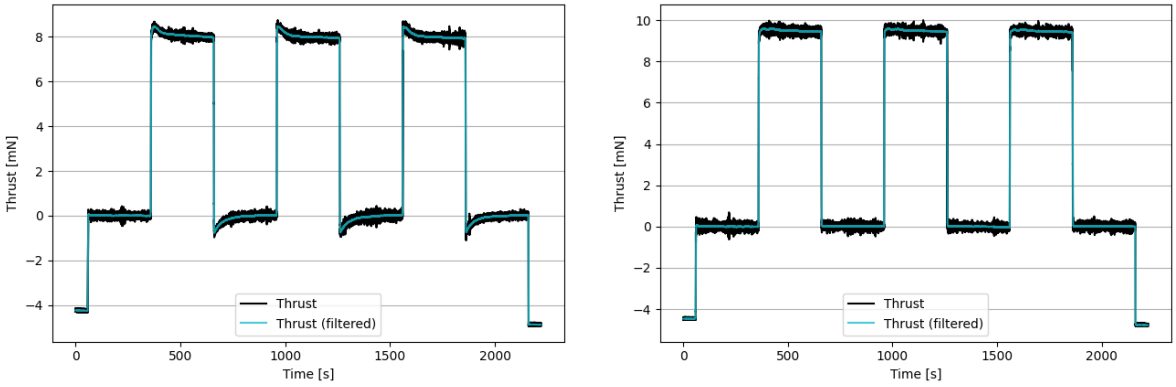

(a) Chamber temperature of 200°C

(b) Chamber temperature of 25°C

Figure 5.3: Baseline corrected thrust at different chamber temperatures.

increasing at higher temperatures. The difference between those experiments and the ones performed in this thesis is that in the experiments by Versteeg the thrust duration was around 20 seconds, with little time recording data after the propellant valve has been shut off, while in this thesis both those periods are sustained for 5 minutes. The longer duration makes it possible to see the effects shown in figures 5.2b and 5.3. To verify that the temperature of the propellant tube is significantly affected by the (absence of) flow of propellant, three thermocouples are placed on the tube and measured over the entire duration of the test. The results of this is shown in figure 5.4. From the figure it can be seen that during periods of propellant flow the temperature of the tube decreases by ≈20, 30 and 35°C as opposed to the absence of flow for the bottom, middle and top thermocouple location respectively. However, there is no significant trend in temperature visible over the entire duration of the experiment which shows that the temperature of the propellant tube is not a significant contributor of the change in baseline over time. With this data it can not be proven that the temperature change of the propellant tube is the only significant contributor of the noticed effect. Since the entire thrust bench is made of thermal conductive materials, a complete solution that includes all dynamics related to thermal expansion is complex and beyond the scope of this thesis. However since the effect is proven to be temperature related, thermal expansion of the thruster mounting is assumed to be the cause of this effect.

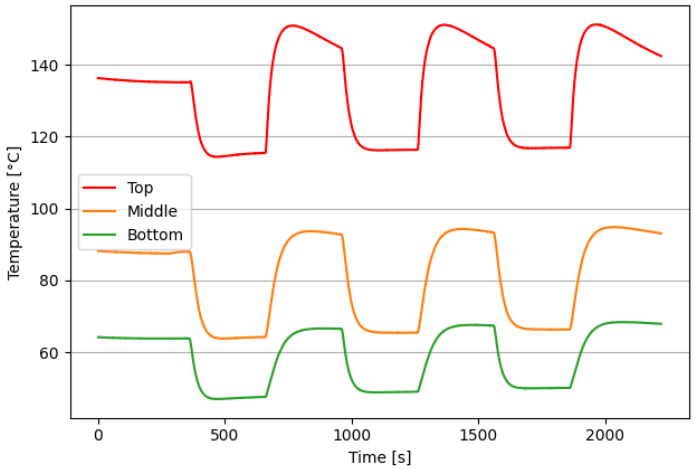

Figure 5.4: Temperature of the propellant tube leading up to the thruster body at 3 locations, see section 3.1.

5.3.2. Thermal expansion correction

At chamber temperatures close to room temperature, the thrust can be determined by simply averaging the produced thrust over the thrust duration. However since thermal expansion at higher chamber temperatures changes the characteristics of the thrust curve, this is no longer possible. When the propellant tube is hot and no propellant is flowing, the pendulum equilibrium is different from the equilibrium position when the propellant tube is cold. Therefore there are two different equilibrium positions of the pendulum, which transition when the propellant valve opens or closes. This effect is not instantaneous as figure 5.4 shows, and so the measured thrust seems to change in the few minutes when the valve is closed. This same effect occurs when the valve is opened and the propellant tube starts to cool down. A stable equilibrium position is reached whenever the temperature of the propellant tube stabilizes. When the experiment starts the tube is hot and the thruster is not producing thrust. The current that is flowing through the actuator coil at that time is the reference current that corresponds to a thrust of zero. However at the end of the thrust period, the propellant tube is cold and the measured thrust therefore has an incorrect reference thrust. This means that the thrust measured at the end of the thrusting period is lower than the thruster is actually producing. This is why the thrust seems to be decreasing right after the propellant valve opens, t_{open}, since the propellant tube is cooling down. In order to know what the actual produced thrust is, the difference between these two equilibrium positions has to be found. In the work by [47] an attempt for this is made using two different calibration points where zero thrust is produced. One calibration point is taken just before opening the valve, and one is taken ±5 seconds after closing the valve. This results in two different measures for the thrust, the difference between the two calibration points is an estimation of the difference between the two equilibrium positions mentioned here. Since the equilibrium position just before closing the valve is not the same as the position after 5 seconds of closing it, this method could use some refinement. Since more data is gathered in this work, the difference in equilibrium difference can be estimated more accurately. After the results are calculated in section 5.3.4, they will be compared to the results from Versteeg [47].

At the point where the propellant valve closes, t_{close}, the thruster is not producing thrust although the propellant tube is still cold and starting to heat up. Fitting the signal after the propellant valve closes and extrapolating it to the time when the propellant valve is closed would give the thrust reference of when the propellant tube is cold. Figure 5.5 shows the measured thrust fitted with a function in the periods after the thruster had produced thrust. The measured thrust in figure 5.5 is fitted with a function of the following shape

$$f(x) = a \cdot e^{bx} + cx + d \tag{5.1}$$

with $a, b < 0$ where x is the time after t_{close} in seconds. Parameters a and b determine the scale

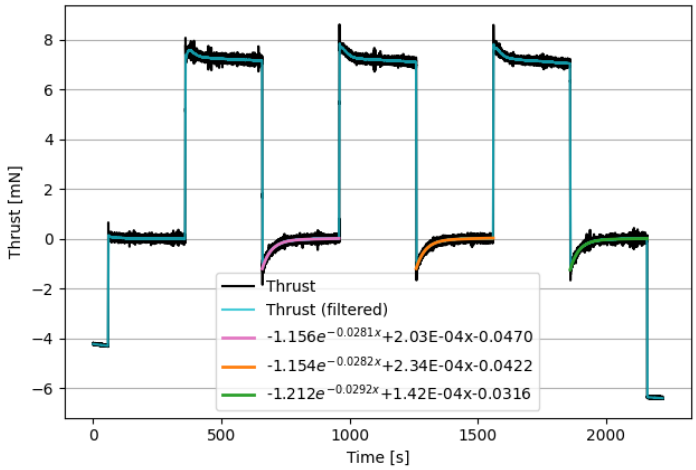

Figure 5.5: Measured thrust change due to thermal expansion fits.

in the xy-plane which corresponds to the amount of drift and the heating rate respectively, while the part $cx + d$ allows for a linear correction based on the inaccuracy when subtracting the baseline from the original signal. This linear correction greatly improves the quality of the fit, of which a closeup is shown in figure 5.6. The intersection between the red vertical, which is drawn at t_{close} line, and the

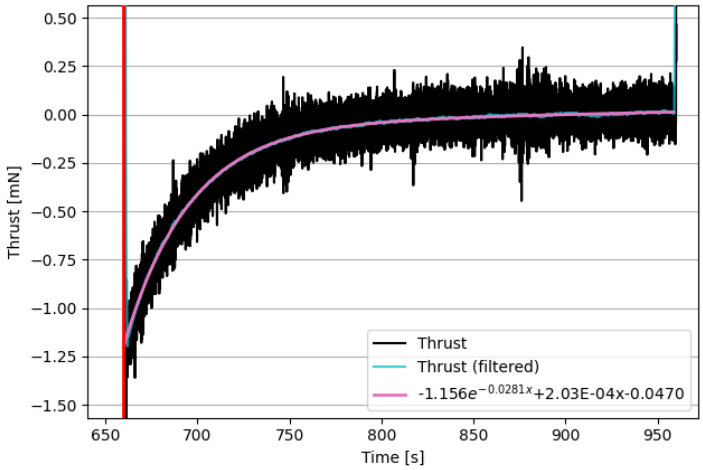

Figure 5.6: Closeup of measured thrust change due to thermal expansion. The intersection between the fit and red vertical line is the difference between hot and cold reference points.

fitted function is the difference between the reference thrust of the hot and cold tube. This difference is called Δ_T and is calculated using

$$\Delta_T = f(0) = a + d. \tag{5.2}$$

Since the state of the valve is recorded with a frequency of 2Hz, the error on t_{close} is 0.25 seconds. This error is included into the error of Δ_T on top of the errors derived from the convolution matrix from the fit. To calculate the produced thrust F_T, the Δ_T is subtracted from the average baseline corrected thrust F_m:

$$F_T = \overline{F_m} - \Delta_T \tag{5.3}$$

The baseline corrected thrust F_m is averaged over the last 50% of the thrust period to not include the transient effects at the start of the firing period. Added on top of the error of F_T is the error of the thrust as shown in table 3.4.

5.3.3. Thruster performance

Using the technique described in the section above the produced thrust was calculated for all experiments using nitrogen. A full list of all the measured parameters per experiment can be found in table A.5. The naming scheme of the experiments is "NIT-$X.Y.Z$" with X being the planned test ID from table 5.1, Y being the number of repeated tests, and Z being the consecutive thrust period inside a single thrust test. From these measured quantities the performance parameters from table 5.4 are calculated and can be found in table 5.8. Note that the consecutive thrust periods are not mentioned individually in this table meaning that they are averaged for brevity (both values and errors individually). Also the heating efficiencies of NIT-1 are not given since these are cold gas tests.

ID	$Re_{t,real}$ [-]	I_{sp} [s]	η_{heat} [-]	$\xi_{I_{sp}}$ [-]	C_d [-]
NIT-1.1	2617±17.8%	63.2±1.5%	-	0.915±2.0%	0.861±9.4%
NIT-1.2	2586±17.8%	63.5±1.4%	-	0.912±2.0%	0.860±9.4%
NIT-1.3	2644±17.7%	63.6±1.5%	-	0.915±2.0%	0.861±9.3%
NIT-2.1	1423±17.6%	77.9±1.5%	0.28±13.9%	0.877±1.7%	0.842±9.3%
NIT-2.2	1424±17.6%	78.4±1.6%	0.28±13.9%	0.882±1.9%	0.838±9.3%
NIT-2.3	1410±17.6%	78.8±1.6%	0.28±13.7%	0.887±1.8%	0.825±9.3%
NIT-3.1	2181±16.8%	78.3±1.4%	0.36±12.6%	0.883±1.7%	0.865±8.5%
NIT-3.2	2162±16.8%	78.9±3.1%	0.36±12.6%	0.890±3.3%	0.858±8.6%
NIT-3.3	2183±16.8%	79.3±2.7%	0.37±12.6%	0.894±2.9%	0.857±8.5%
NIT-4.1	1101±17.6%	84.9±1.9%	0.22±13.8%	0.867±2.1%	0.818±9.4%
NIT-4.2	1112±17.7%	84.5±1.8%	0.22±13.8%	0.860±2.0%	0.826±9.4%
NIT-4.3	1114±17.6%	83.9±1.8%	0.22±13.7%	0.853±2.0%	0.825±9.4%

Table 5.8: Performance parameters of the engine using nitrogen as propellant.

5.3.4. Comparison with previous work

Since the thruster is the same as produced by Versteeg [47] it makes sense to compare these results directly. Figure 5.7 shows the specific impulse as a function of chamber temperature. It has to be noted that in this graph the chamber pressure is not given, and explains in part the disparity between the obtained values for I_{sp} as the chamber pressure plays a small but non-zero contribution to the specific impulse. The error bars on the specific impulse are close to 2% which allows for accurate comparison between the obtained values. For the experiments at room temperature, the values for the I_{sp} are all within each others margin of error with an average difference of only ~0.8%, which validates the results of the nitrogen tests performed at room temperature in this thesis. Comparison of the specific impulse at 200 °C (473 K) to the data from Versteeg shows that the results from this thesis are on average 2.1 seconds higher. This disparity is believed to be mainly due to the fact that in the work by Versteeg in some cases the pendulum could not return to its equilibrium position, which is an indication that the measured thrust is underestimated. If the pendulum can' return to its equilibrium position it is impossible to calculate the results as the type of fit from figure 5.6 can not be made, this leads to inaccurate and inconsistent results. This inconsistency would also explain the decreased precision of the results by Versteeg. If the results are omitted where the pendulum could not return to its equilibrium position, the difference is on average 1.2 seconds, which is with ~1.5% difference within the margin of error of the specific impulse. The results from table A.5 show that the difference in equilibrium position of the pendulum depend on the chamber temperature and mass flow. This makes sense as more mass flow means more active cooling of the propellant tube, while a higher chamber temperature means the tube is cooled more as the difference in temperature between the stored propellant and the tube is greater, also increasing the amount of cooling. The NIT-3 experiment in this work is similar to the experiments TTH-3.3 and TTH-3.4 of the work by Versteeg [47] with respect to mass flow and chamber temperature.

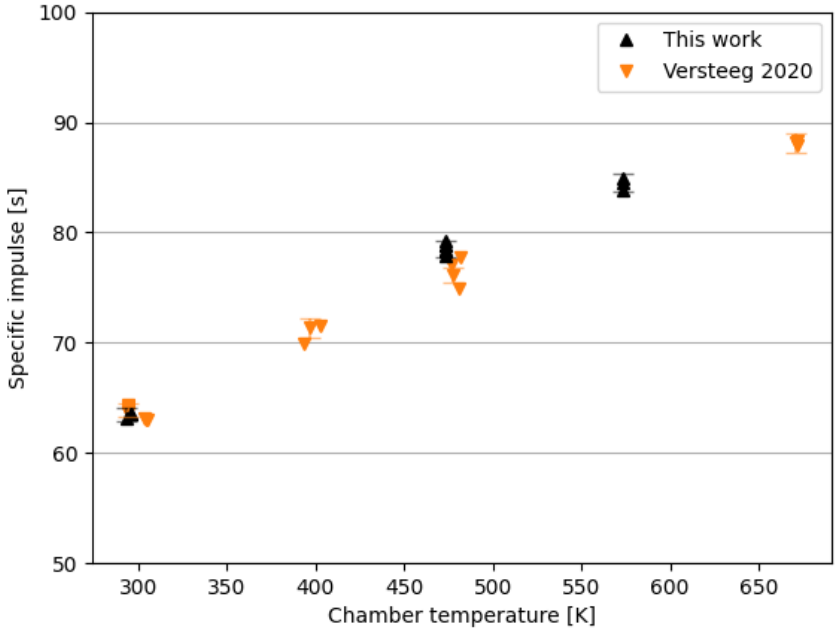

Figure 5.7: Specific impulse of nitrogen as a function of chamber temperature comparison between the results of Versteeg [47] and this work.

The change in measured thrust due to the lower equilibrium position of the pendulum by Versteeg is calculated using the values of $\xi_{F,exp,start}$ and $\xi_{F,exp,end}$ used in the work by Versteeg and is on average an increase of 5.1%. In this work the value is calculated by averaging the ratio Δ_T/F_T and is 6.9%. This slight difference can be explained and is expected as in the work by Versteeg the position is calculated after the tube has recovered for ±5 seconds, and the thrust period is only 20 seconds meaning less cooling of the tube. Also the mass flow of NIT-3 is slightly higher than the work by Versteeg, resulting in more cooling. This could partially explain the slight difference found in I_{sp}.

The discharge coefficient as function of the Reynolds number can be seen in figure 5.8. In this figure the results from this work are compared to the results from Versteeg [47] and Bayt [3]. The data from Bayt was presented in graphs and tabularized by Versteeg. Since the Reynolds number by Versteeg and Bayt are both defined by the throat viscosity instead of the chamber viscosity, the Reynolds number is converted using a factor of $\mu_c/\mu_t \approx 0.878$ for nitrogen and was also used for conversion by Versteeg [47]. The predicted results from both Kuluva and Hosack [21] and Tang and Fenn [40] overestimate the value of C_d compared to the results of the experiment. It has to be noted that the nozzle from Bayt [3] has different values for r_c and r_t which would lead to different expected theoretical values as shown in the graph. The value used for r_c is the design value of 260 µm, while r_t is the taken as half the hydraulic diameter D_h at the throat. The confidence bounds of on the calculated discharge coefficients is around 9% which is largely due to the inaccuracy of the nozzle throat area and the chamber pressure. It can be seen that the values obtained in this thesis of the discharge coefficient are significantly lower as expected by theory, and follow the calculated values of the cold gas tests by Versteeg within 1%. Compared to the results of the hot gas tests by Versteeg, the discharge coefficients are within each others margin of error, but the difference is larger. The hot and cold tests performed by Versteeg used different nozzle dimensions as the thruster was reassembled in between. If the nozzle dimensions were not accurately determined in preparation for the hot experiments, this could explain the difference in similarity found as the expected mass flow is heavily dependent on the throat area. Both experiments, performed in this thesis and the work by Versteeg show however that the expected values for the discharge coefficient does not predict the experimental values sufficiently. Possible reasons for this difference are discussed in section 5.4. The reduction in throat area that is found experimentally is

approximately 2.3x the value that is estimated in the model:

$$C_{d,exp} \approx 1 - \left(1 - C_{d,model}\right) \cdot 2.3 \tag{5.4}$$

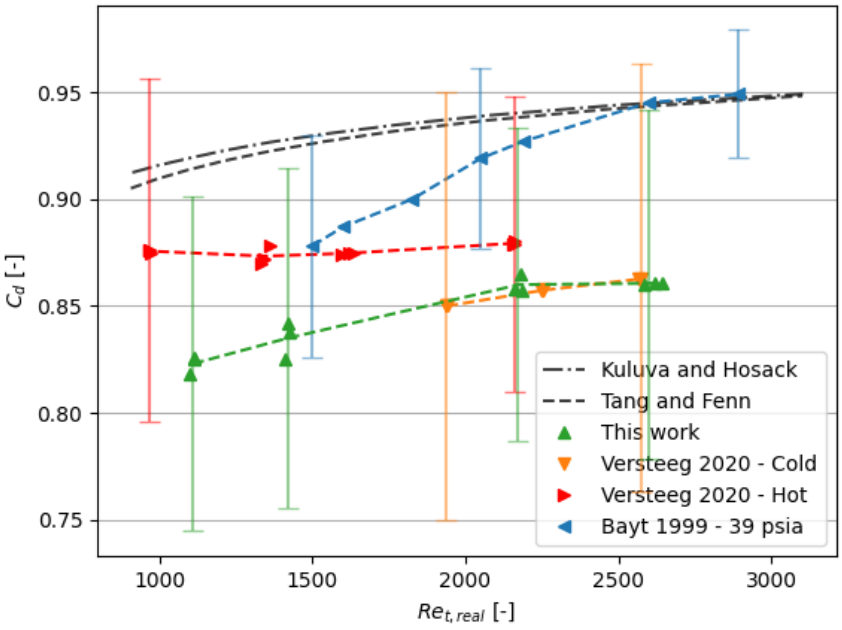

Figure 5.8: Comparison of the discharge factor as function of the Reynolds number at the throat. Theoretical C_d predictions by Kuluva and Hosack [21], Tang and Fenn [40] use the design values of r_c = 260 µm and r_t = 111 µm with $\gamma = 1.4$. Note that the thruster from Bayt [3] has different values for r_c and r_t.

Finally the I_{sp} quality as a function of the Reynolds number is compared to the values predicted by the analytical model and the values obtained in this work and the work by Versteeg [47] and Bayt [3] and can be found in figure 5.9. The values obtained in this work and by Versteeg show similar results within 5% which is in stark contrast to the results of Bayt and the predicted values. The predicted values of ξ_{C_F} are consistently lower than the values obtained through experimentation, especially at the lower Reynolds numbers. Since the values obtained are similar to the work by Versteeg, the results of both experiments are validated and imply that the used model to predict the viscous nozzle losses from equation 2.41 is not accurate for the thruster used. In section 5.4 it is discussed what possible reasons are for the discrepancy between the model and experimental results. The losses estimated in the model overestimate the experimentally obtained nozzle losses by a factor of approximately 2.9x:

$$\xi_{I_{sp},exp} \approx 1 - \left(1 - \xi_{I_{sp},model}\right) \cdot \frac{1}{2.9} \tag{5.5}$$

5.4. Discussion

In the data analysis it is assumed that the propellant tube expands and contracts due to temperature changes caused by whether the propellant is flowing through it or not. It has been shown that the effect of the change in measured thrust immediately after opening and closing the valve is temperature related, as the effect is not present in tests at room temperature, and increases in severity at higher temperatures. This can be seen in figure 5.3 and by looking at parameter Δ_T in table A.5. Although it is highly likely that the thruster mounting twists due to this change in temperature and therefore causes a change in measured thrust, it is not proof that this is the main and only cause of the effect. Testing

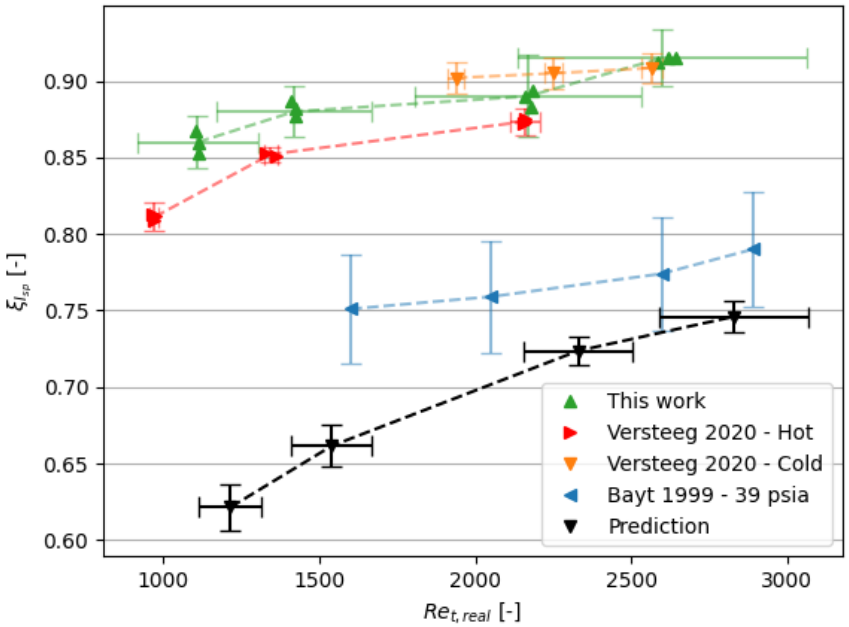

Figure 5.9: Comparison of the I_{sp} quality as a function of the Reynolds number at the throat using nitrogen as propellant in this work and the work by Versteeg [47] andBayt [3]. Predicted values are obtained from table 5.6.

the thruster on a different thrust bench that does not rely on the center of gravity of the setup could potentially resolve this assumption. The given accuracies on the performance parameters given in table 5.8 assume this is the case. Given that on average in the most extreme case $\Delta_T \approx 1.3$ mN for T_c = 300 °C and p_c = 1 bar, this is 18% of the measured 7.1 mN, which results in a large miscalculation of the produced thrust should the assumption be incorrect.

While testing it is unknown what exactly is the cause of the long term drift that is noticed when measuring the thrust. This drift can partly be explained by the heating of the thruster, which heat partly conducts through the thruster mounting changing the center of gravity of the pendulum as the effect was significantly smaller for tests at room temperature than at 200 or 300 °C but the size of which was not consistent enough to be a function of chamber temperature alone. Although not finding the exact cause of this long term drift can be unpleasing, the effect on the measurements is not significant as it can easily be corrected for in the data analysis. The biggest downside of this drift is that over time the thrust might no longer be measured as it can top-out of what the actuator coil can deliver as the actuator coil is maxed out at 10 A to prevent overheating.

In the NIT-3.2 and NIT-3.3 experiments an interesting effect was noticed in which the measured thrust would drop after a fixed amount of time after opening the propellant valve. An example of this can be seen in figure 5.10 of experiment NIT-3.3. The measured thrust drops by ~0.5 mN but no sign of a drop in either the mass flow or chamber pressure can be seen. If the sudden change in measured thrust is noticed at an unexpected time without a change in mass flow or chamber pressure, this can be explained by sliding of the pendulum pivot or the counter weight. However since this effect is found at fixed times after opening the propellant valve, this is very unlikely. Since no significant change in mass flow or chamber pressure is measured, it is unlikely that the measured effect is in fact thrust related. Possible causes for this effect are likely to be sought in the automatic behaviour of some control device used in the experiments due to its consistent behaviour, although no reasonable candidate could be found as they were all deemed unlikely in one way or another. Due to this effect, the error of the produced thrust for the NIT-3.2 and NIT-3.3 experiments are higher than the other experiments with nitrogen.

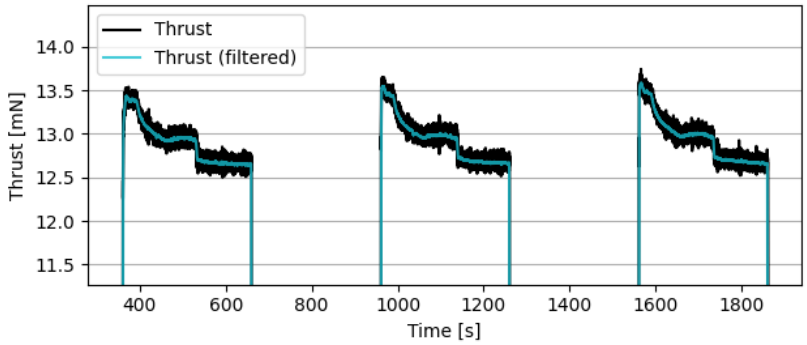

Figure 5.10: Unexpected drop in measured thrust at fixed times after opening the propellant valve.

Overall the accuracy of the produced thrust and specific impulse is (at least at room temperature) very accurate, and the I_{sp} can be calculated within ~1-2% in most cases. The accuracy of the discharge coefficient is lower, between 8-10%, and is limited by the inaccuracy of the nozzle exit and throat diameter measurements.

The values of the estimated quality factors C_d and $\xi_{I_{sp}}$ do not agree with the experimental values obtained. The experimental results are similar to the results obtained by Versteeg [47] which validates both experiments. The errors of the experimental values and prediction do not overlap, which means the used method is not correct for the thruster used. The models did look promising since the parameter ranges such as the Reynolds number, throat radius and specific heat ratio corresponds with the thruster used. The main difference between the assumptions used in the models and the used thruster is that the thruster does not have an axisymmetric (circular) nozzle. The nozzle throat area is in the shape of a rectangle and is not circular which means the assumptions of the boundary layer thickness in the throat can likely not be used for the rectangular shape. This also counts for the boundary layer losses in the diverging section of the nozzle from which the thrust coefficient losses are estimated. It is recommended to investigate the effects of two-dimensional nozzle shape on C_d and $\xi_{I_{sp}}$. However, the cause of the difference in expected and experimental performance may not be just as simple as the two-dimensional nozzle effects, as the thruster by Bayt [3] is also two-dimensional and the results are significantly closer to the modelled performance.

5.5. Conclusion

Thrust tests with a resistojet were conducted using nitrogen as propellant at cold and elevated temperatures up to 300 °C. Due to the thrust bench being sensitive to the Center of Gravity (CoG) of the thruster that is mounted to a hanging pendulum, changes in thermal expansion of the thruster mounting highly influence the measured thrust reducing the measured value by up to 15% of the actual produced thrust at T_c = 300 °C. This effect is up to 10% at T_c = 200 °C and is not present in cold thrust tests. Long duration experiments allowed accurate compensation of these effects which resulted in I_{sp} measurements up to 85 s at T_c = 300 °C with an accuracy of ±2%. Comparison of the results of experiments done by Versteeg [47] where thrust tests with the same thruster were performed showed similar I_{sp} values verifying both experiments. Comparison to data of Bayt [3] and Versteeg [47] of the discharge coefficient for similar Reynolds numbers are within the margin of error and are found to be between 0.82-0.87, although the error on the measured discharge coefficient around 9.5% is high due to the inaccurate measurements of the nozzle dimensions. The obtained discharge coefficients are lower than the theoretical values for C_d predicted by Kuluva and Hosack [21] and Tang and Fenn [40] by a factor approximately 2.3x. The obtained values for the propellant consumption quality $\xi_{I_{sp}}$ with respect to the Reynolds number are in accordance with the results obtained by Versteeg [47] but not with the results from Bayt [3]. The predicted values of $\xi_{I_{sp}}$ show a similar trend but are consistently lower by a factor of 2.9x compared to the experimental values. The differences between the model and experimental values are likely caused by the two dimensional geometry of the rocket nozzle.

6

Water testing

This chapter will describe the experiments that have been performed using water as a propellant. There are three main goals to be obtained by performing these experiments. For one the current VLM design can be validated meaning what parts of the design work well for future VLM design and which areas need to be improved. The same goes for the thrust setup such as the feed system and the mass flow measurements, are the developed methods sufficient or if they still require work. The results of the Resistojet Performance Tool (RPT) will be validated for water to strengthen the (lack of) validity of the model for nitrogen experiments. For example, the usage of nitrogen as propellant could be an irregularity in the model. Section 6.1 describes the main differences between gaseous and liquid testing and problems encountered that were found during exploratory tests. Section 6.2 contains the test plan, and section 6.3 the test procedure of the experiments. The test results are described in section 6.4 and discussed in 6.5. Finally, section 6.6 contains the conclusion of the water thrust tests and will answer the goals set for this chapter.

6.1. Differences between gaseous and liquid propellant

Although resistojets in essence can work with both, the differences between using nitrogen or water as propellant are many. For starters, water can't be used for cold gas propulsion for obvious reasons. Water needs a lot of energy to vaporize which limits the maximum flow and therefore thrust that can be sustained with respect to nitrogen due to the limited amount of power supplied by the energy source. Under gravitational forces gases fill volumes irrespective of thruster orientation, while liquids pool at the bottom while in free fall liquids (especially water) form droplets due to surface tension and spread less throughout volumes. Even if water is heated above its boiling point, small droplets may still exist inside the water vapor thereby reducing performance. This section will list the differences between using nitrogen and water for the used resistojet that impact the testing procedures and analysis of performed experiments that were encountered.

6.1.1. Droplet formation at propellant inlet

In the experiments with nitrogen performed by Versteeg [47] the propellant inlet was oriented on top of the chamber. However for water this presents a problem as it was found that water forms droplets due to its high surface tension which then fall inside the chamber resulting in sudden bursts of chamber pressure and produced thrust. A solution needed to be found in order to provide a steady supply of water vapor to the chamber. One option is to insert metal foam into the propellant tube that breaks up the droplet formation and transfer heat into the liquid water until it eventually vaporizes. This extends the heat transfer element further into the propellant tube. This option requires the propellant tube to be opened up, which is not ideal as it would potentially compromise the sealing capacity of the thruster. This is however considered a potential improvement for future designs. Luckily another much more simple solution exists. The thruster can be mounted onto the pendulum 'upside down' which means the propellant inlet is oriented on the bottom of the thruster. This means that no water droplets form and the water level rises towards the chamber until the wall temperature is hot enough for the water to vaporize. Figure 3.4 shows the heater mounted onto the thrust bench showing the propellant tube

on the bottom of the thrust chamber. This method was experimentally found to be sufficient to prevent small bursts of chamber pressure due to droplet formation.

6.1.2. Propellant rush into chamber

The second problem encountered in preliminary tests using water was that when opening the propellant valve an unexpected large volume of water was dispensed into the chamber. The mass flow was so high that the thruster would lose temperature too quickly and eventually liquid water started to come out of the nozzle. This causes a potentially dangerous situation as there is electrical equipment laying around in the vacuum chamber including power lines to the heaters and actuator coil. When it was noticed that liquid water came out of the thruster, all power supplies were turned off immediately and the propellant valve was closed. A solution for this problem needed to be found in order to continue testing with water.

Before opening the propellant valve, the pressure inside the tube that holds the propellant is around 1 bar, equal to the ambient pressure outside of the vacuum chamber. Since liquid water can be assumed to be incompressible, opening the propellant valve exposes the water to the low pressures of the vacuum chamber and the pressure inside the tube plunges. This sudden fall in pressure inside the tube causes two effects that both contribute to pushing water into the thruster chamber. First, the tube through which the propellant flows outside the vacuum chamber is flexible. This means that when the pressure inside the tube becomes less than the pressure outside the tube, the tube collapses slightly creating an ellipsoidal cross sectional shape instead of a circle as can be seen in figure 6.1. This ellipsoidal shape of the tube has a smaller internal volume, which means the extra volume of water is pushed towards the thruster. The second effect of the sudden drop in

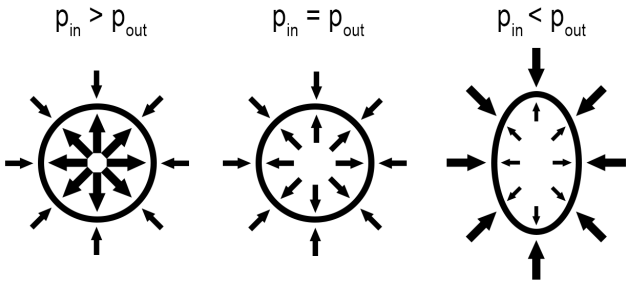

Figure 6.1: Flexible tube cross section depending on pressure inside p_{in} and outside p_{out} the tube. When the pressure outside is smaller or equal to the inside pressure the tube is circular but when the outside pressure is larger the tube shape becomes an ellipse decreasing the volume inside the tube.

pressure inside the tube is that small air bubbles inside the tube and syringe start to grow in size. Also since the solubility of air inside water decreases with decreasing pressures some of the dissolved gas comes out of the water and forms additional bubbles. These bubbles force the liquid water downstream into the chamber. Bubbles forming inside the syringe and tube can be seen in figure 6.2.

One way of solving this problem is by decoupling the water feed pressure from the chamber pressure by inserting a small orifice in the stream close to the chamber that limits and therefore regulates the maximum flow of propellant. In this case the feed pressure just needs to be high enough to reach the limit mass flow. The downside of this solution is that it fixes the mass flow for all experiments, although the chamber pressure can still variate by adjusting the chamber temperature. Another downside is that the setup has to be changed which introduced additional cost and time. A second solution to this problem is setting the mass flow such that the chamber pressure is roughly equal to 1 bar, and limiting the initial rush of propellant by PWM of the propellant valve. Limiting the initial rush of propellant allows the water to vaporize and build up chamber pressure working up to the 1 bar chamber pressure needed to prevent both problems. The PWM functionality of the valve was already implemented by Silvestrini [35], so only implementation into the LabView interface is needed. The downside of using this method is that the chamber pressure should be above 1 bar. For chamber pressures significantly higher than 1 bar the tubing should be checked for leakage and the maximum chamber pressure depends on the maximum power delivered by the heaters. Since this second solution requires significantly less effort

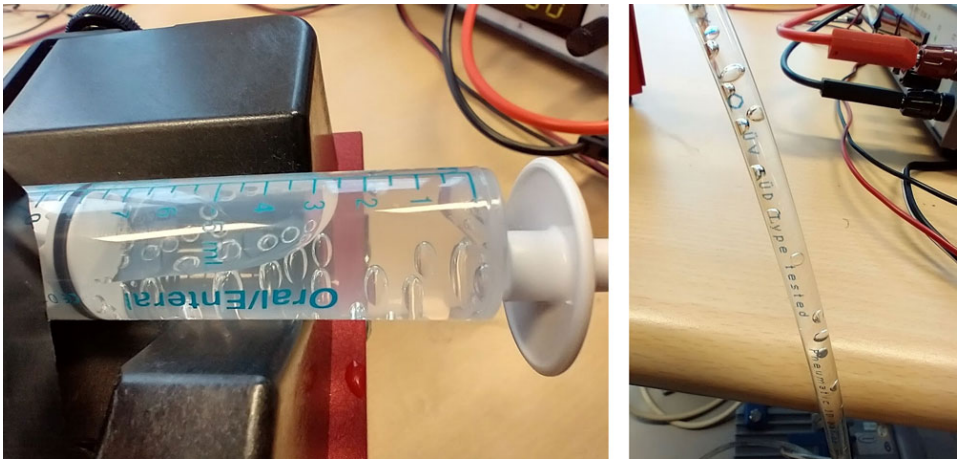

Figure 6.2: Bubbles forming inside the syringe (left) and tube leading up to the vacuum chamber (right) by

and is more feasible, it was chosen to implement the PWM functionality and using a chamber pressure of 1 bar for all liquid water experiments.

6.2. Test plan

This section describes the test plan for the experiments that are performed using water as propellant. The experiments will all be performed at a chamber pressure of 1 bar because of the problems mentioned in section 6.1.2. Although there are possibilities of changing the chamber temperature to get a better description of the thrusters properties, the experiments are only performed at 300 °C in the interest of time. A temperature of 300 °C was chosen as this was previously found to be a safe temperature to operate in without damaging the equipment, while minimizing effects of incomplete vaporization at temperatures closer to the boiling point. Table 6.1 shows the experiment that is going to be performed in this chapter. Note that while the experiment was planned to be repeated three times, one of the experiments was first believed to be compromised which later turned out to be fine for analysis resulting in a total of four repetitions. This is described in section 6.4.3.

ID	p_c [bar]	T_c [°C]
WAT-1	1.0	300

Table 6.1: Planned water thrust tests.

6.2.1. Test objective

The main purpose of this experiment is to gain experience with using liquids as propellant, find out what the biggest challenges are for experimentation and what this means for future thruster design and production at Delft University of Technology. Therefore unlike the nitrogen experiments performed in chapter 5, the aim is not to calculate the accuracy of the performance parameters within a certain accuracy, although it is of interest how the valid the model is for water. From the experiments with nitrogen it is known that the error of the discharge coefficient is around 10% due to the uncertainty in the nozzle dimensions and chamber pressure. If the error on the C_d or $\xi_{I_{sp}}$ quality is higher than with nitrogen, the goal is to find the causes of the decrease in accuracy and provide recommendations for future work to improve this.

6.2.2. Relevant parameters

The relevant parameters for this experiment are the same as for the nitrogen experiments. A difference between the nitrogen experiments and this experiment is the usage of a syringe pump to supply the propellant instead of the pressurized gas. Since the mass flow sensor that was used for nitrogen is not suitable for liquids, the mass flow can not be measured directly. Instead a syringe pump is used

to expel a specified volume of propellant per second which is then converted into a mass flow given the known density of water. Given this, table 6.2 shows the relevant parameters to be measured for the water thrust test. Next to the elements shown in this table, an extra parameter will be recorded is the propellant valve state, which can be opened partly using PWM. Although the value of which is not directly used in the analysis, it can be important for future experimentation to know how fast the valve was opened. Similar to the thrust experiments with nitrogen as propellant, table 6.3 shows relevant parameters that will be calculated from the measured parameters from table 6.2. Finally, table 6.4 shows the performance parameters that are be calculated from the experiment that will be used to describe the performance of the thruster.

Symbol	Description	Location of measurement
$\dot{m}$	Propellant mass flow	Set on syringe pump. Calculated using p_c, see section 6.4.2.
p_c	Chamber pressure	Measured at the end of the pressure sensing tube connected to the thruster. See section 3.1.
p_a	Ambient pressure	Measured inside the vacuum chamber.
T_c	Chamber temperature	Measured on the thruster on the metal profile. See section 3.1.
I_{act}	Current through the actuator coil	Measured internally by the power supply.
I_{heat}	Heater current	Measured internally by the power supply.
V_{heat}	Heater voltage	Measured internally by the power supply.
T_{tube}	Temperature of the propellant tube	Measured at three different locations along the propellant tube. See section 3.1.

Table 6.2: Relevant parameters to be measured for the tests using water as propellant.

Symbol	Description	Dependent on
F_T	Thrust force	I_{act}
P_{heat}	Heater power	V_{heat}, I_{heat}

Table 6.3: Relevant parameters to be calculated for the tests using water as propellant.

Symbol	Description
I_{sp}	Specific impulse
η_{heat}	Heating efficiency
$\xi_{I_{sp}}$	Propellant consumption quality
C_d	Discharge coefficient

Table 6.4: Relevant parameters that are used for describing the performance of the thruster.

6.2.3. Acceptance criteria

Table 6.5 shows the acceptance criteria that have been set to define a successful water thrust test. Criteria AC-WAT-01 ensures that all parameters that need to be measured are being recorded. Criteria AC-WAT-02 ensures that the thrust that is being produced is supersonic. Although the exhaust velocity is not directly measured, it can be calculated if equation 2.10 is satisfied. AC-WAT-03 ensures that the

performance parameters resulting from the analysis can be calculated. Acceptance criteria AC-WAT-04a and AC-WAT-04b ensure that the chamber temperature is withing 5% of the targeted temperature and remains constant (max ±1% deviation, excluding sensor noise) over the course of the experiment. Lastly, criteria AC-WAT-05 ensures that the chamber pressure stays within an acceptable deviation of the targeted value from table 6.1. This excludes the first 10 seconds of the test and only includes the filtered values to exclude the signal noise. A deviation of 10% was chosen as the chamber pressure is determined by the mass flow which is not as easily manageable as with nitrogen. In the end, the main reason to stay close to 1 bar is to prevent the collapse of the flexible propellant tube and expansion of gaseous bubbles inside the feed line.

ID	Description
AC-WAT-01	All parameters from table 6.2 are measured over time through their respective sensors.
AC-WAT-02	The exhaust is supersonic.
AC-WAT-03	The performance parameters from table 6.4 can be calculated.
AC-WAT-04a	The measured chamber temperature remains constant during operation.*
AC-WAT-04b	The average chamber temperature is within 5% of the target.
AC-WAT-05	The chamber pressure remains within 10% of the target.**

* Maximum deviation of ±1% of average value excluding sensor noise, first 10 seconds of startup excluded.

** Excluding sensor noise, first 10 seconds of startup excluded.

Table 6.5: Acceptance criteria for water thrust test

6.2.4. Test predictions

This section contains the values from the analytical model for the experiments that are going to be performed in this chapter. This will make sure the resulting output parameters are within the capabilities of the testing equipment and allows for comparison with the experimental results. The input and output parameters of the analytical model for the performed experiments are shown in table 6.6. The values in this table are the ideal values and thus are uncorrected for the estimated correction factors. The obtained mass flow will act as a guide to what the setting of the syringe pump will need to be in order to obtain a chamber pressure of 1 bar. From table 6.6 the expected mass flow is 9.08 mg/s. Using the results from the syringe pump calibration as shown in equation 4.7, the syringe pump was set to 32.00 mL/hr. From the nitrogen tests, it was found that the total heating power required to keep the temperature stable at 300 °C in the first 5 minutes of the experiment before opening the propellant valve requires around 8.2 Watt. Adding this to P_h, the energy required to heat up the propellant from room temperature up to T_c is 37.4 Watt, which is smaller than the maximum of 50 Watt the two heaters together are rated for.

One possible issue with the predicted values is that at the nozzle exit a pressure of 13.7 mbar and a temperature of 212 K (-62 °C) is predicted, at which water is not gaseous but solid. This is calculated using equation 2.12 but this assumes a constant specific heat ratio γ, the propellant to be gaseous and ignores latent heat of phase changes. The effects of possible condensation of the exhaust gasses on the produced thrust are difficult to model and should ideally be avoided in a new design.

6.3. Test procedure

Experiments with water will have slightly different procedures than the experiments performed with nitrogen. For example the feed system is different with water but also the procedures for the thrust measurement itself will be different. Instead of having three thrust intervals in a single test, the experiments with water will have only one interval. One reason for this is that since water is involved it is expected that some liquid water will remain downstream from the propellant valve for some time which makes multiple consecutive tests difficult. Another reason is that since the mass flow is not measured by a mass flow sensor, it is advantageous to have a single long thrust period so that transient effects are as small as possible. The syringe used has an internal volume of 10 mL and the mass flow is set to 9 mg/s, the maximum thrust time is around 18.5 minutes. Because of this the

		WAT-1	±[%]
Input			
T_c	[K]	573	1.2
p_c	[mbar]	1000	5.0
p_a	[mbar]	5.00	50.0
A_t	[10^3µm^2]	75.32	7.8
A_e	[10^3µm^2]	580.0	1.7
H_t	[µm]	538	1.5
θ	[°]	20	0.0
Output			
Ideal			
γ	[-]	1.30	0.1
F_T	[mN]	12.23	9.1
$\dot{m}$	[mg/s]	9.78	9.3
I_{sp}	[s]	127.5	1.4
c^*	[m/s]	770	0.6
C_F	[-]	1.62	1.2
P_h	[W]	29.2	9.2
Re_t	[-]	1420	8.1
p_t	[mbar]	545	5.0
T_t	[K]	498	1.3
U_t	[m/s]	551	0.6
p_e	[mbar]	13.7	11.3
T_e	[K]	212	2.8
U_e	[m/s]	1198	0.9
Expected			
C_d	[-]	0.929	0.3
$\xi_{I_{sp}}$	[-]	0.663	2.1
ξ_{F_T}	[-]	0.616	2.4
F_T	[mN]	7.53	11.5
$\dot{m}$	[mg/s]	9.08	9.6
I_{sp}	[s]	84.50	2.5
Re_t	[-]	1351	8.4

* Tang and Fenn [40] - Kuluva and Hosack [21]

Table 6.6: Input and output parameters of the analytical model showing the predicted parameters for the tests to be performed using water as propellant.

thrust duration was chosen to be 15 minutes in order to leave some margin for convenience. Since after closing the valve the measured thrust will not be as clean as the experiments with nitrogen, the period before opening the propellant valve will be increased from 5 to 15 minutes to better determine the drift. After the propellant valve is closed again, it is difficult to estimate beforehand how long the recording of data should continue to capture the necessary data to reconstruct the signal drift. When the test was first performed, this end time was not set. During the experiments it was determined that 30 minutes for this is enough. This section will describe the test procedures for the setup, thrust measurements and shutdown of the thrust experiments with water as propellant. The test procedure is separated into four different phases and are in order:

1. Prepare test setup
2. Environment setup
3. Thrust measurement
4. Experiment shutdown

6.3.1. Prepare test setup

This section contains the step by step procedure to make sure all equipment is connected and working. The steps to prepare the test setup are:

1. Turn on equipment that require warm up:
   (a) Turn on the SM-7020, SM-7020-D, ES-030-10, E-030-1 and D-030-1 power supplies (warm-up time: 60 min).
   (b) Plug in the power to the Brooks 5850S 2000sccm mass flow sensor. (warm-up time: 45 min).
   (c) Plug in the power to the Micro-Epsilon DT6220/DL6230 distance sensor DAQ. (warm-up time: 15 min).
2. Connect the test bench to the computer and equipment:
   (a) Install the thruster on the test bench as described in section 3.4.
   (b) Move the test bench inside the vacuum chamber.
   (c) Turn the adjustable feet on the test bench such that the bench is level.
   (d) Connect the connector of the p-T sensor to the NI USB-6008 and NI USB-8451 DAQs.
   (e) Connect the distance sensor cable to the CS2 sensor.
   (f) Connect the propellant feed to the quick connect inside the vacuum chamber.
   (g) Plug in the cables of the actuator coil in the power feedthrough in the vacuum chamber. Make sure the cables are as perpendicular to the coil as possible.
   (h) Plug in the cables of both heaters in the power feedthrough in the vacuum chamber.
   (i) Make sure all connections on the power feedthrough match up to the correct power supplies outside the vacuum chamber.
   (j) Plug in the thermocouples into the NI 9211 DAQ.
   (k) Connect the red and black jumper cables inside the vacuum chamber to the connector pins on the MINSTAC valve. Route the wires over the pivot and parallel to the rotational axis with the other wires. Secure the cable with tape.
   (l) Verify that the pendulum can rotate freely.
   (m) Turn on the computer and open the LabView program.
3. Test if all sensors are working:
   (a) Specify a folder and test name and click **Run** to start the LabView program.
   (b) Verify that all temperature sensors are reading around 20°C.
   (c) Verify that all pressure sensors are reading around 1 atm.
   (d) Open the MINSTAC valve. Slide the valve PWM slider halfway and verify a fast clicking sound from the MINSTAC valve. Close the valve.
   (e) Turn on one of the heaters at 20 Watt and verify that the temperature of the thruster is going up. Turn the heater off. Repeat this step for the other heater.
   (f) Set the pendulum equilibrium position of the pendulum using the counterweights such that it sits anywhere between 500 and 1000 µm.
   (g) Set the setpoint of the pendulum distance to around 75 µm above the pendulum equilibrium and turn on the PID of the actuator coil. Verify that the pendulum is brought to the given setpoint. The current through the actuator coil should be 2±0.5A. Adjust the setpoint distance if the current is not in this range. Turn the PID of the actuator coil off.
4. Prepare the water feed system:
   (a) Connect one end of the water propellant tube into the Swagelok connection to the vacuum chamber.

(b) Open the MINSTAC valve fully to allow air inside the tubing to escape.

(c) Draw water into the syringe and slowly insert it into the tube. Make sure to not create any air pockets in the tube.

(d) The tube can hold multiple syringes worth of water. Fill the tube until the front of the water reaches the vacuum chamber. It takes around an entire syringe (10 mL) to fill the Swagelok interface through the vacuum chamber until the water can be seen again inside the tube in the vacuum chamber.

(e) Very slowly press the syringe until the water can be seen in the propellant tube inside the vacuum chamber. The tube is very small and the propellant will travel very quickly. Continue to fill the tube until the front of the water is around 5-10 cm away from the MINSTAC propellant valve entrance.

(f) Close the MINSTAC propellant valve. This ensures that the water will stay in the same location.

(g) Completely fill the syringe for the last time with water. Make sure there are as little air bubbles in the syringe as possible and connect to the propellant tube.

(h) Place the syringe in the syringe pump, as shown in figure 4.7.

(i) Turn on **(don't start!)** the syringe pump and set the dispensed volume to the desired value. (In this case 32.00 mL/hr).

(j) Open the MINSTAC propellant valve while watching the water level in the tube. Finding the water level can be difficult to spot.

(k) Start the syringe pump which will slowly push the syringe. Turn the pump off when the water level reaches the entrance of the MINSTAC propellant valve.

(l) Close the MINSTAC valve. Slide the PWM slider to zero (fully closed).

5. Stop the LabView program:

(a) Click on the **STOP TEST** button to stop recording data.

(b) Wait at least 5 seconds to ensure all data is being written to the file.

(c) Click on the **Abort Execution** button to stop the LabView program.

6.3.2. Environment setup

This section describes the steps to turn on the vacuum chamber and heat up the thruster. These procedures require the completion of the procedures listed in section 6.3.1.

1. Turn on the vacuum chamber:

(a) Specify a folder and test name and click run to start the LabView program.

(b) Make sure the heating power is set to 0 Watt and the temperature control setpoint to 0 °C.

(c) Make sure the vacuum chamber door is properly closed.

(d) Turn the handle on the vacuum chamber such that the connection to the vacuum pump is open.

(e) Rotate the black knob on the vacuum chamber such that the vacuum chamber is closed off from the outside air.

(f) Turn on the vacuum pump and make sure the pressure sensors in the LabView program show that the pressure is decreasing.

2. Preheat thruster to desired temperature:

(a) Wait for the vacuum chamber to have reached a pressure of 100 mbar or lower.

(b) Turn on the heaters by setting the power level of the individual heaters to max 20 Watt and selecting **Power Control** by clicking the heating control selector button.

(c) Continue heating until the chamber temperature has reached a temperature of 10 °C below the desired temperature. Set the heating power to 0 Watt.

(d) Set the input of the temperature controller to the desired temperature and click the heating control selector button to select **Temperature Control**. The temperature will now automatically rise to the desired temperature.

3. Wait up to 5 minutes for the temperature oscillation to stabilize to an acceptable range (±1 °C) and for the pressure inside the vacuum chamber to reach 5 mbar or lower.

Note: Do not stop the LabView program yet! Stopping the LabView program will stop the control of the chamber temperature. The time between stopping this test and starting the thrust measurements should not be much longer than 10 seconds to keep the chamber temperature stable. The procedures for stopping the current program and starting the measurements for the test are listed in section 6.3.3.

6.3.3. Thrust measurement

This section describes the procedures for performing a thrust measurement. These procedures require the completion of the procedures for the environment setup listed in section 6.3.2. Some of the following procedures are time sensitive so in order not to miss the time window for a certain step, please read the procedure in full and locate all buttons on the LabView interface before starting the first step. At every step try to keep in mind the upcoming procedures. **Important: as mentioned in section 6.1.2, when opening the propellant valve first set the PWM slider to zero, click the button to open the propellant valve (it's still closed as the PWM is set to zero duty cycle), and slowly slide the slider to fully open over the course of ±5 seconds.**

1. Start the measurements:

   (a) Specify a folder and test name to save the upcoming thrust measurement.

   (b) Repeat step 3g of section 6.3.1 since the change in temperature and chamber pressure might change the equilibrium position of the pendulum.

   (c) Turning off pendulum distance control releases the pendulum. Wait until the pendulum distance amplitude has reached a minimum (±30 to 60 seconds).

   (d) Click the **STOP TEST** button to stop the LabView program started for the environment setup.

   (e) Click on the **Abort Execution** button to stop the LabView program.

   (f) Click on **Run** to start the LabView program to start recording for the thrust measurement.

2. Perform the test:

   (a) Perform the actions from table 6.7 at the given time.

   (b) During the experiment, make sure the variables shown in the LabView interface are within the expected values.

3. Stop the test:

   (a) At the end of the experiment, stop recording using the **STOP TEST** button.

   (b) Press the **Abort Execution** button to stop the LabView program.

Time	Actions
0:00	Start recording
1:00	Turn on the actuator coil PID control
16:00	Turn on the syringe pump ⇒ open the propellant valve
31:00	Close the propellant valve ⇒ turn off the syringe pump
61:00	Turn off the actuator coil PID control
62:00	Stop recording

Table 6.7: Actions to undertake during the water thrust measurement.

6.3.4. Experiment shutdown

After the experiment is finished, there are several steps that need to be taken to make sure the experiment is safely shutdown. The thruster can be hot and the vacuum chamber is under low pressure. The following steps should be taken in order to safely shutdown the experiment without damaging the equipment.

1. Turning off power:
   (a) Specify a folder and test name and click run to start the LabView program.
   (b) Make sure the heating power is set to 0 Watt and the temperature control setpoint to 0 °C. Note that the temperature of the thruster is dropping.
   (c) Make sure the actuator coil PID control is off.
   (d) Make sure the MINSTAC propellant valve is closed.
   (e) Stop the LabView program.
2. Stop the vacuum pump:
   (a) Turn the handle on the vacuum chamber such that the connection to the vacuum pump is closed.
   (b) Turn off the vacuum pump. Some air will go through the vacuum pump in the opposite direction to fill the tube leading to the vacuum chamber (where the tube is shut off). If air is moving through the pump in the opposite direction for more than 3 seconds, which can be noted by the sound of the pump being forcibly rotated by the outside pressure, quickly turn the pump back on and verify the vacuum chamber is properly shut off from the pump and try again. Air moving in the opposite direction than what the pump is designed for can damage the pump.
   (c) DON'T TURN THE VACUUM CHAMBER VENT VALVE! Keep the vacuum chamber under low pressure as long as the thruster is still hot to prevent oxidation of the thruster.
3. Turn off the equipment:
   (a) Turn off the SM-7020, SM-7020-D, ES-030-10, E-030-1 and D-030-1 power supplies.
   (b) Unplug the Brooks 5850S 2000sccm mass flow sensor.
   (c) Unplug the Micro-Epsilon DT6220/DL6230 distance sensor DAQ.
   (d) Turn off the syringe pump.
4. Release the vacuum of the vacuum chamber:
   (a) Wait for the temperature of the thruster to be below 40 °C so it can be safely touched. This can take up to several hours. Check the temperature by starting the LabView program.
   (b) Release the vacuum of the vacuum chamber by rotating the vent valve.
5. Dismantle the water feed system:
   (a) Specify a folder and test name and click run to start the LabView program.
   (b) Take the syringe from the syringe pump.
   (c) Disconnect the syringe from the propellant tube.
   (d) Place the end of the propellant tube, which is still filled with water, in a container that can hold the water inside the tubing.
   (e) Make sure the end of the propellant tube is below the thruster so that the water from the propellant tube siphons into the container.
   (f) Open the propellant valve to allow air to enter through the thruster. The water will start to drain into the container.
   (g) If there are small water pockets left in the tube it is possible to pull them out with the syringe.

6. Dismantle the thrust bench:
   (a) Open the vacuum chamber door.
   (b) Disconnect the heaters and actuator coil from the power supply inside the vacuum chamber.
   (c) Disconnect the temperature sensors from the DAQ.
   (d) Disconnect the propellant Swagelok Quick Connect inside the vacuum chamber.
   (e) Disconnect the distance sensor inside the vacuum chamber.
   (f) Disconnect the p-T sensor.
   (g) Carefully take out the test bench from the vacuum chamber making sure no wires are still connected. Note that the test bench is heavy.
   (h) Place the vacuum chamber outside the vacuum chamber and close the vacuum chamber door.
   (i) Dismantle the thruster from the test bench.

6.4. Test results

The test results of the relevant parameters are shown in figure 6.3. The chamber pressure shown in 6.3a shows significantly more noise compared to the nitrogen test in figure 5.1a with pressure spikes in the range of ±200 mbar. As can be more easily seen by the filtered signal, the chamber pressure also seems to rise slowly over time by around 100 mbar in total. The chamber temperature from figure 6.3b shows a larger decrease in temperature when the valve is opened but stays within 10 °C of the target temperature of 300 °C. The ambient pressure in figure 6.3c shows similar pressures compared to nitrogen and maxes out around 5 mbar. The required heating power is with around 36 Watt as expected. The measured thrust in figure 6.3e shows a steady signal drift similar to nitrogen in the first and last ±15 minutes and the thrust period can clearly be recognised. Figure 6.3f shows the temperature of the propellant tube at the same three locations as the nitrogen test. And finally, figure B.1 in the appendix shows the state of the propellant valve where it was slowly opened over a time period of around 5 seconds for future reference. Note that the mass flow is not shown in figure 6.3 since this is not measured using the MFC like was the case with nitrogen testing. The mass flow for these experiments was set through a constant volume flow by the syringe pump. An attempt to estimate an accurate mass flow was made in section 6.4.2. An important difference with the nitrogen thrust test is that with water the measured thrust does not show the characteristic drop as seen in figure 5.1f. Instead, there is a period of ±15 minutes right after closing the valve, t_{close}, where the measured thrust behaves erratically before it returns to a more steady signal comparable to the long term drift before opening the valve and also found in the nitrogen tests. This period of erratic behaviour is also visible in the chamber pressure, chamber temperature, and propellant tube temperatures meaning that there is still some vaporization of the liquid water resulting in produced thrust and chamber pressure. This makes it more difficult to determine the actual produced thrust, as the effect of the thermal expansion of the propellant tube is not directly visible.

6.4.1. Identifying different experiment phases

This section describes the characteristics of the experiment that are seen in figure 6.3. When closing the propellant valve in the nitrogen experiment, the remaining nitrogen trapped downstream of the valve escapes through the nozzle within a second. With water however, there is a significant period of around 15 minutes after closing the valve where the chamber pressure and measured thrust are behaving unpredictably. Figure 6.4 shows the drift corrected thrust (see section 6.4.3) and chamber pressure together with the different numbered phases that are identified in the water thrust experiment. Phase 1 is the phase where drift is measured and the propellant valve is closed so no thrust is produced. Phase 2 is the thrust phase where the propellant valve is open and the syringe pump is on. In phase 3, 4, and 5 the propellant valve is closed and the syringe pump is on, however only in phase 5 are the chamber pressure and measured thrust constant and predictable. Phase 3 is signified by jittery thrust and chamber pressure, whereas the data from phase 4 is more more smooth. It can not be said with certainty what the processes are that cause this kind of behaviour in phases 3 and 4, for which more data is needed. Since the thruster and propellant tube are not transparent, it is difficult to know how

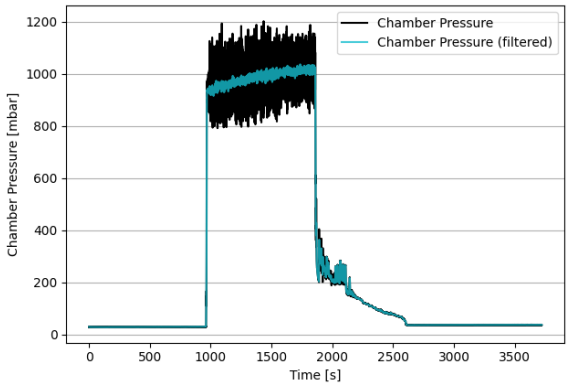

(a) Chamber pressure

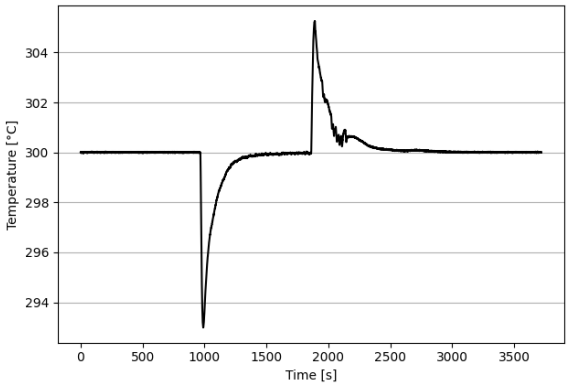

(b) Chamber temperature

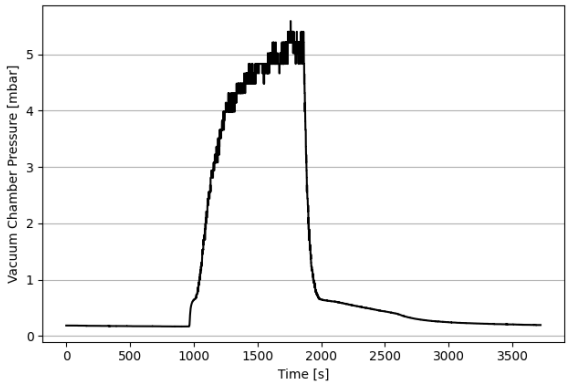

(c) Ambient pressure

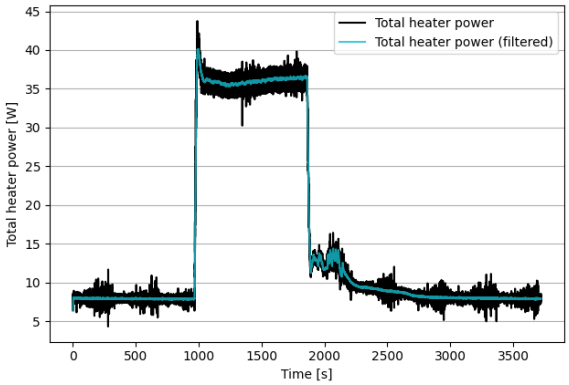

(d) Total heater power

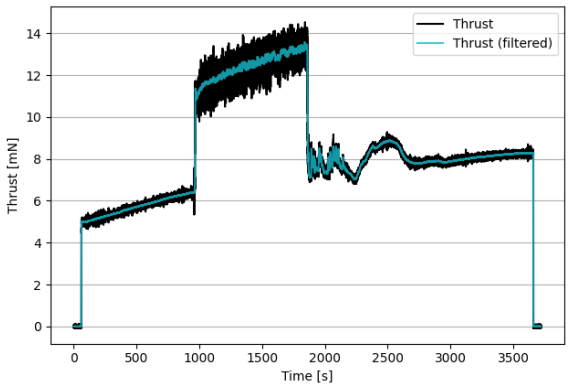

(e) Measured thrust

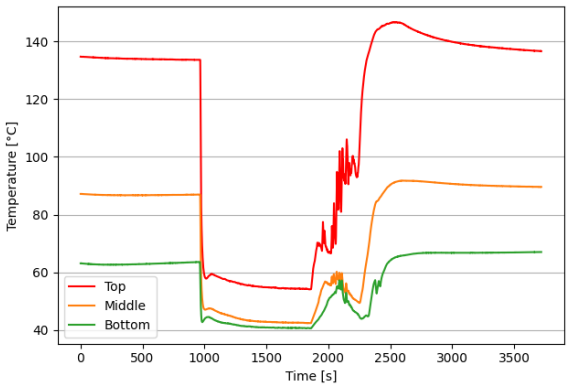

(f) Propellant tube temperatures, see section 3.1.

Figure 6.3: Relevant parameters measured during water thrust test.

much propellant is in the tube and how much of it is boiling. However there is a small plastic tube that connects the propellant valve with the metal propellant tube through which some visual observations could be made. It was observed that at around minute 36 (2160 seconds) gaseous bubble started to appear, which coincides with the transition between phase 3 and 4. These bubbles increased over time and eventually pushing pockets of liquid water up towards the thruster. Around 41 minutes (2460 seconds) in, the plastic tube seemed to be almost void of any liquid, which roughly coincides with the peak in measured thrust in phase 4. A close-up of phase 3 is shown in figure 6.5, which shows the positive correlation between the chamber pressure and measured thrust which indicates that the jittery

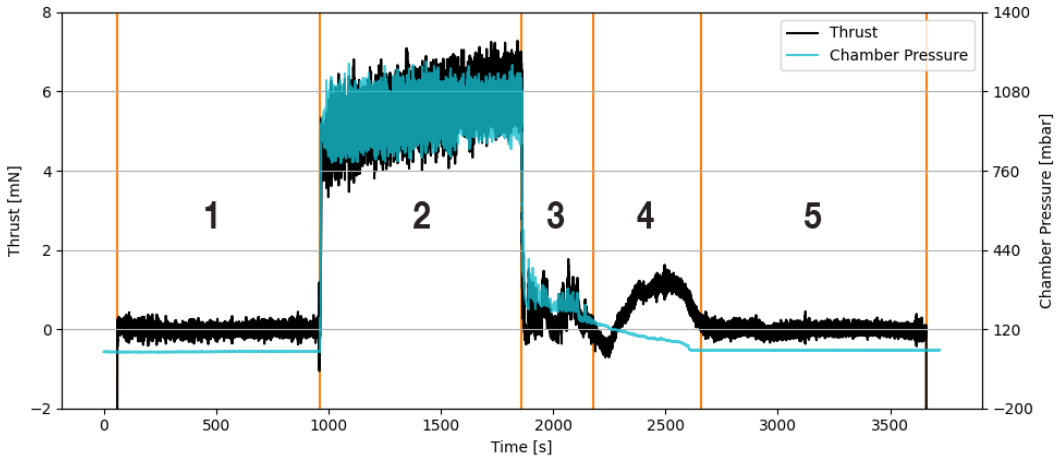

Figure 6.4: Identified phases in the water thrust experiment.

behaviour is not simply a large amount of noise, but actual thrust that is being produced in small bursts. These visual observations and sensor data make it possible to identify processes that could potentially

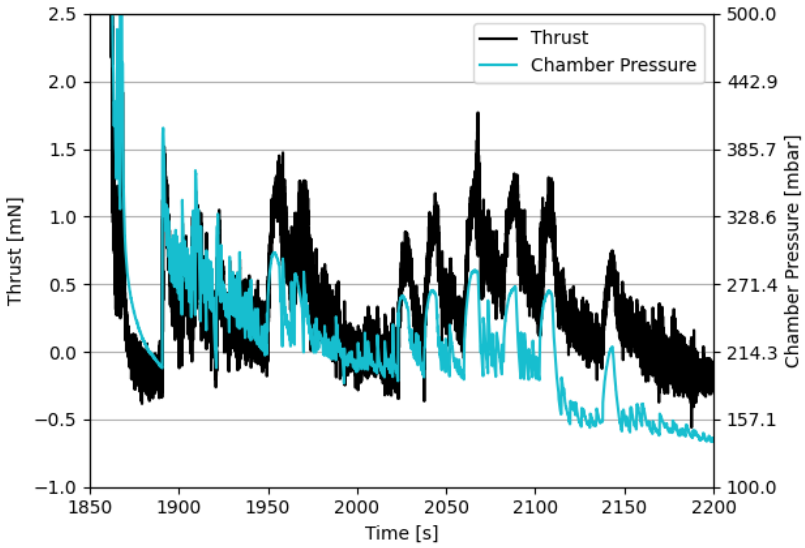

Figure 6.5: Comparison of the measured thrust and chamber pressure after closing the valve showing that thrust is produced in small bursts.

be the cause of the observed behaviour in phases 3 and 4. The bursts of thrust could be the cause of the unsteady formation gaseous bubbles in the liquid water that form from the combination of elevated temperatures together with the decrease in pressure, which evaporates the water but also releases the dissolved air inside the liquid. These pockets of gas form inside the liquid water, rise to the water level inside the tube and eventually pop. This would explain the sudden rises in pressure and thrust. In phase 4 the pressure inside the chamber is slowly but steadily decreasing meaning there are no large bubbles being formed but the water is steadily evaporating. The measured thrust in phase 4 is curious, since it does not corresponds together with the chamber pressure, indicating that it is not actual produced thrust but rather a result of how the thrust is measured and how it is dependent on the CoG of the pendulum, which is influenced by the changing temperatures and change in water level. This could possibly be a point for future research, however it is believed to be more effective to invest in a different

thruster and thrust bench in which these believed causes are not influencing the measurements. More on future recommendations can be read in chapter 8.

6.4.2. Estimating mass flow

Determining the mass flow of water is done in a different way than with nitrogen where it can be measured directly using the mass flow controller. Although the syringe pump is set to a constant volume flow, since the volume between the propellant valve and the chamber is significant, the propellant flow into the chamber when opening the valve and the mass flow lags behind for the duration of the test, as described in section 6.1.2. Looking at figure 6.3a, the chamber pressure rises over the duration of the experiment which can in part be explained by the decrease in chamber temperature in the first half of the experiment, but since the second half of the thrust duration the chamber temperature is constant, this is a clear indication that the mass flow is increasing as well. The rise in chamber pressure is however not constant and the increase is diminishing over time indicating that a constant chamber pressure is reached if given enough time. To find the pressure that the chamber pressure will eventually rise to, the chamber pressure is fit over the duration of the test (minus a 10 second margin) with the following function:

$$f(x) = -a \cdot e^{-bx} + c \tag{6.1}$$

with $a, b, c > 0$ where c is the pressure that the chamber pressure will rise towards over time, from now on called p_0, a and b scaling factors, and x the time in seconds local to the fitting window. A result of this fit can be seen in figure 6.6. Assuming the increase in pressure is due to the recovering mass flow, the chamber pressure at the set mass flow $\dot{m}_{set}$ on the syringe pump is equal to p_0. Equation 2.11 shows that at constant temperature, constant specific heat ratio, and constant throat area (including boundary effects), the ratio between the mass flow and chamber pressure is constant. These assumptions are not far from reality, as the chamber temperature deviates more than 1% for just 20 seconds with a maximum of 1.1%. The changes in pressure and temperature will have a small effect on the Reynolds number, but not enough to change the throat area by a significant amount as 5.8 shows C_d is fairly consistent over a wide range of Reynolds numbers. Also pressure changes of ~10% have insignificant effect on the specific heat ratio. With these assumptions the ratio $p_c/p_0 = \dot{m}/\dot{m}_{set}$ holds true which allows for the calculation of the mass flow during the experiment. For every experiment performed with

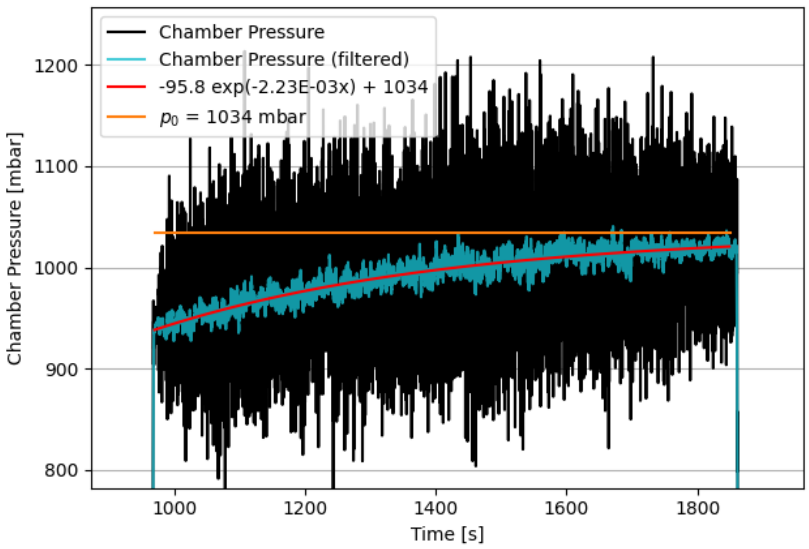

Figure 6.6: Rise in chamber pressure due to recovering mass flow in thrust test with water as propellant.

water, the syringe pump was set to pump 32.00 mL/hour which using the results from 4.2.2 results in a mass flow of $\dot{m}_{set}$ = 8.986 mg/s. The reconstructed mass flow can be seen in figure 6.7.

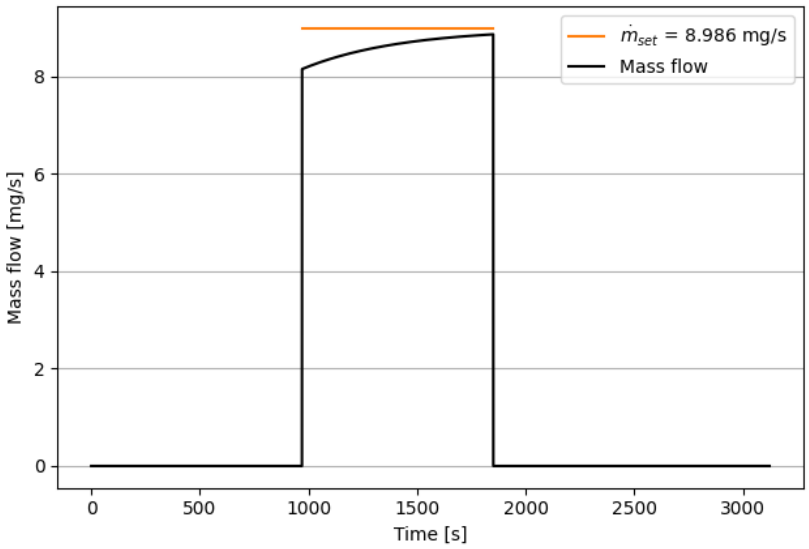

Figure 6.7: Reconstructed mass flow based on the changing chamber pressure during the water thrust test. For reference, $\dot{m}_{set}$ shows the mass flow set on the syringe pump.

6.4.3. Thrust analysis

Applying the same steps taken in section 5.3.1 with nitrogen, the measured thrust is first corrected for the heater power as shown in section 4.4. After this, the long term drift from the measured thrust in figure 6.3e. A long term drift is visible that ranges from ~5 to ~8.25 mN over the duration of the experiment. A fit was made on the first and last 15 minutes of the test so that the erratic behaviour after closing the propellant valve as mentioned before has no influence on the fit. Instead of fitting a quadratic polynomial like with the nitrogen thrust test, a polynomial of order 3 was used as the shape of the drift was more complex than with nitrogen. The thrust from figure 6.8b shows the thrust corrected for

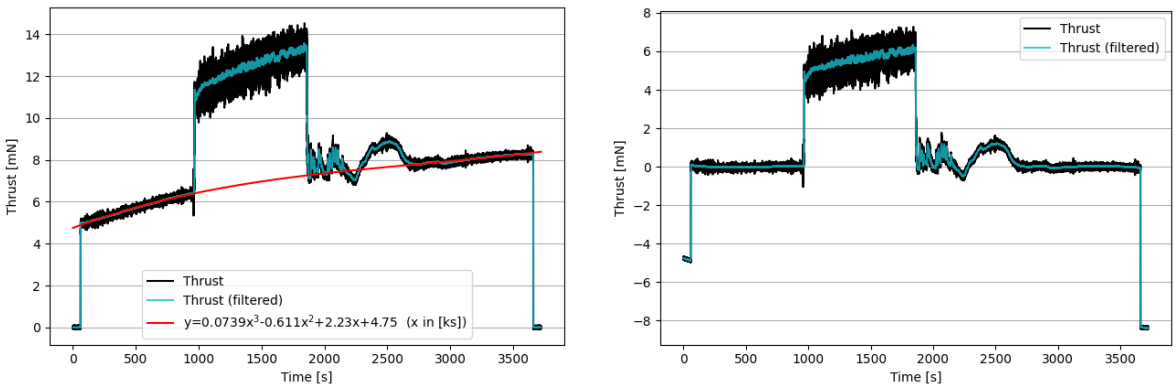

(a) Measured thrust together with the baseline showing in red in terms of kiloseconds.

(b) Baseline corrected thrust

Figure 6.8: Measured thrust and drift correction for water thrust test at 300°C chamber temperature.

the long term drift. However, from the previous experiments with nitrogen it is known that at elevated temperatures the propellant tube cools down due to the flow of propellant and alters the pendulum equilibrium position. The produced thrust is therefore actually higher than the measured thrust shown here. Since there is still leftover water inside the propellant tube when the propellant valve is closed, the water is still evaporating and producing thrust which makes direct measurement on the equilibrium

position like the experiment with nitrogen not possible. In section 6.4.1 it was shown that in phase 3 the chamber pressure and measured thrust still correlate with each other. Since the chamber pressure is linear with the produced thrust, an estimate can be made on what the produced thrust is by comparing the drop in chamber pressure to the drop in measured thrust.

Let $F_{m,end}$ be the (drift corrected) measured thrust and $P_{c,end}$ be the chamber pressure at the end of the thrusting phase, $F_m(t)$ the thrust and $P_c(t)$ the chamber pressure at time t, then the line where the thrust is expected to be zero $F_0(t)$ can be calculated using:

$$F_0(t) = F_{m,end} - \left(F_{m,end} - F_m(t)\right) \cdot \left(1 - \frac{P_c(t)}{P_{c,end}}\right) \tag{6.2}$$

The result of this is shown in figure 6.9 where the data was also fit with an exponential in order to estimate the value of Δ_T, which is the difference in measured thrust due to the difference in equilibrium position due to the thermal expansion of the propellant tube. Comparing this line to the results found in chapter 5 shows a similar drop of similar shape in the pendulum equilibrium position. However the shape of F_0 is not as clean as in the nitrogen case due to the fact that the tube is partially still filled with water. The function to fit the values of F_0 and the calculation of Δ_T is:

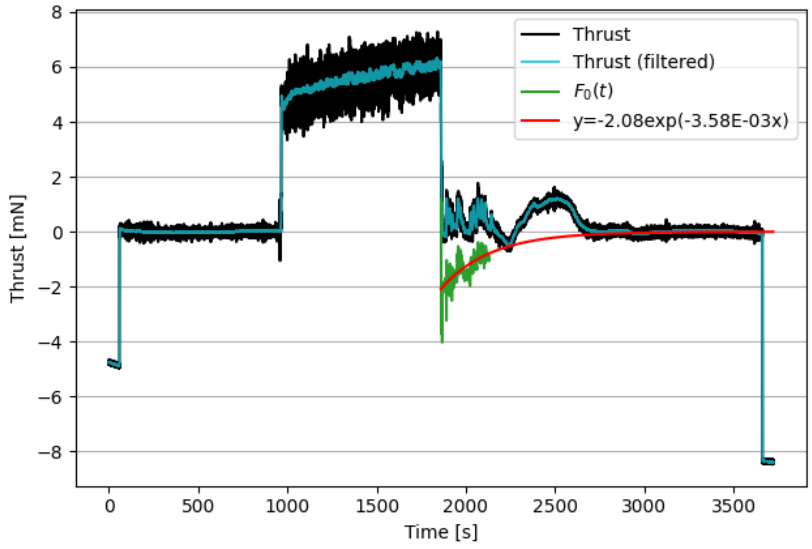

Figure 6.9: Drift corrected thrust showing in green where the thrust is expected to be zero by correcting for the chamber pressure.

$$f(x) = -ae^{-bx} \tag{6.3}$$

$$\Delta_T = f(0) = -a \tag{6.4}$$

with $a, b < 0$ and x being the time after the propellant valve is closed in seconds. The accuracy of the value of Δ_T is difficult to determine due to the various factors that can have an effect on the fit. For one, it is a stretch to assume that the thrust and chamber pressure remain their linear relation over such a big range. For example the kinematic viscosity drops linearly with the drop in chamber pressure, changing the Reynolds number in the throat by a similar amount. Also since the values of F_0 are very susceptible to noise, Δ_T is obtained by a extrapolation of the data, and the shape of F_0 is not a clear exponential, the accuracy of the fit is low. Taking this into account, the error of Δ_T is estimated to be within 1 mN. The produced thrust is then calculated using equation 5.3. The difference with the nitrogen test is that the measured thrust F_m is not averaged over the last 50% of the thrust period, but just over the last minute. This is because the chamber pressure and mass flow are not constant, which will introduce a large error if averaged over a long time period. All values shown for the water experiment are therefore the averages of the last minute. Since the mass flow was determined using the chamber pressure, the

error (in percent) of the chamber pressure is added to the mass flow as well. Finally, on top of the error of F_T is the error of the thrust as shown in table 3.4. Table 6.8 shows the obtained values of the relevant parameters including their statistical errors obtained from the data and equipment errors. As can be seen from the table, the experiment was repeated four times instead of three. This was because for the first test, WAT-1.1, the time after closing the propellant valve was initially set at 20 minutes. It was only after the first experiment that this duration was extended to 30 minutes, which was then performed three times. During the analysis it was found that the test with only 20 minutes after closing the valve could also be analysed with similar accuracy as the other three, resulting in a total of four tests.

ID	T_c [°C]	p_c [mbar]	$\dot{m}$ [mg/s]	p_a [mbar]	P_{heat} [W]	Δ_T [mN]	F_T [mN]
WAT-1.1	300±1.2%	1019±5.1%	8.9±5.2%	6.3±50.1%	36.62±0.7%	-1.76±56.7%	8.28±12.4%
WAT-1.2	300±1.2%	1015±5.4%	8.8±5.5%	5.1±50.6%	36.43±0.9%	-2.08±48.1%	8.20±12.9%
WAT-1.3	300±1.2%	1017±5.3%	8.5±5.3%	5.2±50.2%	36.47±0.7%	-1.87±53.4%	8.30±12.2%
WAT-1.4	300±1.2%	1015±5.2%	8.6±5.2%	5.2±50.7%	36.15±0.7%	-1.56±64.3%	7.94±12.7%

Table 6.8: Water thrust test result data including statistical and equipment error.

6.4.4. Thruster performance

Using the technique described in the section above the produced thrust was calculated for all experiments using water. From these measured quantities the performance parameters from table 6.4 are calculated using the analytical model described in chapter 2 and can be found in table 6.9. The input of the analytical model are the values found of T_c, p_c, and p_a from table 6.8 with their corresponding error.

ID	$Re_{t,real}$ [-]	I_{sp} [s]	η_{heat} [-]	$\xi_{I_{sp}}$ [-]	C_d [-]
WAT-1.1	1336±18.3%	95.2±13.4%	0.724±14.0%	0.752±13.5%	0.889±10.5%
WAT-1.2	1325±19.0%	95.4±14.0%	0.719±14.8%	0.749±14.1%	0.883±11.2%
WAT-1.3	1299±18.2%	99.5±13.3%	0.698±13.8%	0.781±13.4%	0.855±10.5%
WAT-1.4	1309±18.7%	94.0±13.8%	0.713±14.4%	0.738±13.8%	0.868±10.9%

Table 6.9: Performance parameters of the engine using liquid water as propellant.

6.4.5. Comparison to nitrogen and RPT predictions

This section describes the difference in performance values found using liquid water as propellant with respect to the performance obtained using nitrogen and predictions by the Resistojet Performance Tool (RPT). One reason to prefer using water over nitrogen is the high storage density, but also the increased specific impulse due to the lower molecular mass. At a chamber temperature of 300°C, the I_{sp} is around 10s higher for water than for nitrogen. However the error on the I_{sp} for water is with ±14% much higher than the ±1% for nitrogen. This is mainly due to the large inaccuracy of the thrust due to the large error of Δ_T, but in part also due to the increased inaccuracy of the mass flow determined by the pressure sensor. This directly explains the increase in the error of the specific impulse quality $\xi_{I_{sp}}$. The error of the discharge coefficient slightly increased from 9.5% to 11% which is caused by the increased error in the measured mass flow. The heating efficiency η_{heat} is higher with values of 0.70-0.72 compared to 0.22 at the same conditions of T_c = 300°C and p_c = 1 bar. This is since water requires more energy to heat to the target temperature due to the heat needed for vaporization, and is not unexpected. What unexpected is that while the predicted discharge coefficient around $Re_{t,real}$ = 1300 is approximately 0.925 for both nitrogen and water, the obtained discharge coefficient for nitrogen is 0.83, while for water this is 0.87. As the nozzle geometry is the same in both experiments, this discrepancy is thought most likely to be caused by the inaccuracy of estimating the mass flow, meaning the actual mass flow is probably lower than the estimated value. Since it is already known that the model for estimating the discharge coefficient is not adequate for this thruster, it is also possible that the model simply predicts the expected discharge coefficient in a wrong way so the expected value wouldn't be the same for

nitrogen and water at these Reynolds numbers. Since the model is not valid for the thruster used, no decisive conclusion of the cause of this discrepancy of the discharge coefficient can be given. The found propellant consumption quality with a range of 0.74-0.78 with an accuracy of 14% does comply with the expected value of 0.66 as expected by the model, however this is not considered proof that the model in this case accurately predicts the I_{sp} quality. The error of $\xi_{I_{sp}}$ simply increased from 2% to 14% compared to nitrogen which is considered too high to validate the prediction. Since the experimental value of $\xi_{I_{sp}}$ for nitrogen are found to be around 0.87 for a throat Reynolds number of 1300 which is significantly higher than the value obtain with water, this is another indication that the actual mass flow would be lower than the one estimated. The ratio of the actual mass flow versus the derived mass flow is difficult to determine as the comparisons between nitrogen and water can not be made directly. However a rough estimation can be made to show that the actual mass flow is between 5% to 15% lower than the determined mass flow to make the obtained quality factors more in line with the results from nitrogen.

6.5. Discussion

Since the test bench used for the thrust experiment with liquid water is the same as for the experiment with nitrogen, the assumption is made that the pendulum changes equilibrium position due to the change in temperature of the propellant tube. This assumption has a large effect on the magnitude of the thrust being measured. Looking at table 6.8, the measured thrust is corrected by 24% to 34% in the experiments but it is difficult to measure accurately due to the remaining liquid water in the propellant valve. The accuracy of the performance parameters is largely equal to the experiments with nitrogen except for this thermal expansion correction which therefore also increases the error of $\xi_{I_{sp}}$. The large temperature, or more precisely, the CoG dependence is a limitation of the thrust bench which needs to be either solved or properly analysed in order to increase the accuracy of thrust tests at elevated temperatures.

The method of supplying the propellant with use of a syringe pump is not ideal but it can be made to work. Recommendations on how this setup can be made better can be found in chapter 8. There are two main problems with using this feed system which are the flexible propellant feed lines leading from the syringe pump to the vacuum chamber and the air that is dissolved in the water at atmospheric pressure is partially released at lower pressures which forces the water downstream into the thruster. Both these effects limit the operating chamber pressure window, which has to be equal or higher than the outside pressure of ±1 atm. Furthermore it would have been good to have performed experiments at different temperatures, for example an experiment at 200 and 250 °C and at higher chamber pressures, which would also require different mass flows and therefore provide more insight in if the used method of determining the mass flow is correct and accurate.

One effect that was not accounted for is the mass of the propellant inside the thruster during thrust. This mass changes the CoG and therefore the measured thrust. Correcting for this will reduce the measured thrust, but an estimate can not be given without proper analysis. It is difficult to account for this since it is not possible to see the liquid water level during thrust as the thruster is not transparent. Although a simple experiment where filling the tube slowly with the syringe pump and measuring the change in actuator coil current is a good way to estimate the size of this correction. In hindsight this experiment should have taken place, but it was realized too late that this was a viable option.

6.6. Conclusion

Thrust tests with a resistojet were conducted successfully using liquid water as propellant. A syringe pump was used to control the flow of propellant to the thruster. Since the chamber pressure is coupled with the pressure inside the flexible propellant feed lines, the operating chamber pressure was limited to a minimum of 1 bar to prevent the propellant feed lines from collapsing, causing a large mass flow that the thruster can't handle.

Four thrust tests were performed at chamber temperatures of 300 °C at a chamber pressure of 1.0 bar over a duration of 15 minutes. Mass flow could not be measured directly as the equipment is not currently available, but was derived by the change in chamber pressure over time. Comparing

the results to the experiments with nitrogen indicates that the actual mass flow is likely to be around 5% to 15% lower than the one derived but there does not exist enough data to prove this. One way to solve this would be by acquiring a mass flow sensor that is suitable for liquid flow measurements. Produced thrust was found to be 8.0-8.3 mN at a specific impulse of 95-100 seconds with an accuracy of 12-14%. A total of 36.1-36.6 Watt heating power was required with an efficiency of 70-72%. The thruster was found to be capable of performing supersonic thrust tests using water as propellant. To improve the accuracy of future experiments a solution must be found for the thrust bench' dependence of the CoG, which changes during the course of an experiment due to changes in thermal expansion and the additional mass of the propellant inside the thruster. Attempts to correct for the changes in thermal expansion resulted in the largest error contribution.

The Resistojet Performance Tool (RPT) was found to estimate the quality values closer to the experimentally obtained values although this is believed to be mainly caused by the increased inaccuracies of the measurements. More experiments with water as propellant at different conditions with improved accuracies should be done to more accurately compare the results from the model. Although the expected values are within experimentally obtained error margins, the model is not considered valid for the thruster used.

7

Conclusion

The research objective for this work as formulated in chapter 1 states the following:

To perform experimental thrust tests using liquid water as propellant in order to validate the current VLM design and identify areas for improvement for future VLM development.

In order to achieve this research objective, four main research questions were formed. The work performed during the course of this thesis was done in order to give answers to these questions. This chapter will offer direct answers to the research questions by summarizing the work that was performed and the subsequent results that were obtained.

1. *How well can the characteristics of the thruster using liquid water be estimated from theory and how does this compare to nitrogen?*

Experiments with both nitrogen and liquid water as propellant have been performed in this thesis. Besides from the expected changes in performance parameters that can be predicted using the analytical model, several characteristic differences have been noted during these experiments. With liquid water, the chamber pressure increased during the experiment due to the feed system being volume based instead of driven by pressure. In the case of nitrogen, closing the propellant valve and thus shutting off the supply of propellant the remaining propellant downstream from the valve does not produce thrust for a measurable time. However since the density of liquid water is significantly higher than nitrogen, a relatively large amount of mass resides between the propellant valve and the chamber. This volume of water lingers longer than nitrogen as the water slowly evaporates. This resulted in unpredictable production of thrust for as long as 15 minutes after shutdown. This leads to low accuracy of the thrust measurement as the thrust bench is dependent on the change of CoG due to thermal expansion. Therefore the results using water as propellant are less accurate than the results using nitrogen. An analytical model is made based on Ideal Rocket Theory (IRT) and includes corrections commonly used in previous work at TU Delft. The Resistojet Performance Tool (RPT) did not accurately predict the values obtained in the experiments. The estimates for nitrogen are outside of the confidence bounds of the experimental values. Although the estimates of the quality factors for water are closer to the experimentally obtained values, it is believed this is mainly caused by the increased inaccuracies of the measurements. Although the expected values are within experimentally obtained error margins, the model is not considered valid for the thruster used. The difference between the experiment and modelled values is most likely caused by the two-dimensional shape of the nozzle instead of being an axisymmetric nozzle.

2. *How can the current hot gas resistojet design be used for VLM testing using water as propellant?*

Although the resistojet by Versteeg [47] was designed for superheating gas, no adaptions to the design needed to be made in order to use the resistojet as a VLM thruster using water as propellant. There are however a few adaptions on the operational side needed to be made in order to allow for experimentation. Section 6.1.1 described the formation of droplets at the propellant inlet leading to

unstable conditions. This problem was easily solved by mounting the thruster upside down not allowing droplets to form due to the pull of gravity. This solution does now work however under free fall and needs to be reevaluated for a space ready design. One possible solution for space is to extend the heat transfer element into the propellant inlet to where the propellant is still expected to be liquid as this would stop the formation of large droplets. Furthermore, there was a need for the propellant valve to be opened slowly using PWM to reduce the initial rush of propellant towards the chamber during startup, which was described in section 6.1.2. Also it was found that way the heaters were implemented into the thruster was limiting the heat transfer and thus limiting the maximum temperature the thruster can operate at. The low heat transfer caused the heaters to overheat locally at lower temperatures than they were rated for. The heat transfer has been increased using copper grease as described in section 3.5.1 although this may not be a suitable solution for space as the heaters are not fixed into place and can slip out while the grease will likely evaporate in vacuum for an extended duration.

3. *How does the experimental setup need to be modified in order to allow for liquid water thrust tests?*

In order for liquid water tests to be performed the propellant feed system needed to be changed which is described in section 3.3. A feed system for liquids was made by connecting a syringe pump to the propellant inlet of the vacuum chamber. The syringe pump outputs a constant volumetric flow and is therefore not pressure based such as the nitrogen feed system. Liquid mass flow could not be measured directly with the current equipment and therefore the syringe pump was calibrated in section 4.2 to obtain a mass flow estimate, which could then be corrected based on the chamber pressure as described in section 6.4.2. This estimation of the mass flow increases the error of the mass flow compared to nitrogen and section 6.4.5 shows there are signs that the actual mass flow may be between 5-15% less than estimated with the used method. The sensor used to measure the vacuum chamber pressure is not calibrated for water which introduces a large error. Although the accuracy of the vacuum chamber pressure does not have a large influence on the accuracy of the thruster performance, it is part of the setup that should be changed for future water experiments.

4. *What are the areas of improvement with respect to the current VLM design and experimentation?*

The main areas of improvement for thrust tests using liquid water is the reduction in errors of the performance parameters C_d and $\xi_{I_{sp}}$. To say whether the predictions of these performance parameters are valid and accurate, the accuracy of the experimental values should be smaller for improved confidence. Currently only for nitrogen it can be said that the predicted values are not correct. For the experiments with nitrogen, the largest contributor of the errors are the nozzle dimensions. The inaccurate measurements of the nozzle dimensions limit the accuracy of the theoretical thrust and mass flow to $\sim$9%. If the errors of the nozzle dimensions is ignored, the inaccuracy of the thrust and mass flow drop to $\sim$5% where the error of the chamber pressure is the leading inaccuracy. Also the volume of water between the propellant valve and the chamber that resides after closing the propellant valve should be reduced as much as possible as this behaviour is difficult to predict and is a waste of propellant.

8

Recommendations

Over the course of this thesis several areas were identified for improvement. This chapter will discuss recommendations for future thruster design and experimentation.

8.1. Thruster design

This section will discuss the recommendations to improve the design of the thruster used in this thesis. Although the current design is a very good first step in the development of a Vaporizing Liquid Miro-resistojet, as proven by the fact that a thrust test with water has been conducted successfully, there are some improvements that can be made to the design.

One of the problems encountered during experimentation was that the nozzle throat was partially blocked from the inside. The cause of this blockade is not known, but is likely to be a small part from the metallic heat exchanger foam that came loose. It's not inconceivable that this may happen again in the future and therefore not recommended to use for future designs. One slight modification that may resolve this issue is the use of a fine mesh that is placed after the heat exchanger foam that can catch any debris from reaching the nozzle throat. The size of the mesh should be smaller than the nozzle throat so that any debris that clears the mesh should not get stuck inside the nozzle throat. There are many suppliers from which such a mesh can be obtained with mesh sizes smaller than 0.1 mm.

Another problem that was encountered was the heaters breaking down due to the low thermal conductivity causing them to overheat. By applying copper grease in the hole to increase the contact surface and reducing the maximum operating temperature, overheating of the remaining heaters was prevented. Although this solution was enough to continue experimentation, the solution was not completely solved. It is not known to what temperature the heaters can operate safely with the increased thermal conductivity. The heaters could pop out of their fittings when they were heated for the first time by the vaporization of the grease building up pressure on the bottom of the hole. One way to solve this problem is to use heaters with a threaded end so they can't pop out, or use a different method to ensure the thermal conductivity is increased. Drilling precise fittings is not advised, as the precision required makes the solution very expensive. Also, since the holes to fit the heaters into are on the same side as the nozzle exit, copper grease can spill into the nozzle and block it. Although this spilling was not encountered, it is best to completely remove this possibility by drilling the fittings from the other side of the copper blocks. Since the last heater with an internal thermocouple broke down, it would be interesting to order another one to estimate the thermal conductivity of the copper grease solution.

Putting the pressure sensing tube on the other side of the chamber than the propellant tube would be another improvement on the design of the current thruster. In the current design, the liquid water has to come from the bottom to prevent droplets forming at the inlet and falling down into the heated chamber. Having the pressure sensing tube facing downwards creates the possibility of water vapor condensating at the bottom since the temperature at the pressure sensor is below the boiling point. This

creates two problems, first collected water at the pressure sensor changes the CoG of the pendulum which affects the measured thrust. Secondly, the mass flow builds up inside the thruster which is results in a lower effective mass flow. It is not known whether condensation occurs inside the pressure sensing tube. Although some condensation is assumed to occur, it is difficult to estimate how much condensation occurs in order to account for it. By placing the pressure sensing tube above the chamber, any condensed water vapor falls down due to the pull of gravity and will eventually vaporize again thus preventing the buildup of propellant.

Lastly, the largest contributor of the error of the performance parameters for nitrogen were caused by the relatively large error of the nozzle and in particular the nozzle throat dimensions. Improving the accuracy of determining the nozzle dimensions is essential if for future research more accurate measurements are needed.

8.2. Experimental setup

Starting with the most important recommendation for future experimentation is to change or modify the test bench in order to remove its dependence of the CoG. For cold thrust testing with gasses this problem is minimal, but usage of heavy liquids and thermal expansion of the materials cause a change in the equilibrium position of the pendulum affecting the measurement of the produced thrust. Even the cause of the long term drift is not fully understood as it occurs in both heated and cold experiments and is so significant it could be argued that it undermines the validity of the thrust measurement in general. Also it was found that on days with heavy wind the amplitude of the pendulum distance was too large to make accurate measurements. It is recommended to take another look at using other test benches such as the AE-TB-50m which was recently reassembled by Takken [39].

It is also advised to improve the feed system for the liquid thrust testing. Part of this is to invest in a mass flow sensor that are available for liquids. Although it can be difficult to find a solution for the low mass flows that are being used, one possible example is the LG16-0430 from Sensiron [34]. Also the flexible propellant tubes can be improved by making them from a more rigid material that does not collapse when the outside pressure is higher than the inside. Lastly it might be good to deaerate the water before it is inserted into the feed system which can be done by either bringing it to boil or placing it in the vacuum chamber for a while.

The pressure inside the vacuum chamber is currently measured using the VSP 3000 sensor by VACUUBRAND [46]. This sensor is however not recommended for use with water vapor as it is dependent on the gas type. Therefore it is recommended to invest in a sensor that is also capable to measure vacuum chamber pressures for water vapor such as the VSK 3000, which can be used directly with the current setup.

Lastly if the current setup is used for future research it might be good to do more research into the cause of the quadratic relationship between the heater current and the measured thrust. Although this effect is small and can be corrected for, it would be better to find the exact cause of the effect which can then lead to attempts to remove this unwanted correlation between the two. Alternatively, ways of preventing the effect of heater current can be investigated such as rotating the wires around each other or even insulating the wires with an electrical conductor such as aluminum foil.

Bibliography

[1] J Amesz. Conversion of Leak Flow-Rates for Various Fluids and Different Pressure Conditions. pages 1–28, 1966.

[2] Karl Johan Astrom, Bjorn Björn Wittenmark, Karl J. Åström, and Bjorn Björn Wittenmark. Computer Control System Theory and Design. *Prentice Hall*, 1997. ISSN 14337851.

[3] Robert L. Bayt. Analysis, Fabrication and Testing of a MEMS-based Micropropulsion System, 1999. URL https://dspace.mit.edu/handle/1721.1/57601.

[4] Ian H. Bell, Jorrit Wronski, Sylvain Quoilin, and Vincent Lemort. Pure and pseudo-pure fluid thermophysical property evaluation and the open-source thermophysical property library coolprop. *Industrial and Engineering Chemistry Research*, 2014. ISSN 08885885. doi: 10.1021/ie4033999.

[5] JJ Berg, JM Oliveira, JF Congiardo, LK Walls, PT Putman, and MS Haberbusch. Thermal Performance of a Cryogenic Fluid Management Cubesat Mission. Technical report, 2013.

[6] Jefferey J Berton. Divergence thrust loss calculations for convergent-divergent nozzles: Extensions to the classical case. 1991.

[7] R J F Bijster. *Design, Verification and Validation of a Micropropulsion Thrust Stand*. PhD thesis, Delft University of Technology, 2014.

[8] J Bouwmeester, E. K. A. Gill, and C. J M Verhoeven. Advancing Nano-Satellite Platforms : the Delfi Program. In *59th International Astronautical Congress*, 2008.

[9] Jasper Bouwmeester, L. Rotthier, C. Schuurbiers, Wolter (Tno) Wieling, G. Van Der Horn, F. Stelwagen, E. Timmer, and M. Tijssen. Preliminary results of the Delfi-n3Xt mission. *The 4S symposium*, 2014.

[10] Timothy H. Boyer. The force on a magnetic dipole. *American Journal of Physics*, 1988. ISSN 0002-9505. doi: 10.1119/1.15501.

[11] A. Cervone, B.T.C. Zandbergen, D. C. Guerrieri, M. De Athayde Costa e Silva, I. Krusharev, and H. van Zeijl. Green micro-resistojet research at Delft University of Technology: new options for Cubesat propulsion. *CEAS Space Journal*, 9(1):111–125, 2016. ISSN 18682510. doi: 10.1007/s12567-016-0135-3.

[12] DELTA ELEKTRONIKA BV. ES 300 Series - 300W DC POWER SUPPLIES. URL https://www.delta-elektronika.nl/en/products/dc-power-supplies-300w-es300-series.html.

[13] DELTA ELEKTRONIKA BV. SM 1540-D SM 7020-D SM 3004-D Manual, 1992. URL https://www.delta-elektronika.nl/upload/MAN_SM700.pdf.

[14] D. C. Guerrieri, M. De Athayde Costa E Silva, B. T.C. Zandbergen, and A. Cervone. Development of a low pressure free molecular micro-resistojet for cubesat applications. In *Proceedings of the International Astronautical Congress, IAC*, 2015. ISBN 9781510818934.

[15] Robbert J Hamann, Jasper Bouwmeester, and Geert Brouwer. Delfi-C3 Preliminary Mission Results. *Proceedings of the 23rd annual AIAA/USU Small Satellite Conference*, 2009.

[16] International Organization for Standardization. ISO 9300:2005 Measurement of gas flow by means of critical flow Venturi nozzles, 2005. URL https://www.iso.org/standard/34272.html.

[17] E.H.W. Jansen. *Improvement and validation of test stand performance for novel micropropulsion systems*. PhD thesis, Delft University of Technology, 2016.

[18] A N Johnson, P I Espina, G E Mattingly, and C L Merklet. Numerical Characterization of the Discharge Coefficient in Critical Nozzles. In *Proceedings of the 1998 NCSL Workshop and Symposium*, 1998.

[19] I. Krusharev. Micro - Thruster Development: Propulsion System for the DelFFi Mission, 2015.

[20] H.H. Ku. Notes on the use of propagation of error formulas. *Journal of Research of the National Bureau of Standards, Section C: Engineering and Instrumentation*, 1966. ISSN 0022-4316. doi: 10.6028/jres.070c.025.

[21] N. M. Kuluva and G. A. Hosack. Supersonic nozzle discharge coefficients at low reynolds numbers. *AIAA Journal*, 9(9):1876–1879, 1971. ISSN 00011452. doi: 10.2514/3.6443.

[22] Ali Kurmanbay. Design, Fabrication and Characterization of MEMS based micro heater for Vaporizing Liquid Microthruster, 2019. URL https://repository.tudelft.nl/islandora/object/uuid:a9d08ef1-1e95-4a07-b4db-666d51612404.

[23] Kurt J. Lesker Company. Standard Pirani Gauge KJLC PIR, 2017. URL https://www.lesker.com/newweb/gauges/pdf/kjlc-piranigauge-manual.pdf.

[24] H. C.M. Leenders and B. T.C. Zandbergen. Development of a solar thermal thruster system. In *International Astronautical Federation - 59th International Astronautical Congress 2008, IAC 2008*, 2008. ISBN 9781615671601.

[25] P. J. Linstrom and W. G. Mallard. National Institute for Standards and Technology Chemistry WebBook. URL http://webbook.nist.gov/chemistry/.

[26] Rajeev Makhan. Performance of the MEMS Vaporizing Liquid Microthruster using cold nitrogen gas as propellant: An experimental study. 2018. URL http://resolver.tudelft.nl/uuid:aaed2594-d414-4c83-967b-0cd94cccd23f.

[27] Micro-epsilon. Capacitive sensors catalog. URL https://www.micro-epsilon.com/download/products/cat--capaNCDT--en.pdf.

[28] A. Migliaccio, B.T.C. Zandbergen, F.T. Nardini, and M. C. Louwerse. VACUUM TESTING OF A MICROPROPULSION SYSTEM BASED ON SOLID PROPELLANT COOL GAS GENERATORS. *61st International Astronautical Congress*, pages 1–9, 2010.

[29] National Instruments. NI 9211 Datasheet, 2015. URL https://www.ni.com/nl-nl/support/model.ni-9211.html.

[30] A Pappadimitriou. *Performance Evaluation of a Vaporizing Liquid Microthruster using nitrogen and water as propellants*. PhD thesis, Delft University of Technology, 2021.

[31] ProSense. PSNE1000 Single channel syringe pump. URL https://www.prosense.net/en/products/syringe-pumps/syringe-pumps/psne1000/.

[32] Hans Rottländer, Walter Umrath, and Gerhard Voss. Fundamentals of leak detection. *Leybold*, 2016.

[33] Abraham Savitzky and Marcel J.E. Golay. Smoothing and Differentiation of Data by Simplified Least Squares Procedures. *Analytical Chemistry*, 1964. ISSN 15206882. doi: 10.1021/ac60214a047.

[34] Sensiron. Liquid Flow Meter LG16. URL https://www.sensirion.com/en/flow-sensors/liquid-flow-meters/lx-compact-liquid-flow-meters/liquid-flow-sensor-for-monitoring-dynamic-processes/.

[35] Stefano Silvestrini. *Closed-loop Thrust Magnitude Control System for Nano- and Pico-Satellite Applications*. PhD thesis, Delft University of Technology, 2017.

[36] Ernie W Spisz, Paul F Brinich, and John R Jack. Thrust coefficients of low-thrust nozzles. Technical report, NATIONAL AERONAUTICS AND SPACE ADMINISTRATION CLEVELAND OH LEWIS RESEARCH CENTER, 1965.

[37] P E P Stohr. *The characterization and design of a CubeSat Integrated COTS Resistojet thruster*. PhD thesis, Delft University of Technology, 2016. URL http://repository.tudelft.nl/.

[38] George P. Sutton and Oscar Biblarz. *Rocket Propulsion Elements*. John Wiley & Sons, Inc., 8th edition, 2010. ISBN 9780470080245.

[39] Aeilt Jan Takken. *Development of a high-temperature Solar Thermal Propulsion engine*. PhD thesis, Delft University of Technology, 2021. URL https://repository.tudelft.nl/islandora/object/uuid%3Ae6cc6c72-bcfb-4927-a0bf-d935a6ba32f8.

[40] S. P. Tang and J. B. Fenn. Experimental Determination of the Discharge Coefficients for Critical Flow through an Axisymmetric Nozzle. *AIAA Journal*, 1978. ISSN 00011452. doi: 10.2514/3.60854.

[41] TE connectivity. MS5837-30BA ultra small gel filled pressure sensor, 2019. URL https://www.te.com/usa-en/product-CAT-BLPS0017.html.

[42] The Lee Company. 9th Edition Electro-Fluidic Systems Handbook, 2021. URL https://www.theleeco.com/whats-new/9th-edition-electro-fluidic-systems-handbook/.

[43] The Lee Difference. Lee Electro-Fluidic Systems for Clinical Application. URL https://theleedifference.com/.

[44] Thermal Grizzly. Datenblatt Thermal Grizzly Kryonaut.

[45] Thermon. Product Datasheet Thermon T-99, 2021.

[46] VACUUBRAND. Vacuum gauge Set DCP 3000 + VSP 3000, 2018. URL https://www.vacuubrand.com/us/page936.html.

[47] HSE Versteeg. *Novel fabrication method for a hot gas supersonic micro-thruster*. PhD thesis, Delft University of Technology, 2020. URL http://resolver.tudelft.nl/uuid:ac2482ad-0f8e-4569-8bd4-fd11bd6327bd.

[48] W. Wagner and A. Pruß. The IAPWS formulation 1995 for the thermodynamic properties of ordinary water substance for general and scientific use. *Journal of Physical and Chemical Reference Data*, 2002. ISSN 00472689. doi: 10.1063/1.1461829.

[49] Watlow Heating Solutions. Watlow Heater Catalog - Cartridge / Insertion Heaters, 2021.

[50] B.T.C. Zandbergen. *AE4-S01 Thermal Rocket Propulsion Reader*. Number August. 2020.

A Tabulated data

A.1. Leak rate

Test #	ΔP [mbar]	Leak rate [mbar/s]	Leak rate [mg/s]
1	1500	42.39±0.38	0.1178±0.0010
	1250	33.30±0.42	0.0926±0.0012
	1000	25.56±0.36	0.0710±0.0010
	750	17.62±0.35	0.0490±0.0010
	500	10.80±0.44	0.0300±0.0012
2	1500	78.29±0.47	0.2163±0.0013
	1250	60.84±0.34	0.1681±0.0009
	1000	45.83±0.33	0.1266±0.0009
	750	32.87±0.31	0.0908±0.0008
	500	19.89±0.33	0.0550±0.0009
3	1500	71.76±0.35	0.1988±0.0009
	1250	56.04±0.38	0.1552±0.0011
	1000	42.07±0.40	0.1165±0.0011
	750	29.60±0.25	0.0820±0.0007
	500	18.30±0.24	0.0507±0.0007

Table A.1: Leak rate at various pressure differences before reassembly.

Test #	ΔP [mbar]	Leak rate [mbar/s]	Leak rate [mg/s]
1	1500	146.62±0.89	0.4095±0.0025
	1250	117.62±0.56	0.3285±0.0016
	1000	90.15±0.72	0.2518±0.0020
	750	64.25±0.44	0.1795±0.0012
	500	40.78±0.26	0.1139±0.0007
2	1500	145.19±0.97	0.4057±0.0027
	1250	117.18±0.71	0.3274±0.0020
	1000	90.42±0.77	0.2526±0.0021
	750	65.04±0.50	0.1817±0.0014
	500	40.22±0.32	0.1124±0.0009
3	1500	142.68±0.77	0.3988±0.0022
	1250	117.08±0.65	0.3272±0.0018
	1000	89.24±0.46	0.2494±0.0013
	750	63.73±0.43	0.1781±0.0012
	500	39.88±0.31	0.1115±0.0009
4	1500	134.21±0.68	0.3737±0.0019
	1250	106.27±0.56	0.2958±0.0016
	1000	79.21±0.50	0.2205±0.0014
	750	55.35±0.39	0.1541±0.0011
	500	34.62±0.46	0.0964±0.0013
5	1500	138.13±0.85	0.3846±0.0024
	1250	110.83±0.68	0.3086±0.0019
	1000	81.64±0.44	0.2273±0.0012
	750	56.42±0.46	0.1571±0.0013
	500	35.50±0.26	0.0989±0.0007

Table A.2: Leak rate at various pressure differences after reassembly.

Gas		ΔP [mbar] 500	750	1000	1250	1500
N_2	25C	0.105	0.169	0.239	0.316	0.401
	100C	0.071	0.114	0.161	0.213	0.270
	200C	0.047	0.076	0.107	0.142	0.179
	300C	0.034	0.055	0.077	0.102	0.129
H_2O	200C	0.047	0.075	0.106	0.141	0.179
	300C	0.031	0.049	0.070	0.093	0.118

Table A.3: Leak rates in mg/s depending on the gas type, gas temperature and difference between ambient and chamber pressure.

A.2. Syringe pump calibration

Setting [mL/hr]	Weight after 5 minutes [mg]	Average mass flow [mg/s]
10	839.0	2.797
10	855.9	2.853
10	832.0	2.773
20	1695.6	5.652
20	1686.4	5.621
20	1672.2	5.574
40	3377.0	11.257
40	3370.8	11.236
40	3361.4	11.205

Table A.4: Syringe pump calibration results.

A.3. Nitrogen thrust data

ID	T_c [°C]	p_c [mbar]	$\dot{m}$ [mg/s]	p_a [mbar]	P_{heat} [W]	Δ_T [mN]	F_T [mN]
NIT-1.1.1	19±2.4%	989±5.1%	14.9±0.9%	6.6±18.6%	0.0±0%	0.0±0%	9.21±1.2%
NIT-1.1.2	20±2.4%	985±5.1%	14.8±0.9%	6.7±19.1%	0.0±0%	0.0±0%	9.21±1.2%
NIT-1.1.3	21±2.4%	982±5.1%	14.8±0.8%	6.7±18.8%	0.0±0%	0.0±0%	9.20±1.2%
NIT-1.2.1	23±2.4%	993±5.0%	14.9±0.9%	6.2±20.6%	0.0±0%	0.0±0%	9.24±1.1%
NIT-1.2.2	23±2.4%	989±5.1%	14.8±0.9%	6.2±19.6%	0.0±0%	0.0±0%	9.22±1.1%
NIT-1.2.3	23±2.4%	984±5.1%	14.7±0.9%	6.2±20.0%	0.0±0%	0.0±0%	9.21±1.2%
NIT-1.3.1	23±2.4%	1012±4.9%	15.2±0.9%	6.5±19.4%	0.0±0%	0.0±0%	9.46±1.2%
NIT-1.3.2	23±2.4%	1011±4.9%	15.2±0.9%	6.6±20.4%	0.0±0%	0.0±0%	9.47±1.3%
NIT-1.3.3	23±2.4%	1011±4.9%	15.1±0.8%	6.6±19.8%	0.0±0%	0.0±0%	9.44±1.2%
NIT-2.1.1	200±1.5%	991±5.1%	11.5±0.9%	5.1±18.0%	7.83±4.6%	-0.83±2.7%	8.76±1.2%
NIT-2.1.2	200±1.5%	988±5.1%	11.4±0.9%	5.1±17.9%	7.69±2.3%	-0.81±2.3%	8.74±1.2%
NIT-2.1.3	200±1.5%	989±5.1%	11.4±0.9%	5.1±18.4%	7.68±2.3%	-0.81±2.0%	8.76±1.2%
NIT-2.2.1	200±1.5%	996±5.0%	11.5±1.0%	5.0±18.4%	7.75±5.0%	-0.79±2.5%	8.83±1.4%
NIT-2.2.2	200±1.5%	993±5.0%	11.4±0.9%	4.9±18.1%	7.62±2.4%	-0.81±2.9%	8.79±1.3%
NIT-2.2.3	200±1.5%	992±5.0%	11.4±0.9%	4.9±18.0%	7.61±2.6%	-0.79±2.0%	8.77±1.3%
NIT-2.3.1	200±1.5%	995±5.0%	11.3±0.9%	4.9±18.2%	7.66±1.6%	-0.84±1.3%	8.72±1.3%
NIT-2.3.2	200±1.5%	994±5.0%	11.3±0.9%	5.0±17.9%	7.57±2.0%	-0.83±1.3%	8.71±1.3%
NIT-2.3.3	200±1.5%	993±5.0%	11.3±0.9%	5.0±18.2%	7.56±2.3%	-0.83±1.2%	8.70±1.3%
NIT-3.1.1	200±1.5%	1489±3.4%	17.7±0.8%	7.8±20.8%	9.24±1.3%	-0.88±2.2%	13.56±1.2%
NIT-3.1.2	200±1.5%	1486±3.4%	17.7±0.8%	8.0±20.0%	9.07±1.8%	-0.81±2.8%	13.56±1.2%
NIT-3.1.3	200±1.5%	1486±3.4%	17.7±0.8%	7.9±20.4%	9.04±1.8%	-0.90±2.3%	13.64±1.2%
NIT-3.2.1	200±1.5%	1488±3.4%	17.6±0.8%	7.9±20.4%	9.10±1.3%	-0.97±1.4%	13.51±3.0%
NIT-3.2.2	200±1.5%	1483±3.4%	17.5±0.8%	8.0±19.1%	9.02±1.8%	-0.97±1.3%	13.53±3.0%
NIT-3.2.3	200±1.5%	1478±3.4%	17.4±0.8%	8.0±20.3%	8.97±2.5%	-0.97±1.4%	13.56±3.1%
NIT-3.3.1	200±1.5%	1502±3.3%	17.7±0.8%	8.0±19.9%	9.07±1.3%	-1.01±1.1%	13.73±2.4%
NIT-3.3.2	200±1.5%	1498±3.3%	17.7±0.8%	8.1±19.8%	8.95±2.1%	-0.98±1.2%	13.73±2.7%
NIT-3.3.3	200±1.5%	1496±3.3%	17.6±0.8%	8.1±19.8%	8.96±2.1%	-0.99±1.2%	13.73±2.7%
NIT-4.1.1	300±1.2%	991±5.1%	10.1±1.2%	5.6±20.0%	13.53±5.2%	-1.20±1.5%	8.40±1.3%
NIT-4.1.2	300±1.2%	985±5.1%	10.0±1.1%	5.6±19.2%	13.29±2.9%	-1.20±1.4%	8.34±1.4%
NIT-4.1.3	300±1.2%	981±5.1%	10.0±1.1%	5.6±18.5%	13.23±3.0%	-1.24±1.5%	8.35±1.7%
NIT-4.2.1	300±1.2%	988±5.1%	10.2±1.2%	5.0±19.3%	13.49±4.5%	-1.28±1.4%	8.44±1.4%
NIT-4.2.2	300±1.2%	988±5.1%	10.2±1.2%	5.0±18.2%	13.36±2.8%	-1.23±1.5%	8.44±1.3%
NIT-4.2.3	300±1.2%	988±5.1%	10.2±1.1%	5.0±18.6%	13.33±2.8%	-1.18±1.8%	8.41±1.3%
NIT-4.3.1	300±1.2%	991±5.0%	10.2±1.4%	4.8±19.0%	13.45±4.5%	-1.25±1.6%	8.35±1.2%
NIT-4.3.2	300±1.2%	991±5.0%	10.2±1.3%	4.8±19.6%	13.30±2.4%	-1.26±1.5%	8.38±1.2%
NIT-4.3.3	300±1.2%	989±5.1%	10.2±1.3%	4.8±19.0%	13.26±2.2%	-1.28±1.6%	8.39±1.2%

Table A.5: Nitrogen thrust test result data with statistical and equipment errors.

B

Additional figures

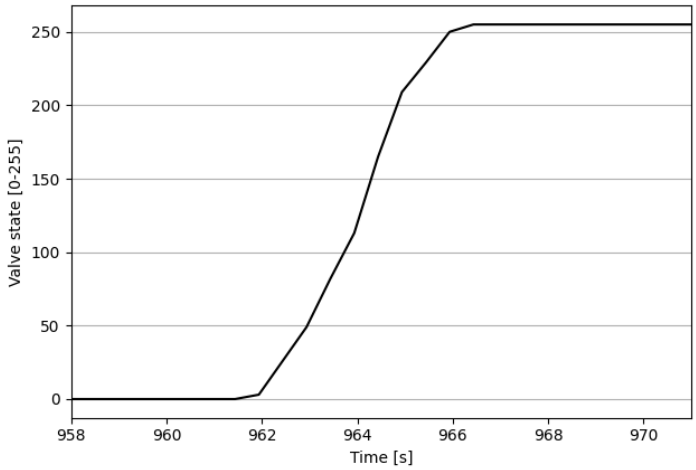

Figure B.1: Propellant valve state when opening the valve during the water thrust experiment. A state of 0 means the valve is fully closed, 255 is fully open.

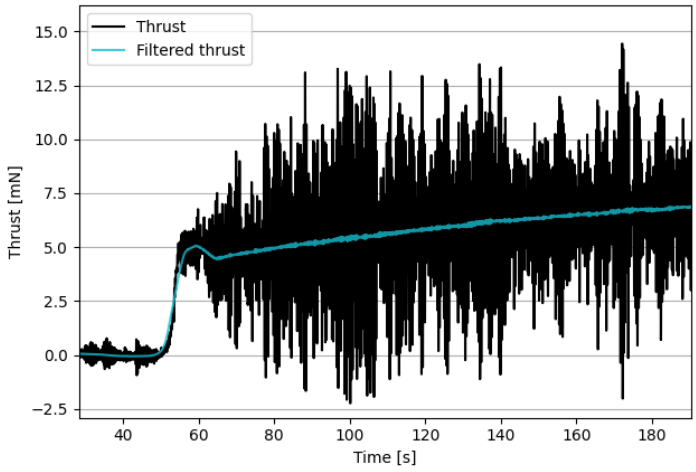

Figure B.2: Poor stability of the PID control resulting in high amplitude, high frequency noise while the time average signal is stable.

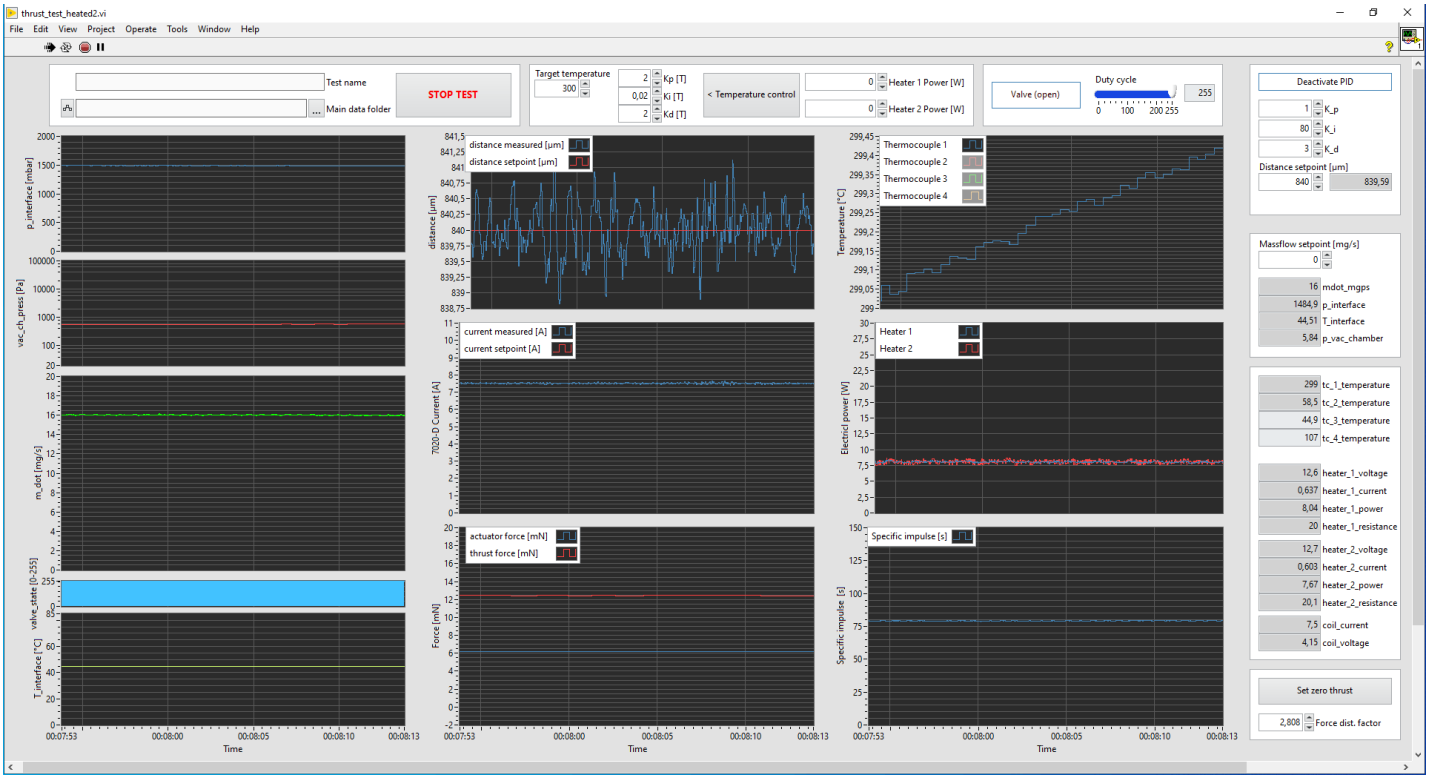

Figure B.3: LabView interface.

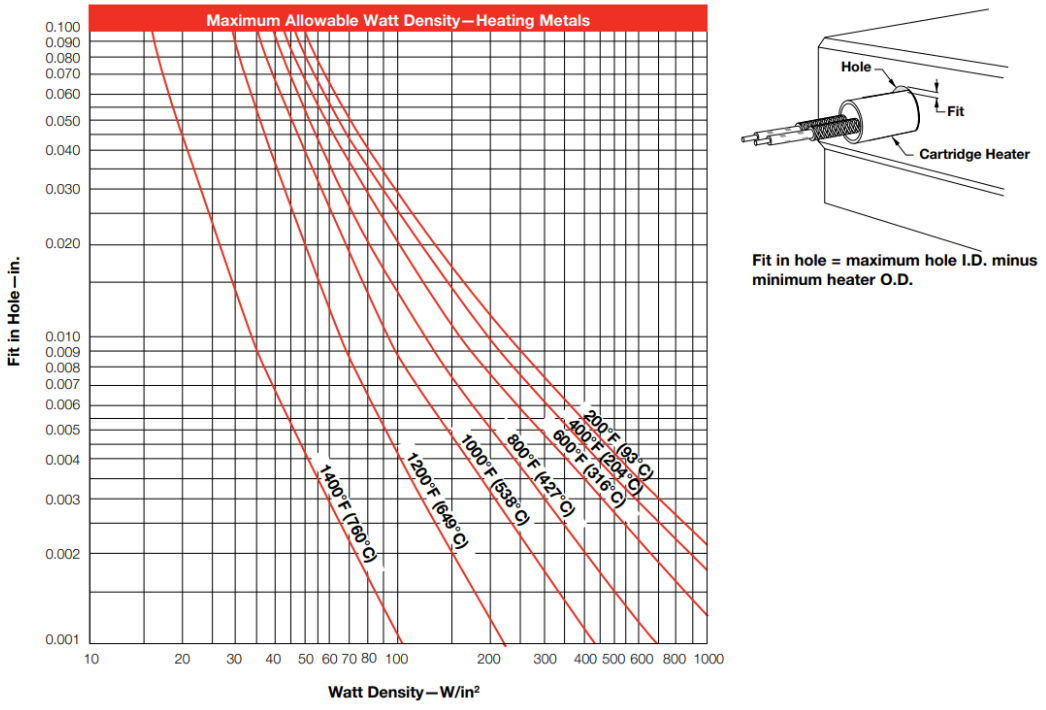

Figure B.4: Maximum allowed Watt density as a function of the fit in hole. Image by Watlow.[49]

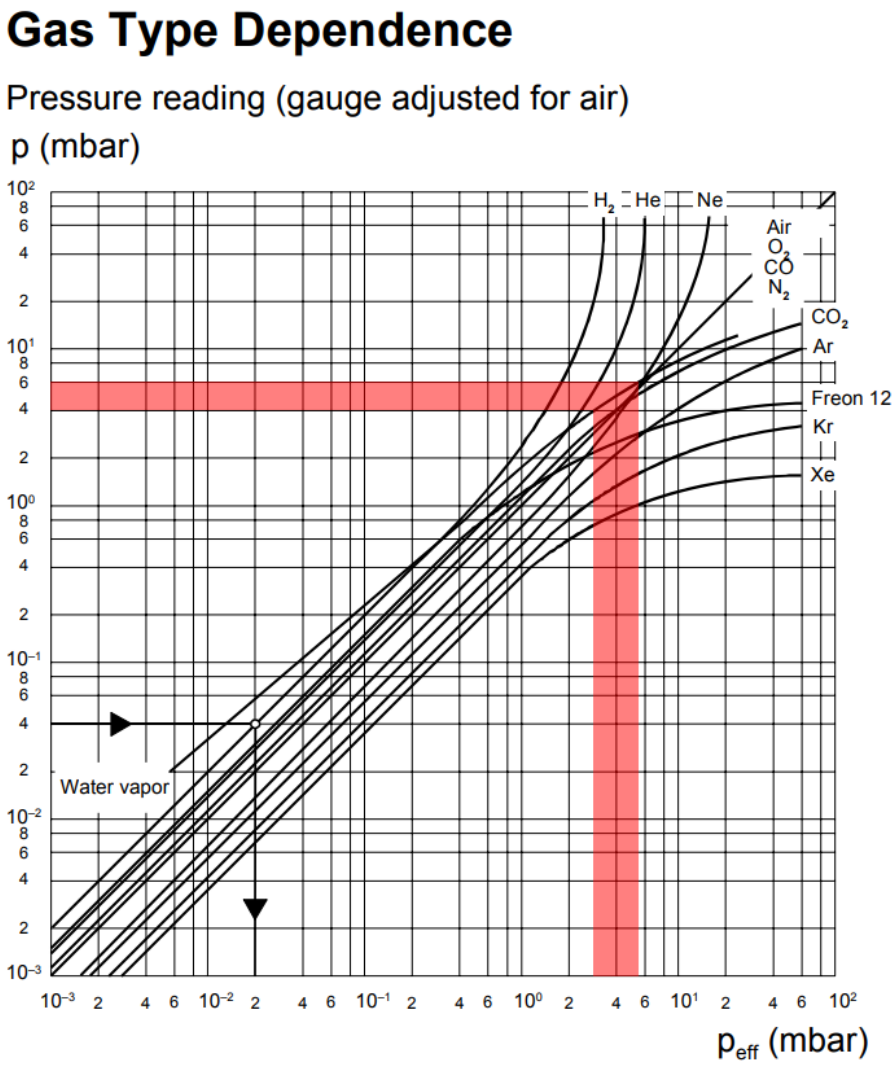

Figure B.5: Gas type dependence of Pirani gauges.[23] Area shown in red marks the water vapor conversion between 4-6 mbar, which is the ambient pressure range where the experiments conducted in this work take place.